DESIGNING STIMULI-RESPONSIVE ENGINEERED LIVING MATERIALS FOR BIOMEDICAL APPLICATIONS

A Dissertation

by

LAURA KATHERINE RIVERA TARAZONA

Submitted to the Graduate and Professional School of

Texas A&M University

in partial fulfillment of the requirements for the degree of

DOCTOR OF PHILOSOPHY

Chair of Committee,	Taylor H. Ware
Committee Members,	Akhilesh K. Gaharwar
	Daniel L. Alge
	Sargurunathan Subashchandrabose
Head of Department,	Michael McShane

May 2022

Major Subject: Biomedical Engineering

ABSTRACT

Engineered living materials (ELMs) that integrate living cells and synthetic materials have been created with stimuli-responsive capabilities. ELMs can harness the biological functions of cells and detect subtle changes in the environment, which enable them to respond in a programmed manner. Importantly, genetic engineering the living component enables the fabrication of ELMs with engineered responses to a wide range of stimuli. ELMs comprised of genetically engineered microorganisms can be programmed to perform desired functions, such as shape-morphing and drug delivery, and thrive in a wide range of environmental conditions. ELMs can be formed using probiotics, providing a multimodal mechanism of action in biomedical devices. This dissertation focuses on a series of studies carried out to understand the fundamental critical tools needed to fabricate ELMs with programmed responses primarily derived from the biological activity of microorganisms. These responses are studied to understand the mechanical changes of the embedding matrix and the chemical changes surrounding ELMs for their potential use in biomedicine.

In the first study, baker's yeast was embedded in acrylic hydrogels to form responsive ELMs capable of mechanical transformation by controlling cell proliferation. Yeast was capable of proliferating within the soft hydrogel matrix, leading to a controllable global expansion of the composite. Genetic engineering of the yeast enabled ELMs that changed in volume in response to specific amino acids and blue light.

In the second study, ELMs with yeast probiotics, acrylic hydrogels, and cellulose nanocrystals were fabricated using direct-ink-write printing. Printed ELMs containing genetically engineered probiotics changed shape into complex structures. Reservoir-based drug delivery capsules were fabricated for on-demand delivery of model drugs in response to specific biomolecules.

Lastly, prokaryotic ELMs were studied to understand long-term bacterial cell release to the surroundings. Materials were prepared with different stiffnesses and concentrations of cells to control cell release from the ELM. In future applications, ELMs made with prokaryotic probiotics can be used in *in vitro* studies to inhibit the growth of uropathogenic strains related to urinary tract infections.

Overall, future advances of ELMs with programmed functions, where microorganisms are programmed to respond to disease-specific stimuli, will offer new applications in drug delivery.

ACKNOWLEDGEMENTS

First and foremost, I would like to express my deepest gratitude to my advisor, Dr. Taylor Ware. His continuous support, guidance, and encouragement have tremendously help me grow as an individual and a researcher. I am very grateful he gave me the opportunity to explore and build a new research branch in living materials in his lab. His continuous excitement and wonderful ideas kept me motivated throughout my studies. I also extend my gratitude and appreciation to my committee members, Dr. Daniel Alge, Dr. Akhilesh Gaharwar, and Dr. Sargurunathan Subashchandrabose.

I would like to thank my collaborator at UT Dallas, Dr. Zachary Campbell for his excitement, knowledge, and support. I also appreciate the help and patience of his students Dr. Vandita Bhat and Tarjani Shukla. I am also grateful for my amazing friends at UT Dallas that made my time at that university more enjoyable.

I would like to thank my lab mates and colleagues, former and current students: Dr. Jennifer Boothby, Dr. Hyun Kim, Dr. Cedric Ambulo, Suitu Wang, Mustafa Abdelrahman, Yoojin Lee, Sasha George, and Manivannan Kalairaj for their roles in my journey. I would like to thank Seelay Tasmim and Mahjabeen Javed for their unconditional support and friendship that have been invaluable throughout these years. I would like to extend my gratitude to the amazing people, staff, faculty, and friends I have met at Texas A&M University.

Finally, I would like to thank my family in Colombia and the United States for always supporting me, loving me, and encouraging me in my pursuit of becoming a

doctor. I cannot thank my husband, Kevin Heckart, enough for always loving me, supporting me, being patient, and helping me to always do my best. His company has been invaluable throughout my doctoral journey. I truly would have not made it this far if it was not for the love and help of all of them. I love all my family and I hope I made each one of them proud.

CONTRIBUTORS AND FUNDING SOURCES

Contributors

This work was supervised by a thesis committee consisting of Dr. Taylor Ware [advisor], Dr. Akhilesh K Gaharwar, and Dr. Daniel L Alge of Department of Biomedical Engineering [Home Department] and Dr. Subashchandrabose Sargurunathan of the Department of Veterinary Pathobiology [Outside Department].

Mahjabeen Javed and Manivannan Kalairaj of the department of Biomedical Engineering at Texas A&M University provided the mechanical and cell viability data of chapter 4. Some images in figures found in chapter 3 were developed in Biorender.

All other work for the dissertation was completed by the student, under the advisement of Dr. Taylor Ware.

Funding Sources

Graduate study was partially supported by grant sources: NIH grant R01NS100788 (to Dr. Zachary Campbell) and by NSF grant nos. 2039425, 1905511, 1752846, 1663367.

.

TABLE OF CONTENTS

Page

LIST OF FIGURES

Page

1. INTRODUCTION TO STIMULI RESPONSIVE ENGINEERED LIVING MATERIALS*

1.1. Abstract

Stimuli-responsive materials are able to undergo controllable changes in materials properties in response to external cues. Increasing efforts have been directed towards building materials that mimic the responsive nature of biological systems. Nevertheless, limitations remain surrounding the way these synthetic materials interact and respond to their environment. In particular, it is difficult to synthesize synthetic materials that respond with specificity to poorly differentiated (bio)chemical and weak physical stimuli. The emerging area of engineered living materials (ELMs) includes composites that combine living cells and synthetic materials. ELMs have yielded promising advances in the creation of stimuli-responsive materials that respond with diverse outputs in response to a broad array of biochemical and physical stimuli. This review describes advances made in the genetic engineering of the living component and the processing-property relationships of stimuli-responsive ELMs. Finally, the implementation of stimuli-responsive ELMs as biosensors, drug delivery vehicles, and soft robots is discussed.

---

* Reprinted with permission from "Stimuli-responsive Engineered Living Materials" by L.K Rivera-Tarazona, Z.T Campbell, and T.H Ware, 2021. Soft Matter. 17, 785-809. Copyright [2021] by Royal Society of Chemistry

1.2. Introduction

Stimuli-responsive materials sense and respond to environmental conditions and enable devices with programmed functionalities, designed for applications in biomedicine,[1,2] wearables,[3,4] sensors,[5,6] actuators,[7–9] electronics,[10] and soft robotics.[11] Typically, the external cues that induce material changes include pH, light, temperature, chemicals, humidity, or electrical fields. In response, these materials can be designed to morph in shape,[12–14] change color,[15] heal,[16] degrade,[17,18] and perform other functions.[19] Stimulus-response in many materials is typically triggered by relatively strong stimuli. Here, we define strong stimuli as changes in environmental conditions that would be likely to cause undesired changes to other materials or living organisms surrounding the stimuli-responsive material. In many proposed applications of stimuli-responsive materials, including a variety of medical devices, the need for a strong stimulus is often a limiting factor. One approach to creating polymers that respond with high specificity to weak stimuli, such as biochemical changes, is to carefully synthesize designed binding motifs on the polymer.[20,21] While some biomolecules might be relatively easily detected, such as enzymes, many less reactive molecules are difficult to detect. Stimuli-responsive materials that respond with high sensitivity has attracted the attention of material scientists to create materials that mimic the functions and behaviors of living organisms. Although significant efforts have been developed,[22,23] it is still challenging to create materials that perform complex biological functions such as chemotaxis, adaptation, growth, and metabolic functions in response to highly specific and weak stimuli. Living organisms respond to weak stimuli in ways that are encoded by the information in the

genome. This response can be inherent to the organism or programmed to enhance sensitivity to surrounding the environment. To survive, cells must process dynamic changes in the form of mechanical and biochemical signals that are poorly differentiated (e.g. diastereomers). Living cells are capable of adapting to their environment, are highly efficient metabolic machines, and are often genetically manipulable.

Engineered living materials (ELMs) integrate living and non-living components. They can harness the biological potential of cells to enable dynamic, self-assembling, and functional materials. [24–27] Previous reviews that describe ELMs focus on engineering biological cells that act as living factories or modulate the performance of novel materials,[25] programming cells to produce materials with functional properties, [26] and integrating cells with synthetic materials to develop sensors and actuators.[27] For example, ELMs have been developed to utilize engineered cells for the synthesis of materials, such as amyloid proteins that form biofilms,[28–30] cellulose,[31] and other polysaccharides.[32] These extracellular materials have been investigated to perform different functionalities, such as self-regeneration and adhesion to surfaces. For the purpose of this review, we focus on describing stimuli-responsive ELMs, where living cells are incorporated within materials and are used to endow materials with stimuli-responsive functions. These materials offer opportunities to program specific responses in devices that require weak and poorly differentiated stimuli to perform diverse functions.

To fabricate stimuli-responsive ELMs, the design of a well-engineered matrix to address control, stability, and survival of the living component is necessary. Several

strategies for cell immobilization in or on polymer materials have been implemented, such as adsorption on surfaces, emulsification, extrusion, coacervation, and spray drying.[33] Synthetic hydrogels are often used as scaffolds and embedding matrices because they provide a protective environment for living cells and allow the exchange of nutrients and waste.[34–36] Strategies used to create ELMs are related to the strategies of tissue engineering, where macroscopic tissues and organs are created by controlling mammalian cell proliferation and differentiation.[37,38] Nevertheless, mammalian cells are fragile. Small changes in their environment can result in death and their growth conditions require well-controlled maintenance for long-term survival. By comparison, bacteria, yeast, and microalgae are substantially more robust. Microorganisms thrive in a wide range of environmental conditions because of their adaptive and metabolic behavior. These living cells act as sensing machines that detect small, weak molecule concentrations or changes in natural or physiological environments. Importantly, advances in genetic engineering technologies enable a wide range of possibilities to design living cells with programmable sensing and functions. Characteristics such as high sensitivity and specificity to weak stimuli, robustness, orthogonality, continuous sensing, and scalability can be achieved.[39,40] In order to build stimuli-responsive ELMs, cells with such characteristics must modulate the physical or chemical properties of the material or modify the surrounding environment upon exposure to external stimuli.

In this review, we briefly present relevant advances in the field of synthetic biology for the design of stimuli-responsive ELMs that sense the external environment and respond in a controlled manner. Next, we explore strategies for the manufacturing

and processing of these materials (Figure 1-1). Finally, we highlight different applications of stimuli-responsive ELMs in the biomedical field.

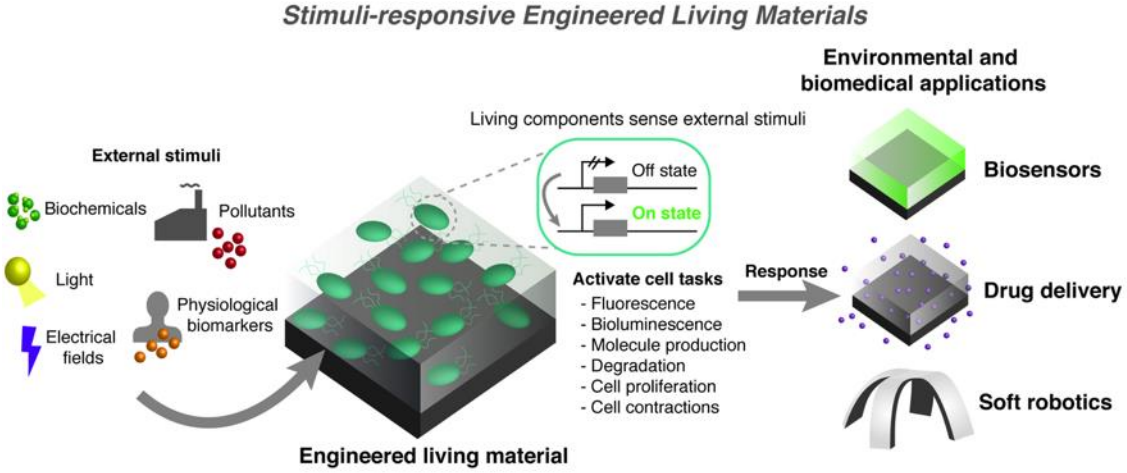

Figure 1-1: Stimuli-responsive engineered living materials. Schematic representation of ELMs that sense the external environment and respond in a controlled manner. Materials that contain genetically engineered living components are capable of sensing specific stimuli. Upon detection, cells can mediate a broad range of ELM responses. These include practical environmental and biomedical applications, such as biosensing, drug delivery, and robotic function. Reprinted with permission from [255]. Copyright (2021) Royal Society of Chemistry.

1.3. Engineered living materials design and processing

The design of materials that actively respond to the environment and perform programmed functionalities can be achieved by incorporating genetically engineered living microorganisms. Living cells such as bacteria, yeast, and microalgae can be tailored to sense and detect changes in their environmental conditions. Encapsulating these cells in materials enables the fabrication of ELMs with stimuli-responsiveness. Genetically engineered cells can be incorporated to engender a range of inputs, such as single chemicals or light, and programmed outputs, such as the production of enzymes or the expression of proteins. Reporters have been in use in molecular biology for decades.

Their application to ELMs enables precise quantification of cell proliferation, fluorescence, bioluminescence, or colorimetric parameters within materials.[41] The union of genetic manipulation and materials science enables the fabrication of stimuli-responsive ELMs for a broad range of practical applications.

1.3.1. Synthetic biology for the development of stimuli-responsive ELMs

Synthetic biology enables the reprogramming of the biological functions of microorganisms to achieve desired and specific responses.[42–45] Engineered prokaryotic and eukaryotic cells can be used as stimuli-responsive elements for ELM devices, where generally weak signals detected by the cells can produce output signals represented by a change in cell proliferation, function, or metabolic activity. These changes can directly modulate the properties or functions of the device, for example, by changing the material's shape to create soft actuators or by releasing molecules locally for drug delivery. One common route to create an ELM is to modify the embedded living components to express reporter genes that encode for proteins that produce measurable signals in response to target stimuli.[46] Common reporters used produce a fluorescent, colorimetric, or bioluminescent signal when a chemical or physical stimulus is detected (e.g., biochemicals, light). Fluorescent reporters such as green fluorescent protein (GFP), from the jellyfish *Aequorea Victoria,* can be employed to identify cells, protein localization, and transcriptional activity. GFP can be readily visualized, is non-toxic for cells, and does not require the presence of substrates other than oxygen for the maturation of the chromophore.[47] Enzymatic reporters such as β-galactosidase, from *Escherichia coli* (*E. coli*) encoded by the lacZ gene, react with an external substrate and

yield a product that can be detected by colorimetric assays.[48] Bioluminescent systems have evolved independently on well over 30 occasions.[49] In eukaryotic applications, the sea pansy (*Renilla*), copepod (*Guassia*), and firefly enzymes are the most common. In bacterial reporters, the *Vibrio* luciferase alpha and beta chains are used to emit light.[50,51] The use of reporters permeates the life science as they have been used extensively to monitor protein-protein interactions, transcription, recombination events, and transduction efficiencies.[47,52,53] Notably, when implementing these reporter systems within materials, ELMs can be leveraged to create biosensing devices that detect specific signals and report by changing the physical properties of the material (e.g., production of visual outputs). The fabrication of stimuli-responsive ELMs offers exciting opportunities in the development of environmental remediation and biomedical technologies.

Gene expression can be activated or repressed.[54] For example, transcriptional induction can occur in response to chemicals such as isopropyl β-D-1-thiogalactopyranoside (IPTG).[55] IPTG causes a transcriptional repressor to be inactivated and enables production of genes under the control of a lac operator sequence. There are a range of promoters that can be utilized to enable a range of chemical stimuli. By coupling sensing elements to reporter genes, cells can report the presence of a specific chemical inducer and initiate production of reporter genes such as GFP (Figure 1-2A).[56,57] Control of gene expression by chemical induction is slow, concentration dependent, and can require generations to reverse. Applications when dynamic control of cell behavior is necessary require more precise controls.[58] Optogenetic switches make use of light to control gene expression. They can provide fine spatial and temporal

control of gene expression. Optogenetic switches have been introduced in bacteria, yeast, and mammalian cells for drug screening, cell signaling, biosynthesis of target molecules, and control of mechanical responses.[58–62] For example, genetically engineered *E. coli* were constructed with an optogenetic switch that activated intracellular drug production upon illumination with blue light.[63] Thermal bioswitches have been constructed with expression systems that activate at different transition temperatures.[64] For example, *E. coli* was modified to express GFP after external induction with focused ultrasound or after detecting fever within a mammalian host.[64] Other genetic circuits have been engineered to sense changes in pH for the dynamic regulation of extracellular organic compounds.[65] For example, when using sugar acids, such as D-xylose, as substrates for cell growth, the substrate oxidates to D-xylonic acid and acidifies the media. This media acidification can be detrimental to cell growth. To address this issue, a genetic circuit that utilized a pH-responsive receptor protein was tested in *E. coli* to control D-xylonic acid accumulation by detecting changes in extracellular pH.[65] Other sensing circuits engineered in living cells have been used for the detection of heavy metals,[66,67] organic compounds,[68] and biomarkers.[69] The responses obtained from these engineered living cells can enable new levels of control over the functions of synthetic materials.

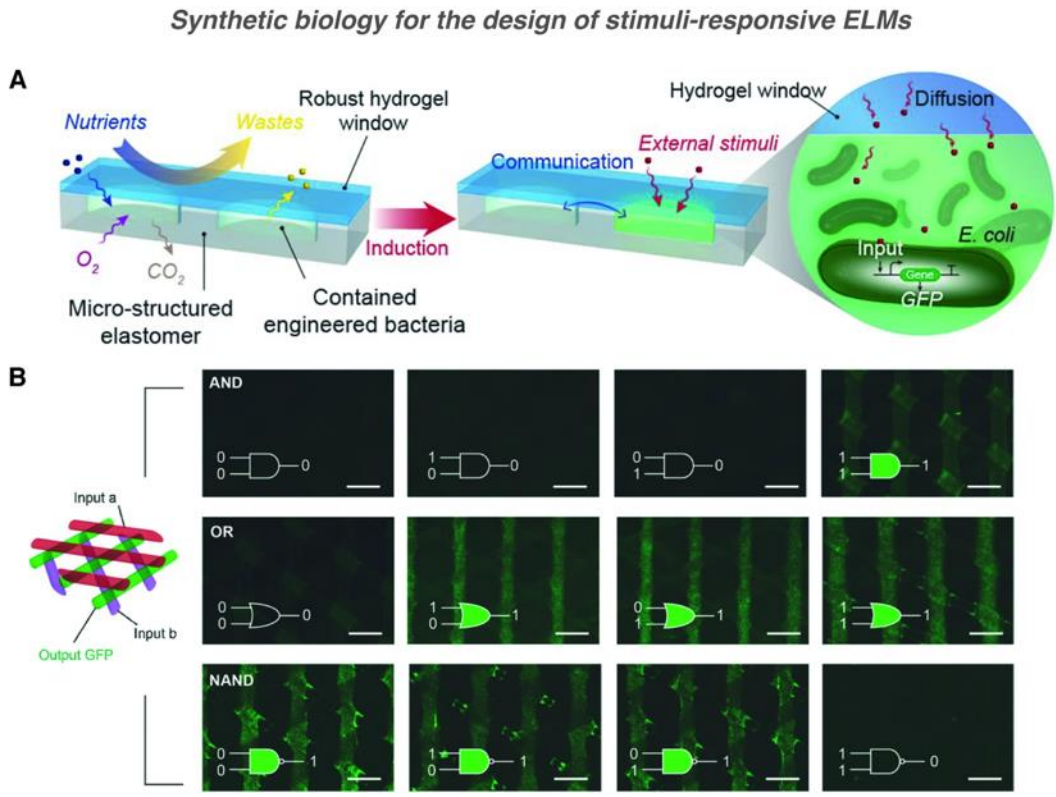

Figure 1-2: Synthetic biology for the design of stimuli-responsive ELM devices. (A) Schematic representation of an ELM with stimuli-responsive properties. The material incorporates living bacteria genetically engineered to express a fluorescent protein (GFP) in response to external stimuli. The living component allows the ELM to produce an optical signal that can be detected and measured. Reproduced with permission from [56]. Copyright (2017) PNAS. (B) Logic gates achieved in 3D-printed, stimuli-responsive ELMs. Programmed bacterial strains embedded in 3D printed structures perform computational operations (AND, OR, NAND). These cells act as outputs that detect the presence or absence of chemical components within the same structure and report by the presence or absence of GFP production after achieving a specific logical function. Adapted with permission from [76]. Copyright (2017) Wiley-VCH.

The development of engineered cells for environmental and biomedical applications has rapidly improved. Methods to optimize genetic circuit performance have focused on lowering limits of detection, increasing selectivity, and modulating dynamic range.[70] Signal processing methods include the integration of logic gates to

detect multiple target stimuli or genetic amplifiers to enhance expression and increase dynamic range to ensure good signal-to-noise ratios.[70–72] Logic gates allow the programmed recognition of multiple inputs to trigger a desired output.[73,74] For example, genetic circuits that respond to both pH and temperature have been engineered to perform complex logical AND or NAND operations involved in the regulation of GFP expression.[75] Programmed bacterial strains have been integrated in 3D structures to perform complex logic functions by interacting with each other and with external chemical inducers (Figure 1-2B).[76] Methods that involve genetic amplifiers have been studied to increase sensitivity and improve transcriptional input signals with large output dynamic ranges. These signal amplifiers have been proposed to be used in environmental applications where pollutants could be detected at low concentrations.[77] For example, an arsenic responsive circuit, built with a fixed-gain amplifier, was engineered in *E. coli* to generate a GFP output signal in response to arsenite concentrations as low as 0.25 μM. Genetically programmed cells that detect the variety of stimuli described above and perform intricate signal processing tasks will open new opportunities in the design of stimuli-responsive ELMs.

Manufacturing methods to introduce engineered cells in appropriate matrices are needed to design stimuli-responsive ELMs. In the next section, we will describe fabrication methods that incorporate living organisms into devices for use in environmental remediation, biosensors, drug delivery, soft robotics, self-healing, and self-cleaning applications.

1.3.2. Processing techniques for the manufacturing of stimuli-responsive ELMs

Processing techniques can be implemented to generate stimuli-responsive ELM devices. Typically, living cells are encapsulated or immobilized in soft matrices by chemical or physical crosslinking, adsorbed on surfaces or membranes, or encapsulated using microfluidic techniques.[78–80] In each of these approaches, traditional materials processing concerns, such as geometric control, microstructural control, and throughput, are combined with a need to maintain the viability of the living cells. We will highlight both 3D-printing and electrospinning as powerful approaches to create ELMs with programmable properties. 3D-printing enables constructs with site-specific control over cell distribution in a pre-designed format. Electrospinning of polymer-cell composites enables the fabrication of fabrics with controllable architecture and mechanics. These processing techniques enable nano, micro, and macroscale control to construct 3D environments suitable for cell encapsulation. As many processing methods to build complex ELM structures described in the literature encompass these techniques, we emphasize relevant work that uses such technologies. Finally, we will also describe additional processing methods for the production of ELMs.

The fabrication of ELMs with 3D printing and electrospinning techniques enables digitally-defined structures. Most frequently, 3D-printed ELMs are printed using extrusion-based techniques, such as direct-ink-write printing. Direct-ink-write printing makes use of biologically active microorganisms contained in a soft pre-gel matrix with shear-thinning properties, typically called “bioink.” Materials with these properties can

be extruded under shear forces and have the ability to maintain the shape of the sheared structure before further crosslinking. Within these bioinks, the unpolymerized matrix should be compatible with the cells and serve as a protective matrix against stresses induced during the printing or electrospinning process and should maintain cellular functions after crosslinking. Hydrogels are typically used in the synthesis of bioinks because they are able to mimic an environment that maintains the biological functions of the living component. Common examples of biocompatible hydrogels include the use of natural and synthetic networks such as agarose, alginate, gelatin, collagen, fibrin, polyacrylamide, polyethylene glycol diacrylate, among others.[81–84] Natural hydrogels offer high biocompatibility and cell viability but typically consist of physically crosslinked networks with weak mechanical properties. Synthetic hydrogels with chemically crosslinked networks permit cellular function and tunability of the mechanical properties. The development of bioinks with enhanced printability and biocompatibility have been explored by introducing functional groups via crosslinking or by using reinforcing materials that can enhance printing and electrospinning resolution.[85] Bioinks with improved mechanical integrity and print fidelity, while maintaining biocompatibility and cellular functions, continue to progress.[86–89]

Strategies that utilize 3D-printing technologies to develop structures with control over cell distribution and cell density have been reported. For example, multiple bacterial species 3D-printed to form living microstructures have been created to study cell-cell interactions and behaviors.[90] In another study, bacterial spores were printed within agarose gels to create living materials capable of surviving extreme conditions

and detecting chemicals or harmful bacteria when germinated.[91] Moreover, digital fabrication platforms have been described to control chemical distribution within 3D printed biohybrid objects and facilitate interactions between genetic constructs and chemical signaling profiles.[92] Other examples used mixtures of alginate and *E. coli* transformed to express red fluorescent proteins. These mixtures were printed on the millimeter-scale to create physically crosslinked structures that responded to external chemical inducers.[93] The development of functional living inks to 3D print multiple bacterial strains has been demonstrated in the design of living materials with pre-determined functionalities for biomedical applications (Figure 1-3A).[94,95] Besides the advances in bacterial processing, other microorganisms such as yeast and microalgae have been utilized to manufacture ELMs. For example, *Saccharomyces cerevisiae* has been printed within high-resolution scaffolds at low and high cell concentrations for the production of ethanol from glucose fermentation.[88,89] Microalgae were deposited in a layer-by-layer manner to create algae hybrids and study microalgal cell behavior and long-term viability.[96] Microorganisms from multiple kingdoms, like bacteria, algae, and yeast, were distributed within the same 3D-printed structure to study viability and cellular growth behaviors (Figure 1-3B).[97] This approach could offer new understandings in the way different species behave within the same encapsulating structure or provide methods to create ELMs for cell-cell communication and interactions with the external environment or the encapsulating matrix.

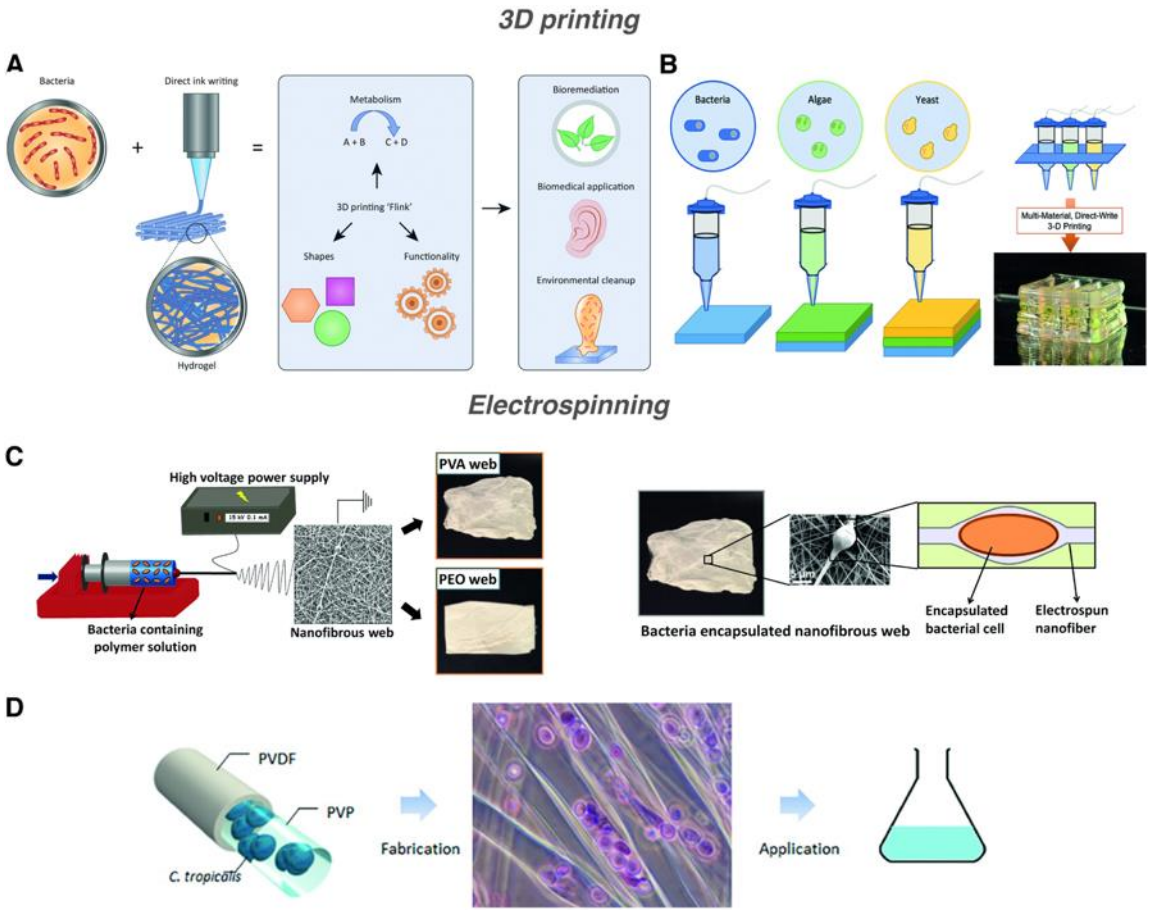

Figure 1-3: Fabrication strategies for the development of stimuli-responsive ELMs. (A) Schematic representation of a 3D printing process for the fabrication of functional printable living materials that can be implemented in biomedical and environmental remediation applications. Reproduced with permission from [95]. Copyright (2018) Elsevier Ltd. (B) 3D printing approaches can be used to build structures that contain multiple cell types. Adapted with permission from [97]. Copyright (2020) Wiley-VCH. (C) Schematic of an electrospinning process for the encapsulation of bacteria within nanofibrous webs. Picture and SEM micrograph of bacteria encapsulated in electrospun fibers. Reproduced with permission from [99]. Copyright (2017) Elsevier Ltd. (D) Yeast cells were encapsulated in core–shell polymeric nanofiber. Micrographs showing yeast cells encapsulated within the fibers. Reproduced with permission from [100]. Copyright (2015) American Chemical Society.

Electrospinning is a highly versatile processing method that utilizes electrostatic forces to assemble micro/nanometer-scale non-woven polymeric fibers with high porosity and large surface area. It has been implemented in the encapsulation of

microorganisms for delivery systems of probiotics, molecule sensing, agriculture, wastewater bioremediation, and drug delivery (Figure 1-3C, D).[98–100] Probiotic *Lactobacillus* species are viable in encapsulated polyethylene oxide nanofibers after electrospinning.[101] In the encapsulation of fungi, *Kluyveromyces lactis* and *S. cerevisiae* were combined with polyvinyl alcohol or cellulose acetate to produce electrospun ELM nanofibers. These structures can remove aflatoxin B2, which is a toxic metabolite with adverse effects produced by fungi found growing on agricultural products.[102] In general, 3D-printing and electrospinning approaches allow the top-down fabrication of structures that contain living organisms. One major advantage of these additive processing strategies is that both processes facilitate the fabrication of ELMs with multiple species. The co-location of multiple species is a physical strategy that can be used to complement genetic engineering strategies to enable greater functionality in response to a single stimulus or the ability to respond to multiple stimuli. These approaches mirror work where disparate synthetic materials are built into responsive structures; for example, structures that respond to both temperature and pH can be fabricated.[103] Incorporating multiple species in one structure could enable high specificity and selectivity to a variety of external stimuli, for example, by reporting the presence of multiple biomarkers in the same environment.

Additional techniques used for the fabrication of ELMs include wet spinning and roll-to-roll processes.[104,105] Both wet-spinning and roll-to-roll techniques are highly scalable. For wet spinning methods used in ELMs, polyvinyl alcohol (PVA) microfibers containing dispersed *Micrococcus luteus* or *Nitrobacter winogradskyi* bacteria were used

for gold sequestration and nitrate bioremediation, respectively. Using energy-dispersive X-ray spectroscopy and transmission electron microscopy, it was shown that the embedded *M. luteus* had successfully sequestered the gold into the composites. For bioremediation, the fibers encapsulating *N. winogradskyi* were capable of oxidizing nitrite and it was demonstrated by observing a decrease of nitrite concentration surrounding the fiber.[104] A roll-to-roll continuous coating process was demonstrated to build an ELM based on engineered *Bacillus subtilis* endospores. The cells were encapsulated in a PVA hydrogel and were cast onto a nonwoven poly(ethylene) terephthalate support. It was observed that cells retained functionality during this process as they were capable of generating a fluorescence signal after IPTG sensing.[105]

In summary, the combination of synthetic biology and materials science offers new methods to develop stimuli-responsive ELMs with well-defined functions. High specificity to a variety of molecules can be programmed into cells to produce composites that sense, respond, and modify the physical or chemical properties of the material itself or the surrounding environment. By implementing processing tools to control the spatial distribution of cells, living responsive devices for biomedical applications can be designed.

1.4. Applications of stimuli-responsive engineered living materials

The applications described in this section focus on ELMs with stimuli-responsiveness for and biomedical challenges. The combination of synthetic biology tools to address the control of living cells and processing techniques allows the

fabrication of ELMs to build devices for sensing in biomedical applications, devices for drug delivery platforms, and soft biohybrid robots.

1.4.1. Biomedical applications

1.4.1.1. Biosensing technologies for molecule detection and diagnostics

The integration of genetically engineered cells into materials enables stimuli-responsive ELM wearables for healthcare monitoring. Non-living, sensing wearables have been extensively studied to monitor temperature,[106] strain,[107] pressure,[108] and metabolites found in body fluids[109,110] with selectivity and high sensitivity.[111,112] They offer significant advantages for non-invasive and continuous real-time monitoring for diagnostics, especially when the wearables are designed to collect data wirelessly. Nevertheless, incorporation of electrodes, flexible printed circuits, and power supply units are still needed to design high-performance, functional devices. Stimuli-responsive ELMs to build wearables that do not require the use of power for data collection and processing, show significant promise in the screening of weak stimuli, such as target biomarkers, for diagnostics. For example, materials integrating bacteria programmed with genetic circuits have been fabricated as living wearable sensing patches that adhere to the skin and wearable gloves with chemical detectors at the fingertips.[56] These devices consisted of tough, stretchable polyacrylamide-alginate hydrogel and silicone elastomer covalently bonded to create bilayers encapsulating different genetically engineered *E. coli* strains. These strains express GFP when detecting chemical stimuli, such as N-acyl homoserine lactone (AHL), IPTG, and rhamnose (Rham). Interactions between these chemicals and the living material are created via chemical diffusion through the

hydrogel, where expression of GFP is observed as an output reporting signal when each bacterial strain detects their specific cognate inducer. As a result, the ELM sensing patches and gloves became fluorescent in their presence.[56] The same research group developed a 3D-printed living, stretchable tattoo that integrates these multiple GFP-expressing bacterial strains for the detection of chemicals applied on human skin. 3D-printable bioinks were synthesized that contained the programmed *E. coli* strains, Pluronic F127 diacrylate micelles to provide rheological behavior, photoinitiator to allow further crosslinking, and nutrient media to maintain cell viability. Upon exposure to each chemical inducer on the skin, a specific region of the tattoo produced fluorescence (Figure 1-4A). The wearable device was capable of resisting skin deformation without showing any signs of detachment or damage.[76] Responsive ELMs for wearable textiles have utilized genetically engineered *E. coli* patterned on cotton or plastics, by inducing cell adhesion in response to colored light. An *E. coli* strain was designed to encode a *csg*BAC operon, controlled by a blue light promoter, involved in the synthesis of curli fibers that anchor the formation of biofilms. Additionally, it included another promoter involved in the production of GFP under green light. To create wearable ELMs, the engineered bacteria were first adhered on cotton fabric by forming a biofilm in response to blue light. Then, ELM response was assessed by incubating the living fabric and shinning green light at 532 nm to induce expression of GFP. GFP fluorescence was then visualized under blue-light transillumination. Living fabrics exposed to green light showed 65% more fluorescence than fabrics not induced by green light.[113] ELMs with a hygroscopic response to sweat have been used to build

smart garments.[114] The wearable was designed by incorporating moisture-responsive *E. coli* onto moisture-inert films, like latex, to create ventilating flaps in a running suit. The responsive flaps in the suit opened when detecting body sweat from a wearer during exercise. The suit could control body temperature and could effectively remove body sweat (Figure 1-4B, C). Additionally, the same study designed a fluorescent running shoe prototype that incorporated GFP-expressing *E. coli* on the ventilating flaps. The shoe's flaps bent and exhibited increased fluorescence intensities when humidity conditions increased around the sole of the shoe.[114] In general, even though these ELM wearables utilize engineered strains for proof-of-concept monitoring of chemicals and physical stimuli, devices that detect physiologically relevant molecules could open future work in the fabrication of stimuli-responsive ELM biosensors for real-time point-of-care diagnostics.

Materials used to sense biomolecules for the development of medical technologies are highly desired for their use in diagnostic applications and early detection of diseases. One approach is to use stimuli-responsive polymers for sensing weak stimuli, by including recognition units such as phenylboronic acid-based polymers that detect sugars and respond with a change in diffraction,[115] wettability,[116] or fluorescence quenching.[117] These materials are stable in physiological conditions, but frequently have poor selectivity for saccharides. Other approaches utilize enzyme-functionalized materials that contain moieties for the catalysis of specific reactions which, in turn, leads to physicochemical changes in the material. Such methods include color-changing hydrogels that respond to analytes, including urea and glucose.[118,119]

Often, these enzyme-functionalized hydrogels suffer from poor stability because of their sensitivity to environmental conditions.[120,121] Stability and selectivity can be achieved with the use of molecularly imprinted polymers for the specific detection of biomarkers related to different diseases, like phenylketonuria, cancer and immune-suppressant disorders.[122,123] Often times, these polymers have poor water compatibility that can affect sensing performance and affinity.[124] Stimuli-responsive ELMs offer unique advantages in next generation biosensing technologies for detection and diagnostics.

Detection of physiologically relevant molecules, that are usually weak in nature, with stimuli-responsive ELMs has been achieved with biological paper analytical devices (bioPADs),[125,126] tough hydrogel biocontainment platforms,[127] and a wireless analytical device.[128] bioPADs composed of filter paper, ink, genetically engineered yeast, and hydrogel have been designed to detect doxycycline at concentrations down to 0.3 μg/mL. The living yeast biosensors utilized *S. cerevisiae* strains transformed with tetracycline responsive plasmids, linked to the red fluorescent reporter protein yEmRFP. The plasmids contain a reverse tetracycline transactivator, rtTA, capable of activating in the presence of the antibiotic doxycycline. The detection of the antibiotic promotes the transcription of the reporter gene to generate a readable fluorescent signal. The bioPAD was designed using paper filter printed with patterns that served to spot a pre-gel solution of sodium alginate containing the yeast. The gel was then crosslinked by submerging in calcium chloride to entrap the cells in the paper device. Results showed that bioPADs were capable of producing fluorescent signals when exposed to physiological fluids of human urine or bovine serum spiked with doxycycline (Figure 1-

4D, E).[126] *In vitro* sensing of physiological molecules can also be performed using tough polyacrylamide/alginate hydrogel biocontainment beads. These beads encapsulate engineered probiotic *E. coli* efficient in the detection of heme. Heme sensing is possible because cells carry an outer membrane hemin receptor (chuA) and a bioluminescent reporter. When heme is internalized through this transporter, it interacts with the transcriptional repressor HtrR, to then generate a bioluminescent signal from expression of the bacterial *luxCDABE* operon. The tough biocontainment ELMs were capable of sensing heme released from defibrinated blood and producing a significant increase in bioluminescence activity.[127] A monitoring device suitable for *in vivo* sensing of gastrointestinal molecules has been previously demonstrated by incorporating the above-mentioned heme responsive bacterial strain in a wireless readout capsule. The ingestible micro-bio-electronic device (IMBED) combines bacteria with microelectronics to enable local sensing of disease-related biomolecules (heme, AHL, thiosulfate) associated with the state of disease in the gastrointestinal tract. IMBEDs were built to detect bioluminescence generated by the engineered bacteria, using phototransistors that convert the signal to a digital code and transmit it wirelessly to an external device (Figure 1-4F). The capsule was deposited into the stomach of a porcine model of gastrointestinal bleeding, and detection in response to heme was achieved in less than an hour after deployment (Figure 1-4G). Small amounts of the molecule were able to be detected with high specificity and sensitivity.[128]

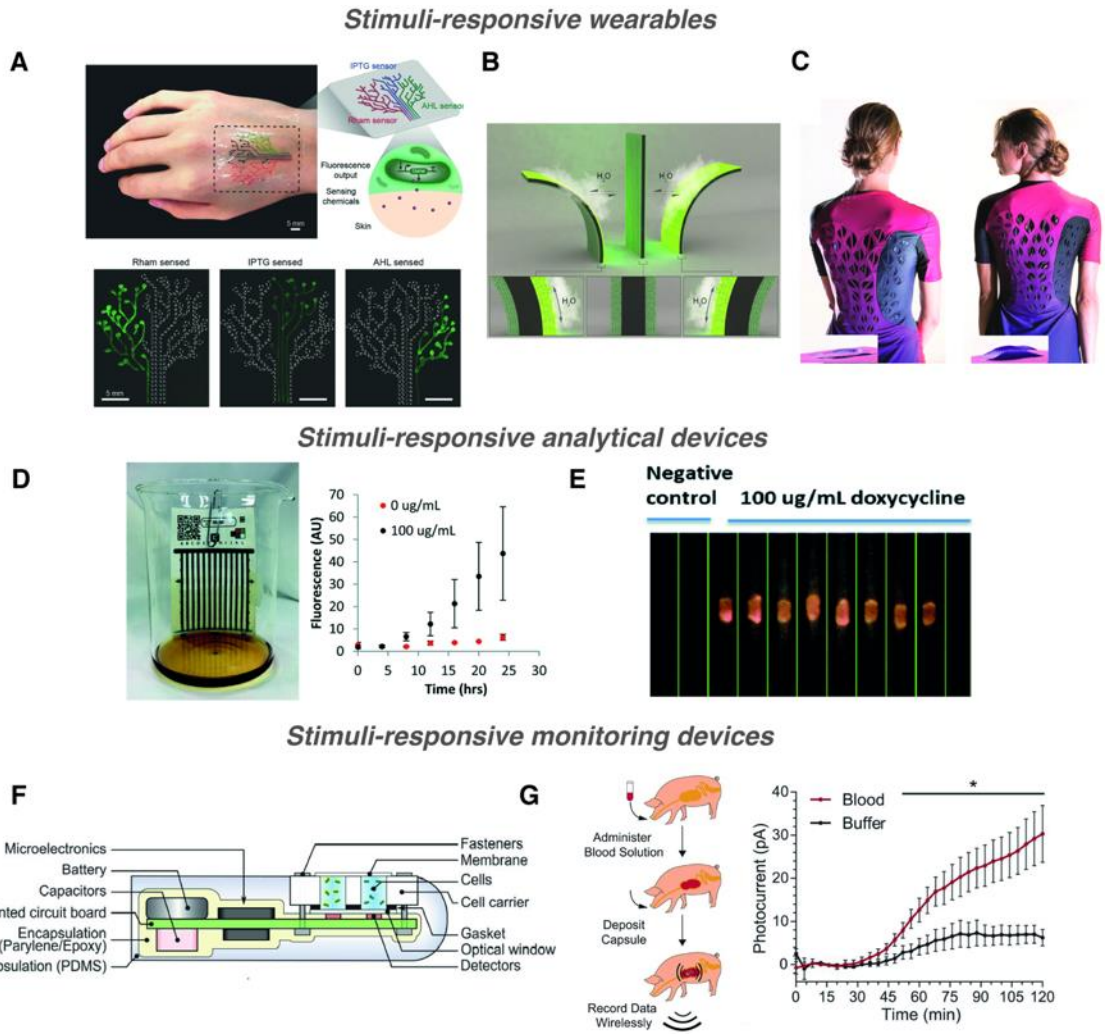

Figure 1-4: Stimuli-responsive ELMs for wearable, analytical, and monitoring devices. (A) 3D-printed ELM tattoo encapsulating engineered bacteria that sense different chemicals on the skin. The tattoo is capable of reporting the presence of chemicals by emitting fluorescence. Adapted with permission from [76]. Copyright (2017) Wiley-VCH. (B) Moisture-responsive films that change shape under humidity conditions. (C) Smart wearable suit with flat ventilating flaps before exercise (left) and bent flaps after exercise. Adapted with permission from [114]. Copyright (2017) exclusive liscensee American Association for the Advancement of Science. Distributed under a Creative Commons Attribution NonCommercial License 4.0 (CC BY-NC) http://creativecommons.org/licenses/by-nc/4.0/. (D) Fluorescent bioPAD spotted with modified yeast embedded in a hydrogel matrix. The device was developed in a reservoir of media containing doxycycline (left). Fluorescence was monitored over time in bioPADs treated with or without 100 μg mL−1 of doxycycline (right). E) Device treated with 100 μg mL−1 of doxycycline was imaged in a fluorescence lightbox. Adapted with permission from [126]. Copyright (2020) Royal Society of Chemistry. (F) Electrical system diagram of the ingestible, monitoring device. (G) Schematic of a porcine model

of gastrointestinal bleeding. Blood was administered, capsule was then deposited, and collected data was wirelessly transmitted (left). Photocurrent measurements over time of the device in the presence or absence of blood. Data was collected from the porcine model of gastric bleeding (right). Adapted with permission from [128]. Copyright (2018) American Association for the Advancement of Science.

1.4.1.1.1. Ongoing challenges and future directions

Stimuli-responsive ELMs for wearable, analytical, and monitoring biosensors offer great opportunities in detection and monitoring of physiologically relevant molecules. The key advantages of using ELMs to detect molecules related to disease states include that the biosensors are highly sensitive and specific and can report through the activation of gene expression. However, their implementation in real-world biomedical applications is a key challenge. When using ELM wearables, living cells entrapped in fabrics or hydrogels are prone to dehydration and may have limited nutrient exchange with the human body. One potential opportunity to overcome this limitation is to engineered cells to survive for long periods of starvation or utilize available molecules, such as those found in sweat, as a form of energy source.[129] Future studies could have a focus on developing wearables that use engineered cells for targeted drug delivery, monitoring disease-related biomarkers, and measuring body temperatures on the skin. Analytical ELMs based on paper scaffolds provide control of nutrient and oxygen diffusion for efficient cell viability. They are generally suitable for high-throughput analysis of body fluids and are compatible with cells.[130] Wearables and analytical paper-based devices provide information from biomarkers found in blood, saliva, sweat, tears, and urine. However, one of the most important advantages of utilizing stimuli-responsive ELMs, is their versatility to be used for *in vivo* monitoring.

For example, the gastrointestinal tract provides a rich source of biomarkers related to health and disease state. Genetically engineered cells have been studied to sense levels of gut biomarkers, report disease, and deliver therapeutics.[131] Nevertheless, a key challenge is that many biomarkers of interest cannot be detected because their receptors have not been fully studied or have not yet been identified.[132] This issue limits biosensor applicability. Some strategies described in this section use ELMs to monitor biomarkers related to gut disease. However, when translating these strategies for use *in vivo*, different aspects, such as the highly acidic environment of the stomach, areas of near anaerobic conditions, and highly variable transit time need to be considered to ensure sensor performance.[133] In addition, when building ELMs, a major design consideration is the selection of strains that colonize or do not colonize the gut if cell leakage from the device is present. Some strains colonize the gut without disrupting the microbiome, and others could generate serious side effects.[134] We expect that future advances in synthetic biology greatly expand the use of stimuli-responsive ELMs that could be effective in the detection and quantification of complex, highly specific molecules for healthcare applications.

The design of ELM biosensors with stimuli-responsiveness to physiologically relevant biomolecules is of great interest in creating wearable or monitoring devices. Synthetic biology tools could enable the development of microorganisms that respond to multiple stimuli and could open new ways to facilitate the design of ELMs for personalized medicine. The use of microorganisms can be further explored to design ELMs for delivery of therapeutics. In the next section, we expand on the use of stimuli-

responsive ELM devices that sense the environment and produce molecules for the design of drug delivery platforms.

1.4.1.2. Drug delivery platforms

Integrating biological and synthetic components is a promising strategy to obtain specific control of drug delivery. Stimuli-responsive polymeric materials, such as responsive drug-loaded microcarriers, are often functionalized to recognize biological changes in the body that alter material properties such as solubility, shape, or state of aggregation.[135,136] Materials that perform these functions are desired to enable on-demand delivery of therapeutics, with spatial and temporal controlled release triggered by strong physical, chemical, or biological stimuli.[137] Different stimuli such as temperature, magnetic fields, ultrasound, light, pH, redox gradients, and enzymes have been investigated for the potential release of drugs at specific areas within the body.[138–143] These stimuli are often strong and non-specific and when used in physiological conditions, they can be triggered at undesired sites or they can disrupt the environment surrounding the material. Materials that carry a payload and detect these stimuli can change shape, burst, degrade, or solubilize. However, the local changes associated with disease are often subtle, which complicates the design of synthetic materials that can sense and respond to this disease state by releasing a drug. New design concepts that use metabolically-engineered bacteria or fungi have been proposed as they avoid previous drug manufacturing, drug encapsulation, and drug stability.[144,145] Synthetic biological therapies that use engineered bacteria have been reported for cancer therapy and diagnosis,[146–149] treatment for genetic conditions,[150] therapies for infectious

conditions,[151] and treatment for gastrointestinal disorders.[152] However, some issues with colonization of these microorganisms could generate undesirable immune responses or infections. Microorganisms could freely circulate within the body or deliver a drug in a non-specific location, making these approaches complicated for clinical translations.[144] ELMs with stimuli-responsiveness to biological molecules or specific cues, may offer opportunities where living cells can be contained and used to deliver drugs at specific locations within the body. Importantly, the use of ELMs may provide ways to remove microorganisms when their functions are complete.

Towards the development of drug delivery ELMs, encapsulation of bacteria has been reported to endow materials with drug-producing capabilities. A study that utilized a bacterial strain of *Serratia marscescens* developed a stimuli-responsive ELM for the production of prodigiosin.[153] This red-pigmented metabolite, produced by the bacteria, has been found to have antimicrobial and anticancer activities.[154] Silica matrices were used to encapsulate the bacterial cells and nutrients were provided as external stimuli to induce the production of prodigiosin. Production of this metabolite was observed within the matrix but appeared to be slower than the production obtained from freely suspended cells. The inclusion of quorum sensing molecules to the media, such as acylated homoserine lactones (5 μM), appeared to enhance viability and increase prodigiosin production by 20% more than the production obtained in the absence of these molecules.[153] In another report, probiotic bacteria, *E. coli* Nissle 1917, was transformed to encode GFP and to secrete model proteins. Cells were entrapped in electrospun polyethylene glycol-polylactide porous fibers and further immobilized by adsorption or

covalent binding to the surface of the fibers.[155] These porous fibers allow sufficient nutrient diffusion for cell growth and protein secretion when exposed to chemical stimuli. ELMs were incubated in the presence of the chemical inducer IPTG (1 mM) to induce cell proliferation. The structures were capable of undergoing fluorescence by expression of intracellular GFP and also secrete the proteins into media.[155] This strategy serves as a proof-of-concept approach for the development of drug delivery devices that use probiotics for the potential release of therapeutic drugs in the body. Another drug delivery approach utilized light to spatially and temporarily control intracellular drug production in bacteria. This study made use of an endotoxin-free *E. coli* strain encapsulated in agarose hydrogels.[63] This strain was programmed to express a *vioABCE* operon for the metabolic production of deoxyviolacein (dVio), a bacterial metabolite with anti-bacterial, anti-fungal, and anti-tumor activities.[156,157] The *vioABCE* operon was placed next to the optogenetic plasmid pDawn, to build a genetic circuit with light-responsive capabilities for the production of dVio (Figure 1-5A). It was found that, when the ELM was exposed locally to blue light, *in situ* production of dVio was obtained (Figure 1-5B).[63] In addition, drug production led to a change in color of the material to a dark purple and the development of weak fluorescence when the material was exposed to light intensities of 1.38 mW/cm^2 (Fig. 6A). Nevertheless, the drug remained in the bacterial cytosol and was only released when a nonionic surfactant was provided to the hybrid material.[63] Similar to this approach, the same group developed an ELM using *E. coli* encapsulated in agarose gels that delivered a protein in response to blue light.[158] Bacteria were constructed with a streptadivin-binding peptide containing RFP. The ELM

was capable of expressing RFP protein within the gel and secrete it to the surrounding growth media using blue light. Fluorescence changes within the ELM were observed, and protein secretion of around 40 ng per 10 μL of bacterial hydrogel was obtained within a day of pulse-cycle light illumination.[158] In the next approach, *E. coli* was engineered to produce a cell-adhesive protein on the bacterial surface.[159]

Bacteria were engineered to express an RGD adhesive miniprotein along with a red fluorescent protein when sensing the presence of a photoactivatable version of IPTG (PA-IPTG). Bacteria were immobilized on poly-D-Lysine coated nexterion slides and induced with PA-IPTG and a light source. This stimulus activated miniprotein expression in the cell membrane and the production of RFP. To study the presence of the miniprotein produced, mouse embryonic fibroblasts were seeded on the materials. These fibroblasts displayed integrins that interacted with the proteins and adhered to the ELM. Additionally, it was observed that RFP could eventually secrete outside of the bacteria, which opens up opportunities to target drug delivery in mammalian cells.[159] These approaches enable the specific control of light for spatio-temporal control of bacterial metabolic functions for drug production. Further studies could be investigated towards the implementation of material processing techniques that allow better diffusion of nutrients and penetration of light for secretion of drugs.

The design of materials that actively secrete drugs to the surroundings are highly desired. To create drug-releasing ELMs, an antibiotic-producing fungus, *Penicillium chrysogenum*, was encapsulated in a sandwich-like structure for the production of penicillin. The structure consisted of a nanoporous top layer for diffusion of nutrients, a

middle layer made of agar and the living component, and a bottom layer for mechanical support. The resulting ELMs were capable of maintaining sustained release of penicillin for days when the materials were provided with sufficient external nutrients. The nutrients diffused through the top layer and allowed the fungi to grow and release penicillin on top of the ELM surface. Further, the material could effectively inhibit the growth of penicillin-sensitive *Staphylococcus carnosus* within one day.[160] In other studies, the use of bacteria, such as *Lactococcus lactis*, was harnessed to control the behavior of human mesenchymal stem cells (hMSCs) upon addition of peptides, such as nisin.[161] Bacteria were engineered to express human fibronectin to support stem cell adhesion and to secrete a bone morphogenic protein (BMP-2) that induces osteogenic differentiation in hMSCs. Addition of nisin as an external stimulus promoted fibronectin expression on the bacterial cell membrane and the secretion of BMP-2 to the extracellular environment. To build ELMs, engineered bacteria were cultured on different materials, such as poly(ethyl acrylate) or collagen, to allow biofilm formation and adherence to the substrate. ELM function was tested using different concentrations of nisin. After adding 10 ng/mL of this molecule to the ELM, fibronectin expression was induced, and subsequent hMSC adhesion was obtained. In addition, bacterial cells were capable of secreting high concentrations of BMP-2 (200 ng/mL) that contributed to osteogenic differentiation of hMSCs.[161] These stimuli-responsive ELMs are suitable for delivery of proteins to the surrounding environment and enable strategies that can be used for stem cell research or drug-delivery platforms. The same group utilized a droplet microfluidic device to construct compartmentalized microgels that encapsulated both of

the previously described bacteria and hMSCs within the same structure. The microgels served as extracellular matrices to study osteogenesis upon addition of extracellular nisin.[162] This versatile encapsulation platform enables strategies to study drug production and symbiotic cellular interactions. An approach that utilized the proliferation of living microorganisms to build oscillatory platforms for controlled release of model proteins has been investigated.[163] This strategy utilized pH-responsive chitosan capsules containing genetically engineered *E. coli* built with a genetic circuit that causes oscillations in cell density over time (Figure 1-5C). By introducing nutrients as external cues, bacteria were capable of proliferating and undergoing partial lysis by expressing toxins upon reaching sufficiently high cell densities within the capsule. Accumulation of toxins caused cell lysis and a decrease in cell density, but partial decrease allowed growth recovery and, therefore, the generation of growth oscillations for multiple cycles. Cell proliferation and subsequent lysis led to a change in pH of the surrounding media and, eventually, the shrinkage of the chitosan capsules to squeeze out bacterial lysis protein products. Swelling was observed by controlling the lysis rate after shrinking when glucose was added, and by replenishing the capsules with fresh media periodically. The model protein released from the capsules was β-lactamase, and its presence in the surrounding media was detected by adding a substrate to measure enzymatic activity (Figure 1-5D).[163] This ELM platform demonstrates the active feedback control that can be mediated by the interactions between engineered cells and stimuli-responsive materials to create drug delivery platforms. Genetically-engineered *E. coli* with cell surface-displayed adhesin proteins and triggered drug secretion enable multifunctional

ELMs. The bacteria were able to be retained in dextran-based hydrogels by displaying a calcium-dependent, glucose-binding adhesin. The adhesin protein (*Mp*A), derived from Antarctic bacterium *Marinomonas primoryensis* binding proteins, was expressed on the surface of the cells. When the chemical IPTG was present, the protein could bind glucose with high affinity. Additionally, to create a stimuli-responsive ELM, cells were also transformed to express and secrete bacteriocin lysostaphin. This molecule was secreted to target and inhibit the growth of pathogenic bacteria, *Staphylococcus aureus*, when the ELM was exposed to the monosaccharide arabinose (Figure 1-5E). The results showed that upon exposure to arabinose, the device was activated for the in situ secretion of lysostaphin, which diffuses out of the cells and inhibits the growth of methicillin-resistant *S. aureus*.[164] The bactericidal activity was tested when the hydrogels were placed on agar plates streaked with *S. aureus*, in the absence or presence of IPTG and/or arabinose. Bactericidal activity against *S. aureus* was induced by adding arabinose and observed by the development of inhibition zones around the periphery of the ELMs (Figure 1-5F).[164] This work demonstrates the application of an engineered living material with specific responses to biomolecules for drug secretion and enables the design of devices for therapeutic applications. Further work could be focused on the implementation of 3D printing to build structures that allow higher cell biomass retention and that improve the efficient secretion of drugs.

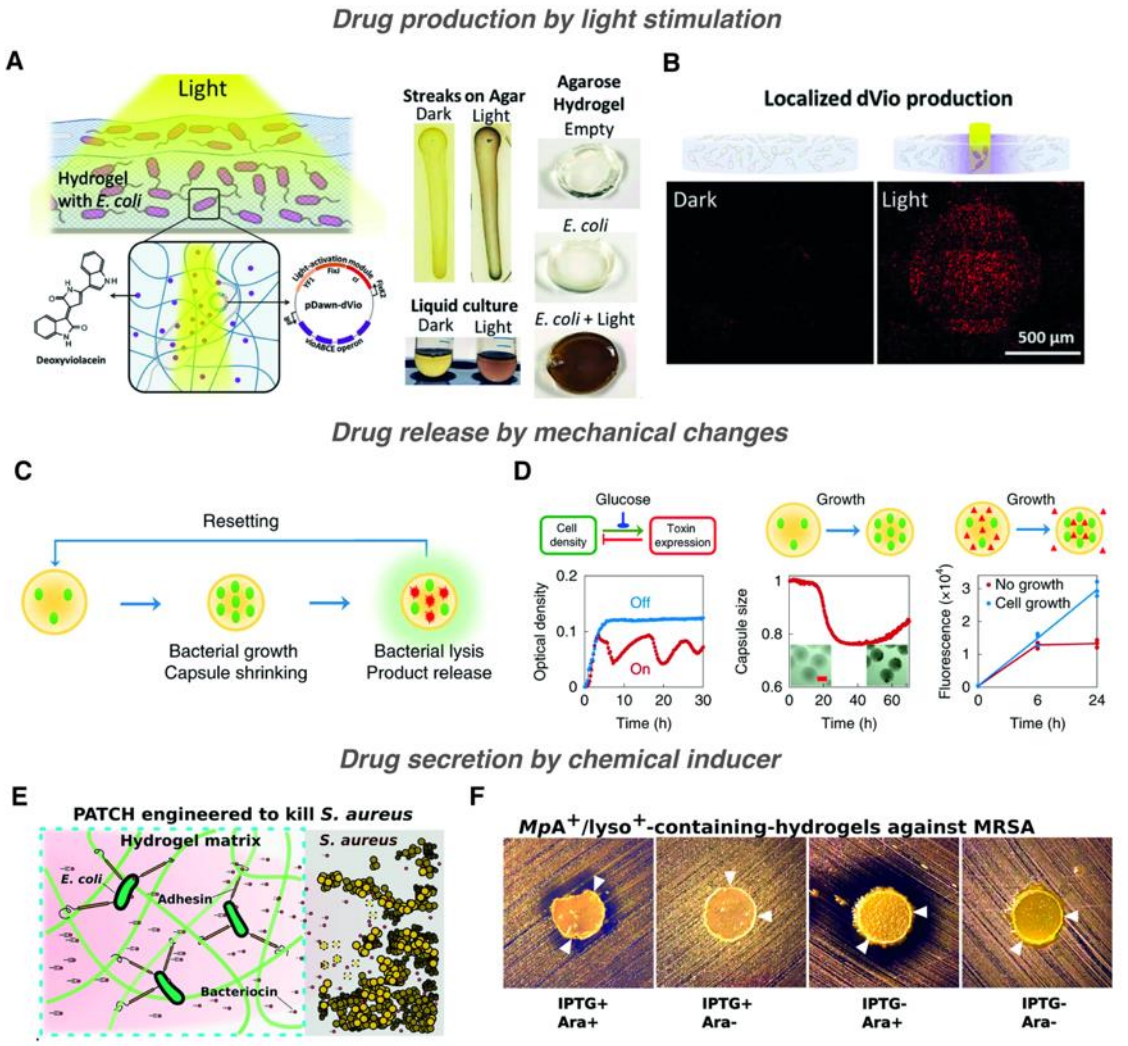

Figure 1-5: Stimuli-responsive ELMs for drug delivery applications. (A) Schematic of a light-responsive ELM. Bacteria was engineered with a pDawn-dVio plasmid to enable the production of the drug deoxyviolacein upon light illumination (left). Bacterial cells cultured on agar, liquid media or encapsulated in agarose hydrogels were capable of producing the drug and a change in color in response to light (right). (B) Patterned light exposure allowed the production of drug locally and was detected by epifluorescence microscopy. Adapted with permission from [63]. Copyright (2018) Wiley-VCH. (C) Schematic representation of beads encapsulating bacteria that shrink in response to cell growth and swell in a reversible manner to enable an oscillatory behavior. Bacteria undergo lysis at sufficiently high cell densities and then release model molecules to the surroundings. (D) Oscillatory behavior can be turned off by adding glucose to the media. Capsules shrink in response to cell growth. Capsules that shrink lead to an increase in fluorescence intensity as compared to capsules that do not shrink. Adapted with permission from [163]. Copyright (2019) Nature Publishing Group. (E) Schematic of the ELM encapsulating engineered bacteria that produce and secrete

an antimicrobial enzyme against methicillin-resistant *S. aureus*. (F) Antimicrobial activity of ELMs placed on Mueller–Hinton agar plates streaked with methicillin-resistant *S. aureus*. Adhesin and lysostaphin functionalities by cultivating ELMs in the absence or presence of IPTG and/or arabinose. Adapted with permission from [164]. Copyright (2020) American Chemical Society.

1.4.1.2.1. Ongoing challenges and future directions

Stimuli-responsive ELMs could facilitate long-term delivery of therapeutics that may be impossible to obtain with traditional or purely synthetic stimuli-responsive materials. The key advantages of using ELMs are that a variety of stimuli can initiate drug delivery and that the drug could be synthesized within the ELM. As described in this section, production of model drugs and therapeutics from ELMs usually involves the use of engineered microorganisms. In these studies, cells are modified to express heterologous genes that encode a molecule of interest only when an exogenous stimulus is applied. This enables the targeted delivery of therapeutics only when and where required. Nevertheless, the release of some drugs to the surroundings using ELMs is a key challenge. Some drugs that are synthesized within the cells require exportation through the cell membrane and must diffuse out of the ELM. Exportation is often limited to small molecules that may be able to cross the microbial cell membrane freely. However, for larger molecules this exportation usually requires the engineering of cells with appropriate secretion systems. These systems can have limited capacity and become saturated, leading to drug retention. Alternative strategies involve cells programmed to lyse to release their cargo. In addition, when building stimuli-responsive ELMs, the encapsulating matrices could be designed to further modulate diffusion of therapeutics out of the material. Another key advantage of these materials is their use as gut

therapeutics. ELMs could be used to detect relevant biomarkers found in the gastrointestinal tract and control targeted drug delivery. As described previously, ELMs have been reported to sense disease related gut biomarkers, but the integration of a therapeutic approach in this area remains to be studied. We expect that drug delivery from ELMs may be most compelling when the properties of both the living cell and the synthetic material are used to control the release profile.

1.4.1.3. Soft robotics

Engineered living materials with the ability to sense their environment and respond mechanically are of great interest for the fabrication of soft biohybrid robots. Soft robots are capable of performing functions for healthcare applications, benefiting from their ability to adapt, undergo complex motions, and increase compatibility with the mechanics of the body.[165,166] Soft robots that are made of stimuli-responsive soft materials, including electroactive polymers,[167] pneumatic elastomers,[168] shape memory polymers,[169,170] liquid crystal elastomers,[171,172] or hydrogels[173,174] may enable untethered systems with sensing and shape-changing abilities. Each of these materials requires strong, external power sources to change shape, and the delivery of this power, such as by heating the material, may be incompatible with the environment surrounding the robot.[175,176] In this context, engineered living cells enable soft robots that are, at least partially, chemically powered by the metabolism of the cells. So far, we have described on ELMs mainly composed of microorganisms, which provide exceptional control mechanisms for creating stimuli-responsive ELMs with the advances of synthetic biology tools. Mammalian cells offer unique capabilities, including coordinated and

synchronized actuation for the design of soft robots. The pioneering work that placed the foundation for building soft biohybrid robots utilized rat ventricular cardiomyocytes seeded on polydimethylsiloxane (PDMS) to create muscular thin films. Upon exposure to electrical stimuli, cells underwent synchronized contraction and relaxation that caused the underlying films to transform from 2D to 3D shapes, and perform functions such as gripping, pumping, walking, and swimming.[177] Building on this work, cardiomyocytes were used to fabricate jellyfish-like soft robots that achieve complex swimming behavior.[178] Other research studies that take advantage of contraction and relaxation properties of cells utilized a range of muscle cell types, including skeletal muscle myotubes, smooth muscle cells, stem cell-derived cardiomyocytes, among others.[179–182] The ability of cells to respond to chemicals in the environment has also allowed the fabrication of color-changing biosensors with actuating capabilities powered by cardiomyocytes.[183,184] In one example, neonatal rat ventricular cardiomyocytes have been cultured and oriented on *Morpho menelaus* butterfly wings to function as beating components and cause structural color shifts. Upon addition of isoproterenol, cardiomyocytes were stimulated to increase beating frequency, which resulted in an increase in the degree of structural color changes. Studies in this field offer advances for creating self-reporting platforms to evaluate drug effects on mammalian cells.[184] The biohybrid methods described so far are able to function at high energy efficiencies and harvest energy from surrounding nutrient solutions.

Optogenetics enables the realization of soft biohybrid robots with fast and precise control over multiple muscle units, necessary to power locomotion and achieve

coordinated robotic maneuvering. Cardiac and skeletal muscle cells have been modified to express light-gated ion channels, Channelrhodopsin-2, to create blue-light-sensitive constructs.[62,185–187] An interesting approach, where cardiac cells were patterned onto a four-layered architecture, yielded a tissue-engineered artificial stingray with phototactic control on sequential muscle cell activation for undulatory locomotion (Figure 1-6A).[185] The stingray was guided along an obstacle course by modulating the frequency of the applied light and controlling directional turns (Figure 1-6B). Another biohybrid robot based on optogenetics utilized skeletal muscle cells to fabricate bioactuators with 2D directional locomotion and rotational steering in response to both electrical and optical stimulation.[186] Further, the same group optimized the system by developing strategies to drive healing and remodeling after mechanical damages.[187] These approaches are promising for creating soft robots, but the maintenance of mammalian cell cultures needs to be carefully controlled. As a result, these devices are highly unlikely to persist for long periods of time in various environments.

A strategy that developed a method to actuate a skeletal muscle cell-based biohybrid robot in air has been described.[188] Collagen hydrogel and a system of tubes to perfuse culture medium were used to encapsulate skeletal muscle tissue and maintain the necessary humidity conditions for cell viability. Electrical stimulation was applied through embedded electrodes to induce tissue contractility when the robot was operated in the air (Figure 1-6C). This stimulation allowed the control of the deformation of the biohybrid robot and was demonstrated by pushing a bead in air (Figure 1-6D). Although this system gradually dries out, its contractility function was continuously maintained for

1 h without any damage to the skeletal muscle tissue.[188] Insect muscle cells have relatively longer-term viability and can tolerate fluctuating changes in temperature, pH, or oxygen, and thus, they have been studied to create robust soft robotic actuators.[189,190] In addition, the use of motile microorganisms expands on the use of living cells to create microrobots that have better stability in a wide range of environmental conditions and that can be genetically modified to complete complex functions. Microrobots have been described in soft robotic reviews where motile bacteria, microalgae, and mammalian cells sense the environment and are manipulated by external stimuli. Their fabrication is of potential use in applications for specific targeting and delivering of cargo or for powering 3D micromotors.[191–193] Nevertheless, these types of devices are only manipulated for their use at the microscale, due to the fixed size of the biological units. Methods that focus on the sensing and responsive capabilities of microorganisms to drive actuation in macroscale soft robots, by applying external stimuli, are also of interest in this review.

Many materials in nature undergo shape transformations in response to environmental conditions such as humidity. Hygromorphic materials have been studied to produce actuators that operate by changes in moisture found in the skin or the air. Studies that use the hygroscopic properties of natural cells, to convert energy from humidity gradients have made use of bacterial spores as building blocks for the design of macroscopic actuators.[194] Bacterial spores from *B. subtilis* possess a cortex that is hygromorphic, have long term survivability, and do not require the addition of a nutrient source to maintain its hygromorphic behavior.[195] These spores have been applied in the

fabrication of stimuli-responsive ELMs as they can reversibly expand or shrink to changes in relative humidity. For example, in one study 3 mg of these spores were coated on 0.5 mm or 0.75 mm thick latex sheets treated with poly-L-lysine to improve adhesion.[194] After fabrication, the ELMs have an initial curvature at a relative humidity of 15-20% from laboratory conditions. This curvature starts decreasing when the ELM is subjected to increasing relative humidity. The ELMs have a fast, reversible response because the spores respond mechanically within ~0.4 s after exposure in humid conditions and within ~0.5 s of water release. Because of these unique responses, ELMs were applied to harvest energy, and it was observed that the spores delivered an average power of 0.7 μW with an estimate of ~233 mW/kg for electrical power.[194] These materials were further studied to create ELMs that undergo complex transformations. Bioprinting techniques were used to spatially localize *B. subtilis* spores on flat substrates.[195] These materials were capable of undergoing complex 3D folding in response to relative changes in humidity. Another report utilized the same bacterial spores to build structures using photolithography and UV-curable resins.[196] Spores were mixed within the resin and then UV-cured on top of a polyimide substrate to build the devices. Further, the polyimide substrates were laser cut and patterned with the spore/UV-resin solution through photolithographic masks. This design allowed ELM actuators to undergo complex changes in shape under relative humidity conditions. These materials presented work and power intensities at a maximum of 0.44 MJ/m^3 and 54 kW/m^3, respectively.[196] These hygromorphic ELMs could be used in future applications for energy harvesting and soft robotics.

Yeast proliferation within polymer materials has been harnessed to drive mechanical actuation in macroscopic structures. Baker's yeast, *S. cerevisiae*, encapsulated in polyacrylamide hydrogels, were capable of proliferating within the matrix when essential nutrients were provided (Figure 1-6E).[197] Cell proliferation led to the material expanding its volume up to 200% more than when nutrients were absent (Figure 1-6F). Genetic engineering of the yeast enabled high control of shape-change by using specific biogenic amines, such as L-histidine, that triggered cell proliferation within the composite. The engineered yeast could sense external stimuli and respond by irreversible expanding the polymeric matrix. By patterning cell viability, complex structures such as helical geometries could be obtained (Figure 1-6G). Optogenetic switches were also engineered in the yeast and enabled the spatiotemporal control of ELM actuation when the materials were exposed to a light intensity of 2.7 mW cm^{-2}.[197] We note that this approach utilized visible light at a weak irradiation intensity to induce shape change in the ELM. Many strategies in traditional stimuli-responsive materials, built to change shape, require UV or visible light at strong irradiation intensities of 100 mW cm^{-2} or higher.[198,199] High intensities may cause overheating and undesired health effects, such as tissue damage when ELMs are used for biomedical applications. However, it is important to note that parameters such as irradiation time and wavelength of light need to be considered when making this comparison.[200]

A method that developed a soft robotic gripper utilized an interfacial module that allowed the communication between living bacteria, the external environment, and electronics embedded in soft materials.[201] The interface module allowed the

biocontainment of engineered bacteria to detect environmental signals that then where converted into cellular and to electronic signals. The soft robotic gripper consisted of *E. coli* carrying the plasmid *pIV_GFP* to allow the synthesis of GFP in the presence of chemical inducer IPTG. Cells were cultured, retained by membranes, and housed within a PDMS chamber to create a biolayer. Then, a flexible printed circuit board (FlexPCB) and pneu-nets were combined with the biolayer and mounted to a 4-DOF robotic arm (Figure 1-6H). This device was designed to produce a fluorescent signal in response to IPTG, allowing the electronic components to detect the signal and distribute it to a central processing unit to initiate robotic decision making and actuation. To initiate the process, the device was incubated in the absence or presence of IPTG and allowed to measure and store the data of the cell fluorescent output. After incubation, the gripper 'decides' whether or not to deploy a round object into the media. When the device detects the presence of IPTG, it alerts the system and does not deploy the object. In the absence of IPTG, the system then decides that it is safe to grab and deploy the object (Figure 1-6I).[201] This approach demonstrates the possibility of combining genetically engineered living microorganisms, electronics, and soft materials to create a responsive, actuating device that communicates with the external environment and excels at a decision-making process.

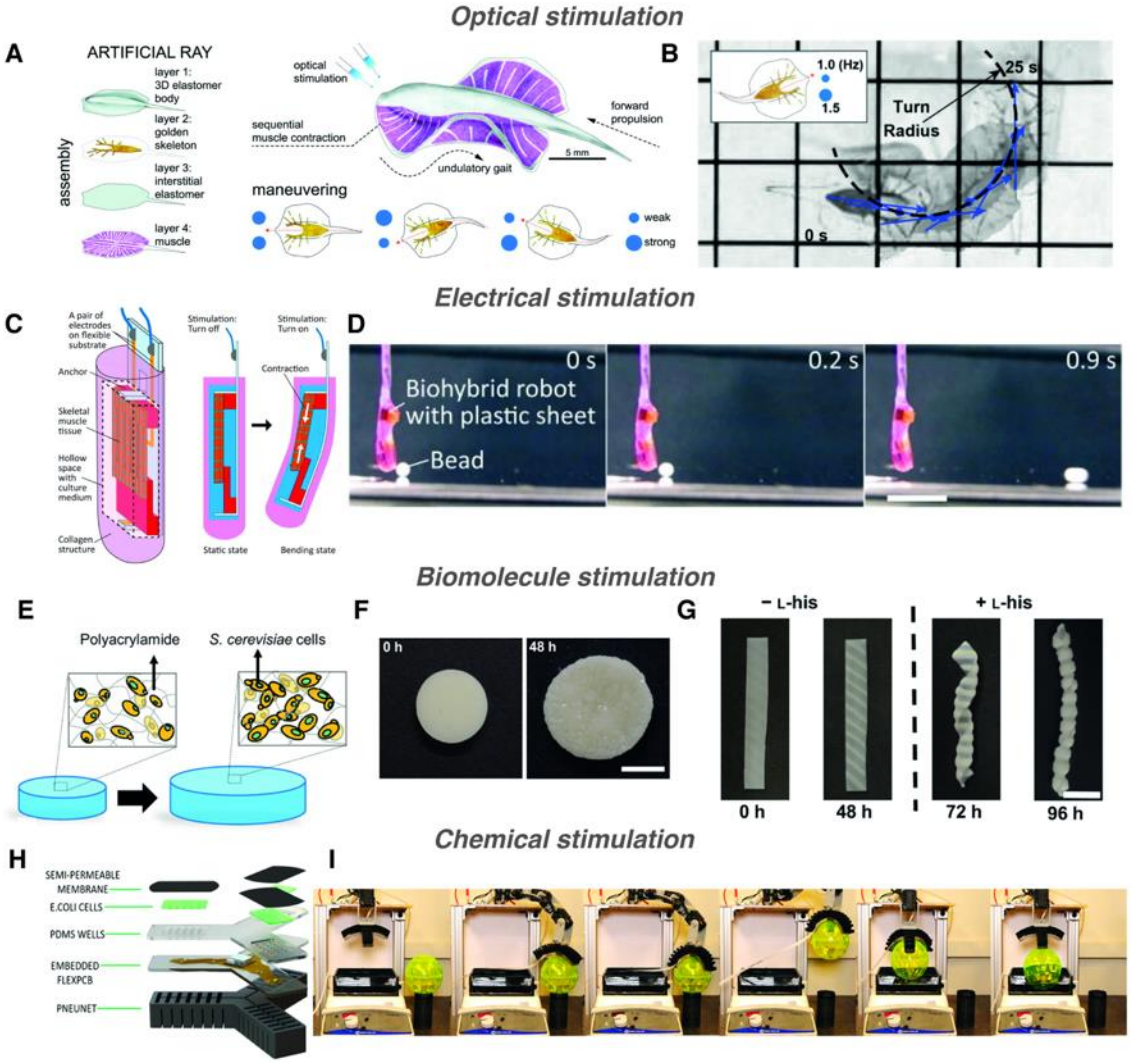

Figure 1-6: Soft biohybrid robots actuated by external stimulation. (A) Soft robotic ray composed of genetically engineered cardiomyocytes in an elastomeric body. The robot was controlled by optical stimulation to induce sequential muscle cell activation and locomotion. (B) Asynchronously triggering modulated by light frequency with 1.0/1.5 Hz paired pulses resulted in directional turns. Adapted with permission from [185]. Copyright (2016) American Association for the Advancement of Science. (C) Biohybrid robot composed of skeletal muscle tissue encapsulated in collagen structure. Upon applied electrical stimulation, the biohybrid robot actuates in air. (D) Motion control was demonstrated by pushing a bead through deformation of the collagen structure from muscle contractions (scale bar: 1 cm). Adapted with the permission from [188]. Copyright Yuya Morimoto, Hiroaki Onoe, Shoji Takeuchi, *APL Bioeng.*, 2020, 4, DOI: http://10.1063/1.5127204; licensed under a Creative Commons Attribution (CC BY) license. (E) Schematic representation of a shape-morphing living composite that changes in volume in response to yeast proliferation. (F) Living composite before and after incubation shows an increase in volume (scale bar: 7 mm). (G) UV-patterned

an antimicrobial enzyme against methicillin-resistant *S. aureus*. (F) Antimicrobial activity of ELMs placed on Mueller–Hinton agar plates streaked with methicillin-resistant *S. aureus*. Adhesin and lysostaphin functionalities by cultivating ELMs in the absence or presence of IPTG and/or arabinose. Adapted with permission from [164]. Copyright (2020) American Chemical Society.

1.4.1.3.1. Ongoing challenges and future directions

Within this section, we described using the mechanical nature of living cells that respond to an external stimulus to drive ELM mechanical deformation. The key advantages of using living cells to control or drive mechanical motion include that the device is chemically powered and can respond to weak and poorly-differentiated stimuli. However, further work is required in a number of areas regarding ELM-based soft robots. Durability is one key challenge. At one end of the spectrum, hygromorphic bacterial spores in fabrics use only the biophysical characteristics of the spores and do not involve processes at the cellular level. This limits the number of stimuli that can be used, but the ELMs should be quite durable. By contrast, in studies involving the use of mammalian muscle cells, the cellular environment, from fabrication through use, needs to be carefully controlled to ensure functionality of the device. The speed of response is another key challenge. Muscle-based or hygromorphic spore-based ELMs can respond on the order of seconds. Actuators based on cellular proliferation are slow which limits their use to applications that do not require rapid or reversible motion. We expect that living cells will continue to be used to control traditional actuators and to serve directly as actuators in applications where chemical powering of the robot is critical, such as in small, untethered, and implanted robots, and in applications where autonomous response to biochemical or weak physical cues is desired.

1.5. Objectives of the dissertation

The objectives of this dissertation are to understand the fundamental mechanisms needed to create an engineered living material platform capable of sensing highly specific and predetermined cues and responding by undergoing mechanical deformation. This dissertation elucidates the fundamental relationship between cell proliferation of microorganisms and mechanical shape changes of biomaterial matrices used to design ELMs. A series of studies, where the combination of genetic engineering, materials science, and fabrication techniques is presented to enable a new strategy for creating shape changing ELMs that could potentially be used in building biosensing or drug delivery devices for biomedical applications. The combination of these fields represents a significant advancement in the use of ELMs as active soft matter.

2. SHAPE-MORPHING LIVING COMPOSITES*

2.1. Abstract

This work establishes a means to exploit genetic networks to create living synthetic composites that change shape in response to specific biochemical or physical stimuli. Baker's yeast embedded in a hydrogel forms a responsive material where cellular proliferation leads to a controllable increase in the composite volume of up to 400%. Genetic manipulation of the yeast enables composites where volume change on exposure to L-histidine is 14× higher than volume change when exposed to D-histidine or other amino acids. By encoding an optogenetic switch into the yeast, spatiotemporally controlled shape change is induced with pulses of dim blue light (2.7 mW/cm^2). These living, shape-changing materials may enable sensors or medical devices that respond to highly specific cues found within a biological milieu.

2.2. Introduction

Materials that change shape enable mechanical activity in devices, such as smart garments, sensors, microfluidics, or drug delivery platforms.[114,202–204] In these devices, traditional actuators, like solenoids, are too large, heavy, or power intensive to be used.

Shape change in synthetic polymers and gels can be triggered using temperature, electric fields, or chemicals.[205–208] The specificity of the response is dictated, and limited, by the physical characteristics of the material.[209] One approach to induce specificity in the physical characteristics of a hydrogel is to build polymer networks from biomacromolecules, such as DNA, allowing the detection of analytes that directly bind to these constituents.[20] Binding of designed DNA sequences can induce 100-fold volumetric hydrogel expansion by successive extension of cross-links, using a DNA hybridization cascade. In the design of chemically responsive hydrogels, this mechanism is limited to detection of analytes capable of highly specific binding motifs. In living organisms, direct DNA binding is not the typical mechanism by which sensing occurs. Genetic information in cells encodes components that enable appropriate responses to a wide range of specific chemical and physical cues.

Composites that combine the tunable properties of synthetic materials and the responsive nature of living organisms represent a powerful strategy to imbue multifunctionality in a single material. Several living composites have been previously reported including self-healing concrete,[210] ethanol-producing three-dimensional (3D)–printed hydrogels,[211] gels that self-heal using photosynthesis,[212] and wearable fluorescent biosensors.[56] However, these living composites lack the ability to respond mechanically to environmental cues. One example of a mechanically active living composite is a bilayer of an elastomer and mammalian muscles that bends through contraction and relaxation of the muscle cells.[177] However, muscle cells only thrive over a very narrow set of conditions, limiting the range of applications where these materials can be used.

Notably, shape change in living organisms is not limited to contraction of muscles. Tissue morphogenesis in animals and plants is controlled, in part, by cellular proliferation.[213,214] However, a strategy that harnesses proliferation of living cells to control the shape change of synthetic materials has yet to be reported.

Here, we describe hybrid materials where living *Saccharomyces cerevisiae* (i.e., baker's yeast or brewer's yeast) embedded within a polyacrylamide hydrogel proliferates in response to a combination of environmental cues, which induces shape change in the composite (Figure 2-1A). By controlling cell loading or hydrogel stiffness, we control the magnitude of volume change in the composites. This shape change is further controlled by patterning proliferation within a monolith. Critically, yeast provide a versatile platform for genetic engineering of the conditions required for proliferation. Using this control, we design composites that respond only in the presence of a single chirality of a single amino acid or to brief pulses of dim visible light. We harness this shape change to create microfluidic channels that respond selectively to fluids flowing through the channel.

2.3. Results and discussion

S. cerevisiae is an ideal model organism to realize responsive, living composites. These unicellular organisms thrive within solid matrices,[211] are much stiffer (1 to 10 MPa)[215]than many hydrogels (10 to 100 kPa)[216], and are known to survive over a wide range of conditions.[217] Our key observation is that as these stiff cells proliferate within a solid hydrogel matrix, a global increase in volume is observed. We hypothesize that this volume increase is not due to ordinary swelling of a hydrogel, but instead is attributable

to local displacement of the hydrogel by proliferating cells. After the composite is exposed to the appropriate conditions for cell growth, a marked increase in cell count can be observed (Figure 2-1B). To quantify the effect of proliferation on macroscopic volume change, living composites were polymerized with pre-gel solution [0.9 billion to 1.1 billion cells/ml; 6 weight % (wt %) of dry yeast]. Composites were incubated in YPD (yeast extract, peptone, D-glucose) medium at 30°C for 48 hours. YPD contains the necessary nutrients for the yeast, and hence, cell proliferation–induced shape change occurs, resulting in a change in area of 124.2 ± 10.3% and a volume change of 200.9 ± 2.4% (Figure 2-1C). By incubating composites in medium without a fermentable carbon source (D-glucose), the area of the disk only increased by 6.3 ± 0.4%, as the yeast are incapable of proliferation (Figure 2-1D and Figure A-1). Similarly, hydrogels without encapsulated yeast incubated in YPD only undergo a volume change of 1.2 ± 0.5% (Figure A-2). The shape change of the living composites in rich medium is also not attributable to passive cell size changes; cell viability is required for shape change to occur. We pattern cell viability, using ultraviolet (UV) light (254 nm) exposed through a mask, in living composites covalently bound to glass (Figure 2-1E). Only the regions of the hydrogel not exposed to UV, the letters "ALIVE," contain viable cells and undergo a volume increase on exposure to YPD. This expansion is greater than 110% of the initial film thickness after 36 hours (Figure 2-1F and Figure A-3). Shape change is accompanied by a change in topography, from smooth to rough, as the growing colonies deform the surface in a heterogeneous manner at the submillimeter scale. The described

experiments show that yeast proliferation is the primary mechanism associated with volume change in these hybrid living materials.

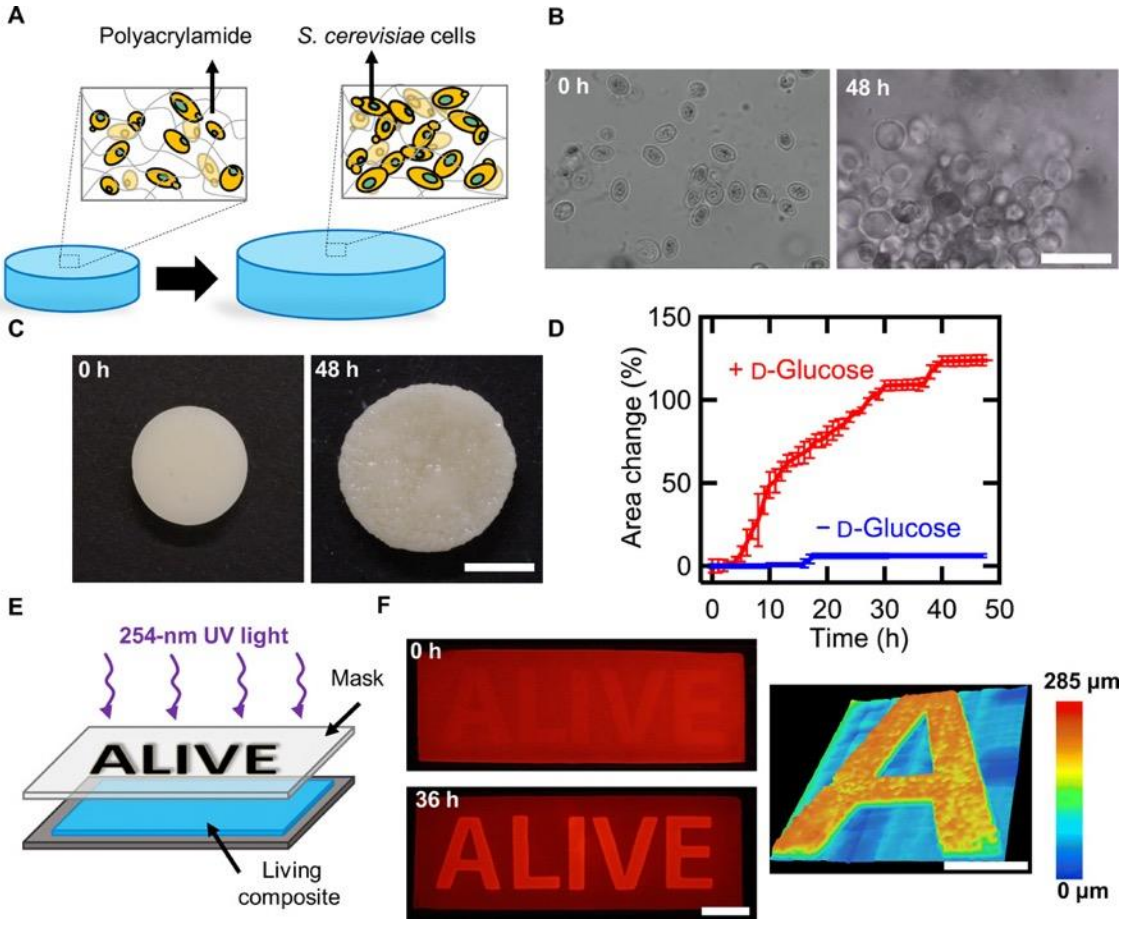

Figure 2-1: Controlled expansion of polyacrylamide gels by proliferation of yeast. (A) Schematic of shape change in living composites. In YPD, yeast proliferate and cause expansion in the polymer matrix. (B) Optical micrographs of a living composite before and after growth in medium. Scale bar, 30 µm. (C) Macroscopic expansion of a living composite gel with 6 wt % yeast. Scale bar, 7 mm. (D) Area change over time of a sample with 6 wt % yeast in the presence of medium with and without glucose. (E) Photopatterning process of a living composite. (F) Fluorescence images of a living composite after UV patterning (top) and after incubation in YPD (bottom). Scale bar, 10 mm. Topography of an initially flat living composite after exposure to YPD (right). Scale bar, 5 mm. Each data point represents the mean (n = 3), and error bars represent SD. Trend lines are only intended to guide the eye. Reprinted with permission from [197]. Copyright (2020) exclusive licensee American Association for the Advancement of Science. Distributed under a Creative Commons Attribution License 4.0 (CC BY).

Proliferation-driven shape change can be tuned by controlling the initial composition of the living composite (Figures 2-2A, B). On varying the initial concentration of yeast from 1 to 18 wt %, the volume change after 48 hours increases from 123.8 ± 3.9% to 337.2 ± 17.4%. This volume change is accompanied by a concomitant increase in dry mass, which varies from 177 ± 11% to 320 ± 35% (Figure 2-2A). While we observe that some cells escape from the composite and proliferate in the medium, this increase in dry mass suggests that most of the cells are retained in the hydrogel matrix. We also note that the shape of the grown composites is largely stable for over 128 days in deionized water at room temperature (Figure A-4). The increase in dry mass and shape stability further supports our hypothesis that CO_2 production or passive swelling from the hydrogel matrix is not the mechanism responsible for shape change. This mass change represents material that can be produced on demand with only as much external intervention or equipment as is needed to ferment grape juice. In the case of materials with 18 wt % yeast, the solid components of the as-synthesized composites are 35.9% polymer and 64.1% yeast. After growth, the yeast content increases to 85.6%. These growing composites may provide opportunities to produce materials directly from renewable feedstocks or even waste streams.[218]

The mechanical properties of the hydrogel matrix also control the proliferation-induced shape change. By altering the feed ratio of cross-linker from 0.05 to 0.6% (w/v), at constant yeast loading (6 wt % dry yeast) and acrylamide concentration [10% (w/v)], the Young's modulus of the composites after synthesis increases from 8 ± 1 kPa to 204 ±

16 kPa. As stiffness increases, the volume change during cell proliferation decreases from 255.8 ± 7.3% to 107.9 ± 1.2% (Figure 2-2B and Figure A-5). We attribute this decrease to increased elastic resistance to the expanding colonies, perhaps resulting in limited cell proliferation. Given the tradeoffs between composite stiffness, yeast loading, and volume change, we selected composites with 0.1% (w/v) cross-linker and 6 wt % yeast for further studies, as these composites have relatively high initial elastic modulus and large stimulus response (Figure A-6).

Spatial control of volume change can be programmed to yield composites that morph controllably from 2D to 3D. Informed by previous work where spatially controlled swelling is used to guide shape selection in hydrogels,[219–223] we fabricated composite disks (12 mm in diameter and 0.5 mm in thickness) and used UV light (254 nm) to kill cells in programmed areas (insets of Figures 2-2C, D). After irradiation, no shape change is observed when the hydrogel is equilibrated in water, indicating that the passive swelling of the gel is not substantially altered. After incubation in YPD, spatially controlled proliferation induces a 2D to 3D transformation. The flat disk shown in Figure 2-2C grows in area in the center of the disk while being constrained around the perimeter, resulting in a hemispherical cap (+ Gaussian curvature). By contrast, the disk depicted in Figure 2-2D grows along the perimeter while being constrained in the center, resulting in a saddle-like geometry (− Gaussian curvature).

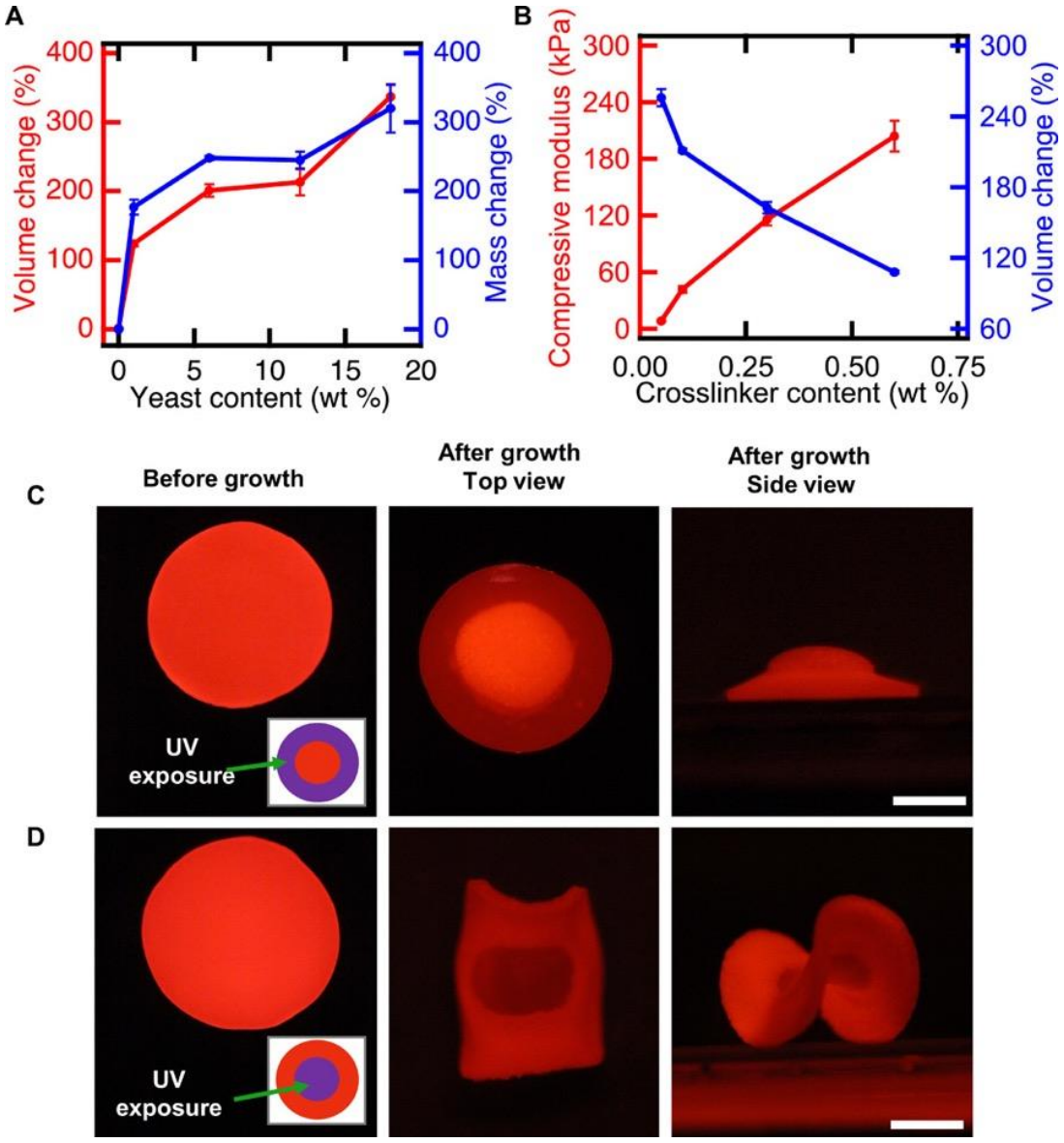

Figure 2-2: Shape change of living composites can be controlled. (A) Volume and mass change of living composites as a function of yeast content. (B) Compressive modulus and volume change as a function of cross-linker content. (C) Flat disk exposed to spatially patterned UV light (left) in a 3-mm-wide ring pattern (inset). After incubation in medium, a hat-like structure with positive Gaussian curvature is observed (center, right). Scale bar, 5 mm. (D) Flat disk exposed to spatially patterned UV light (left) in a 6-mm inner circle (inset). Upon incubation in medium, a saddle-like structure with negative Gaussian curvature is observed (center, right). Scale bar, 5 mm. Each data point represents the mean (n = 3), and error bars represent SD. Trend lines are only intended to guide the eye. Reprinted with permission from [197]. Copyright (2020) exclusive licensee American Association for the Advancement of Science. Distributed under a Creative Commons Attribution License 4.0 (CC BY).

Programming of the stimulus that induces shape change of living composites can be achieved by genetic manipulation of the yeast. *S. cerevisiae* is a model eukaryote commonly used for heterologous protein expression.[224–226] The yeast strain we use (L40) is deficient in L-histidine metabolism. This metabolic feature, termed auxotrophy, prevents proliferation in the absence of L-histidine in the growth environment (Figure 2-3A). This strain was used to fabricate composites that morph into 3D helical shapes only in the presence of L-histidine. Rectangular free-standing films were patterned with UV light to cause cell death in the areas indicated in Figure 2-3B. Incubation for 48 hours in selective medium lacking L-histidine did not affect the shape of the composite. When these composites were incubated in medium containing L-histidine, the flat films morph into a helix (Figure 2-3C). Over 48 hours in medium lacking L-histidine, disks of these composites only increase in volume by 20.7 ± 6.1%, despite the other 20 amino acids, D-glucose, and nitrogen base present in the medium. The same composites were then incubated for another 48 hours in otherwise identical medium containing L-histidine, resulting in a volume change of 278.3 ± 12.9% (Figure 2-3D and Figure A-7). Critically, these composites remain dormant during periods of unfavorable conditions and then respond when conditions match those programmed by the genetics of the yeast. The ability to withstand unfavorable conditions stands in stark contrast to the fragile nature of cells from multicellular organisms. To further demonstrate the biochemical specificity of these composites, volume change of living composites was measured for samples incubated in medium containing L-histidine and compared to the volume change of samples grown in medium with D-histidine and without any histidine. Much like the

composites exposed to medium lacking L-histidine, the inclusion of D-histidine into the medium did not lead to substantial volume change at the end of an incubation period of 72 hours, as D-histidine is not naturally incorporated into proteins (Figure 2-3E and Figure A-7). Previously, hydrogels that swell by recognition of a single enantiomer of a chiral molecule have been achieved through molecular imprinting; however, the volume change in these materials is often less than 20%.[227] Notably, the reported living composite exhibits a volumetric change up to 20× larger than the volume change observed in imprinted hydrogels.

Microfluidic devices fabricated with living composites respond with specificity to the fluid flowing through the channels. We fabricated responsive microfluidics by using replica molding to form channels within a living composite. All cells were rendered inviable with UV light except for the cells within two of the microfluidic channels (Figure 2-3F). Flow of a fluorescent fluid is then used to visualize the performance of these devices. Before flowing medium containing L-histidine, the channels are all open, and the intensity of the fluorescence is similar across the device (Figure 2-3G). After flowing medium with L-histidine through the inlet, the two microchannels with viable cells grow in volume, resulting in the channels becoming blocked, while the other channels remained open. By contrast, similar devices exposed to otherwise identical medium lacking L-histidine have all channels open (Figure A-8). These smart microfluidic devices could enable strategies for biosensors that directly manipulate the flow of fluid without external intervention, traditional sensors, or actuators. While materials that respond to biochemical cues are ideal for devices that

change autonomously with their environment, diffusion limits the ability of these cues to generate on-demand shape change with control in space and time.

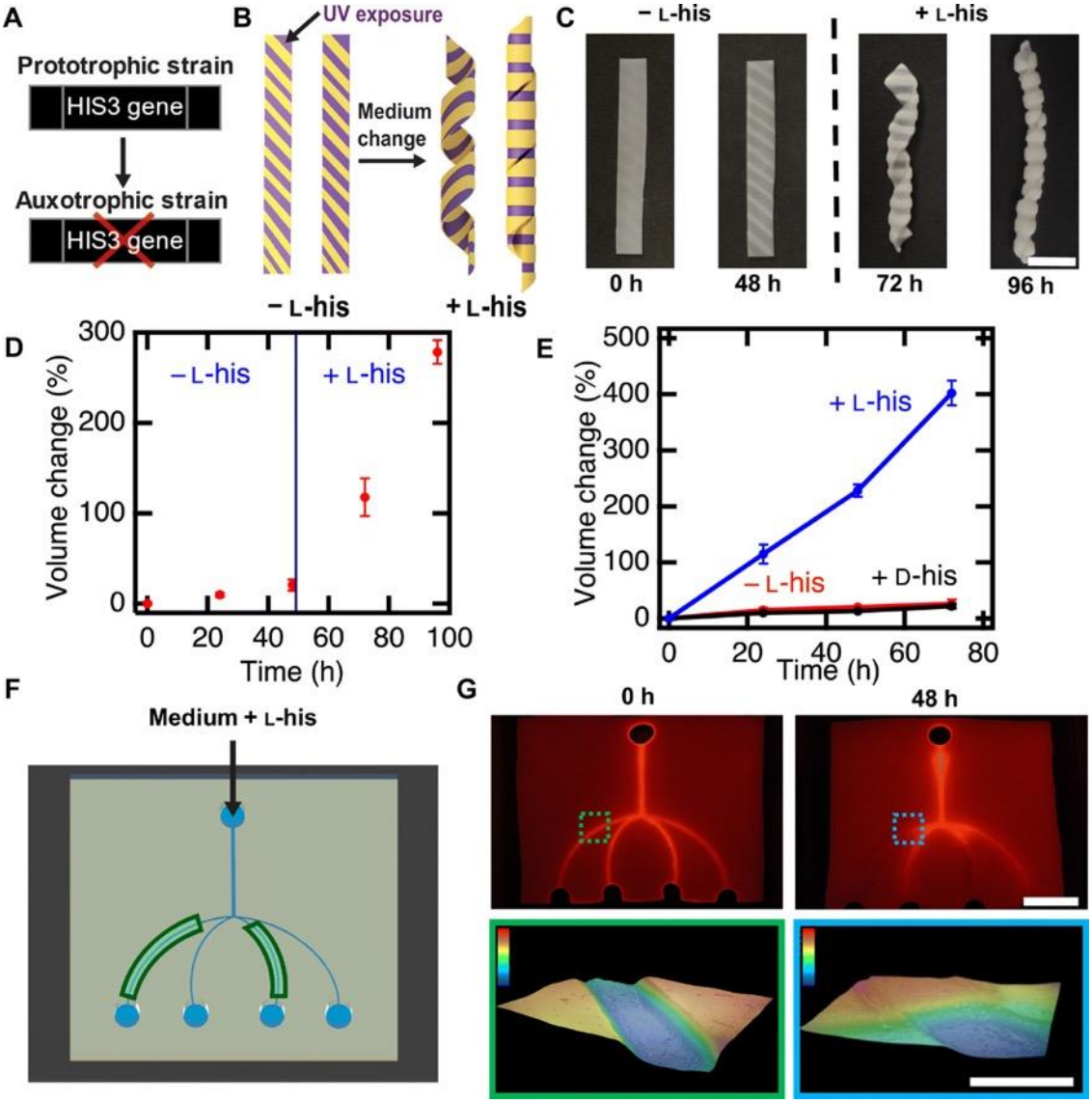

Figure 2-3: Genetic engineering enables controlled composite response to specific cues. (A)Deletion of the *HIS3* gene results in failure to proliferate in medium lacking histidine. (B) Schematic of a UV-patterned living composite with growth triggered by the amino acid L-histidine. (C) UV-patterned living composites with auxotrophic yeast do not substantially change in shape in medium lacking L-histidine. Shape change into a helical structure after incubation in medium containing L-histidine. Scale bar, 10 mm. (D) Volume change over time for auxotrophic living composites before and after L-histidine exposure.

(E) Volume change over time for auxotrophic living composites incubated in medium lacking histidine, with D-histidine, or with L-histidine. (F) Schematic of a living microfluidic device where the composites forming the channels indicated in green contain living auxotrophic yeast. (G) Fluorescence image of fluid traversing the microfluidic device before exposure to medium (top left). Scale bar, 10 mm. Fluorescence image of fluid traversing the microfluidic device after medium containing L-histidine flows for 48 hours through the channels. Topography of a living channel before and after (color scale, 0 to 0.3 mm) growth (bottom). Scale bar, 1 mm. Each data point represents the mean (n = 3), and error bars represent SD. Trend lines are only intended to guide the eye. Reprinted with permission from [197]. Copyright (2020) exclusive licensee American Association for the Advancement of Science. Distributed under a Creative Commons Attribution License 4.0 (CC BY).

Optogenetic switches can be engineered into yeast to enable photoresponsive composites, where shape change can be spatiotemporally controlled. We generated a yeast strain to express a photoresponsive transcriptional switch that induces gene expression after illumination with blue light (455 nm). This strain has two *Arabidopsis thaliana* proteins in a yeast two-hybrid system.[228] Blue light stimulation induces binding of CRY2 fused to the LexA DNA binding domain and CIB1 Gal4 activation domain chimera. In the presence of light, the *HIS3* gene is activated, enabling cellular proliferation in the absence of L-histidine (Figure 2-4A). We also generated two additional strains: a positive control that does not require light for activation of *HIS3*[229] and a negative control that lacks the CIB1 protein and is auxotrophic for L-histidine with or without blue light. The metabolic activity of the experimental strain is more than 100× higher when exposed to light than when kept in the dark, as measured by a β-galactosidase assay, which probes *lacZ*, a reporter gene, activity (Figure 2-4B and Figure A-9). In the negative control strain, the metabolic activity is low in blue light and in the dark, while the positive control presented high metabolic activity in both conditions.

Optogenetic control of histidine auxotrophy enables photocontrolled cellular proliferation and therefore shape change in living composites. We fabricated composites from each of the three different strains described above and exposed each composite to brief, dim pulses of blue light (2.7 mW/cm^2, 2 s on, 2 min off) or darkness (Figure 2-4C). Over 72 hours, living composites made with the experimental strain undergo a volume change of 315.9 ± 2.1% when exposed to light and a volume change of 86.2 ± 5.7% when kept in the dark (Figures 2-4D, E). By comparison, the positive control composites undergo a volume change of more than 260% in both light and dark, and negative control composites grow only 103.1 ± 20.1% in the light and 10.2 ± 5.3% in the dark (Figure 2-4E and Figure A-9). We note that traditional photoresponsive polymers, which use light to power shape change, typically require irradiation intensities of more than 100 mW/cm^2.[198,230] By comparison, these living composites rely on light to trigger an optogenetic switch that has been optimized by evolution. The activation of this switch subsequently enables a metabolically powered change in volume. As a result of this pathway, the time-averaged intensity required is at least 2250× smaller than traditional photoresponsive polymers.

The combination of patterned cell viability and patterned light illumination can be used to provide spatiotemporal control of complex shape change in living composites composed of transformed yeast with the optogenetic switch. The cell viability within a film of the living composite was patterned using UV light to leave only two circular regions on the film with viable cells (Figure A-10). As shown in Figure 2-2C, proliferation should lead to the formation of a hemispherical cap. By exposing these two

regions sequentially. Each region sequentially actuates from flat to hemispherical (Figure 2-4F).

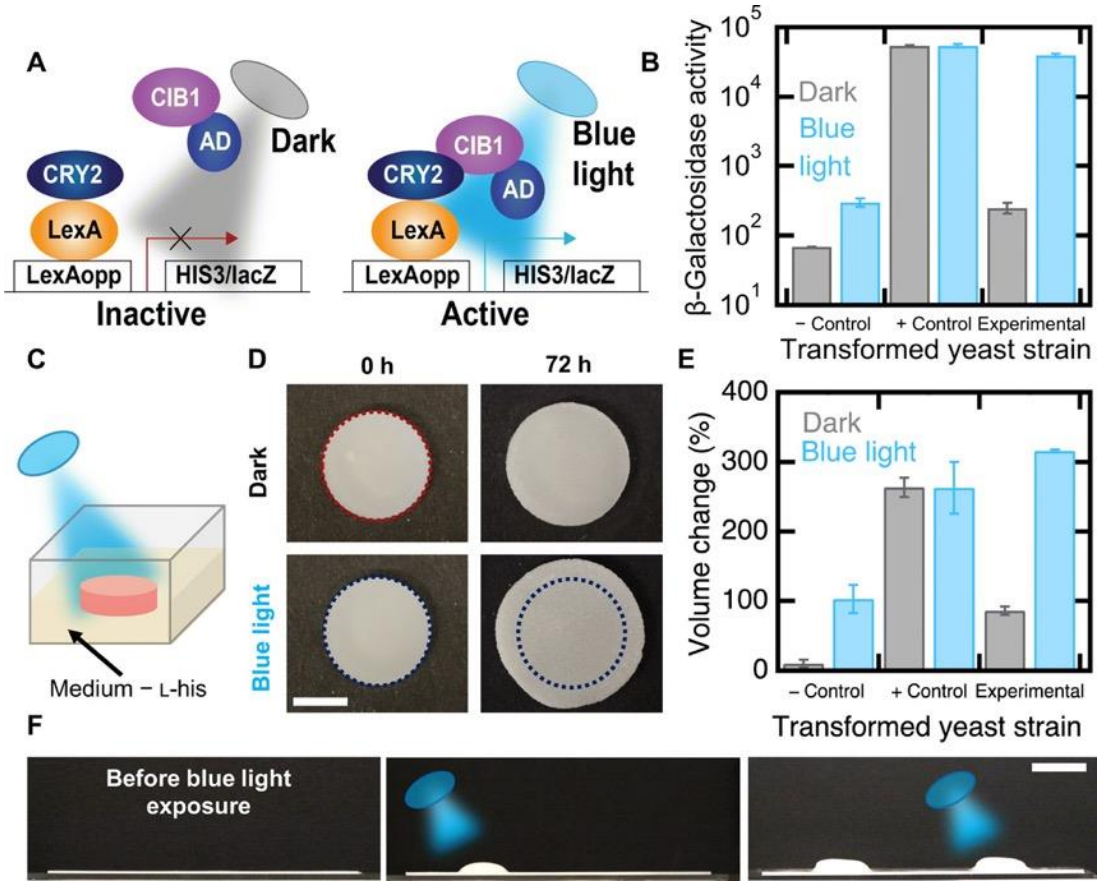

Figure 2-4: Genetic engineering enables optogenetic control of shape change. (A) Schematic of a light sensitive yeast two-hybrid. Blue light induces expression of *HIS3* and *lacZ* reporters by inducing conformational changes in CRY2 to favor interaction with CIB1. Reporter genes are transcribed by recruitment of the Gal4 activation domain (AD). (B) β-Galactosidase assays of an auxotrophic strain lacking CIB1 (negative control), a strain not auxotrophic for L-histidine in the dark (positive control), and the auxotrophic strain depicted in (A) (experimental). (C) Schematic of a living composite irradiated with blue light in growth medium lacking L-histidine. (D) Volume change of living composites with experimental yeast irradiated with blue light or kept in the dark. Scale bar, 5 mm. (E) Volume change of living composites with each yeast strain when exposed to blue light or kept in the dark. (F) Patterned photoresponsive living composite with the experimental yeast strain in medium lacking L-histidine where blue light is first targeted on the left side and then the right side. Scale bar, 10 mm. Each data point represents the mean (n = 3), and error bars represent SD. Reprinted with permission from [197]. Copyright (2020) exclusive licensee American Association for

Living composites undergo cell proliferation–induced shape change controlled by the initial composition of the composite or by patterning regions of viable cells. These materials capitalize genetic control of biological mechanisms, namely, cellular proliferation, to enable responsiveness in topography or shape in response to specific cues. A host of devices from drug delivery platforms to environmental sensors could be enabled by these findings.

2.4. Materials and methods

2.4.1. Materials

Acrylamide, *N*,*N*′-methylenebisacrylamide (MBAA), ammonium persulfate (APS), *N*,*N*,*N*′,*N*′-tetramethylethylenediamine (TEMED), 3-amino-1,2,4-triazole (3-AT), L-histidine, adenine sulfate, sulforhodamine B, bisphenol A ethoxylate diacrylate (BPA) (512 g/mol), and poly(ethylene glycol) diacrylate (PEG-DA) (700 g/mol) were purchased from Sigma-Aldrich. The photoinitiator Irgacure 369 (I-369) was donated by BASF Corporation. Methacryloxyethyl thiocarbonyl rhodamine B (PolyFluor 570) was purchased from Polysciences. Commercial yeast (*S. cerevisiae*, active dry yeast, Fleischmann's) was purchased from Tom Thumb (Richardson, TX). Yeast extract, yeast nitrogen base without amino acids, peptone, D-(+)-glucose, D-histidine, and trypan blue were purchased from Fisher Scientific. TPM [3-(trimethoxysilyl) propyl methacrylate] was purchased from Acros Organics. Rain-X was purchased from Wal-Mart (Richardson, TX). All chemicals were used as received without further purification.

2.4.2. Genetically engineered yeast strains and plasmids

The genotype of the L40 yeast strain is *MATa ade2 his3 leu2 trp1 LYS::lexA-HIS3 URA3::lexA-LacZ* (American Type Culture Collection, MYA-3332).[231] L40 yeast were transformed with experimental constructs CRY2 LexA DNA binding fusion in the expression vector pDBTrp (pDBTrp-LexABD-CRY2FL) (plasmid no. 78210, Addgene) and a separate CIB1 Gal4 activation domain fusion vector pGADT7 (pGal4AD-CIB1) (plasmid no. 28245, Addgene). pDBTrp-LexABD-CRY2FL, along with the pGADT7 empty vector, was used as negative control. In the positive control, we made use of a previously described interaction between *Caenorhabditis elegans* FBF2 (residues 121 to C terminus fused to the Gal4 activation domain present in pGADT7) and CPB1 (residues 1 to 80 fused to the LexA DNA binding domain encoded by pBTM116).[229,232]

2.4.3. Mold construction

For volume change and mechanical testing experiments, molds were made of two glass slides (75 mm by 51 mm) previously cleaned with Rain-X to avoid gel adhesion. Slides were separated with 1-mm or 500-μm rectangular spacers, wrapped with parafilm closing one of the open sides, and fixed using binder clips.

For living composite coatings, molds (75 mm by 25 mm) with one glass slide cleaned with Rain-X and one treated with a methacrylate-functionalized silane were assembled. The two glass slides were separated with two 250-μm polystyrene spacers on each side and fixed with binder clips. For the silane treatment, glass slides were cleaned following a similar process described in the literature (*37*).[233] Briefly, glass slides were

sonicated for 5 min in acetone and isopropanol mixtures and rinsed three times in dH_2O. Afterward, substrates were sonicated for 30 min in a mixture of water and Alconox cleaner (Alconox Inc., USA), rinsed, and stored in dH_2O overnight. For silanization, glass slides were modified for 30 min with a 5% (v/v) mixture of TPM in toluene at 65°C. Then, the slides were rinsed with toluene, dried with N_2 gas, and baked on a hot plate at 120°C for 5 min.

2.4.4. Determination of cell density

To determine cell concentrations in active dried yeast, cell density was measured with a UV/visible spectrophotometer by observing the optical density at 660 nm. Briefly, 50 ml of mixture with 0.6 g of yeast in dH_2O was prepared. Then, a 1:10 dilution was made by mixing 0.1 ml of the mixture with 0.9 ml of dH_2O. Diluted samples were pipetted into a 1-ml cuvette for spectrophotometer measurements. Optical densities between 1 and 1.1 were measured, which correspond to numbers of cells of 1.89×10^7 and 2.25×10^7 cells, respectively. These results indicate that the active dried yeast contained between 15 billion and 18 billion cells/g.

2.4.5. Preparation of living composite materials with active dried yeast

Polyacrylamide hydrogels with embedded yeast were prepared at room temperature by free radical polymerization of acrylamide monomer and MBAA cross-linker. Stock solutions of acrylamide (0.4 g/ml) and MBAA (0.02 g/ml) were prepared in dH_2O to create polyacrylamide gel precursor solutions. All pre-gel solutions were prepared with a final concentration of 10% (w/v) acrylamide. Pre-gel solutions were prepared with a final concentration of 0.1% (w/v) MBAA and pre-gel solution (~1

billion cells/ml), unless otherwise noted. To polymerize these solutions, a 10% (w/v) APS stock solution was added at 1% of the total solution volume, and TEMED was added at a ratio of 0.1% of total solution volume. Polymerizing solutions were then vortexed for 3 s and quickly pipetted into molds. Filled molds were flipped every 45 s, while polymerization occurred to avoid yeast settling. After 10 min, polymerized living composites were demolded and rinsed three times with dH_2O to remove unpolymerized acrylamide residues. Living composites were stored in dH_2O for 24 hours before mechanical testing and volume change experiments. For mechanical testing and volume change experiments, pre-gel solutions were prepared with 0.05, 0.1, 0.3, and 0.6% (w/v) MBAA and 6% (w/v) yeast [pre-gel solution (~1 billion cells/ml)]. To test volume change and Young's modulus with varying yeast content, composites with final concentrations of 0, 1, 6, 12, and 18 wt % yeast were prepared.

2.4.6. Area, volume, and mass change quantification of living composites embedding active dried yeast

Living composites embedded with commercial active dried yeast were cut into 10-mm-diameter disks. The dimensions of each disk were measured before incubation. Samples with varying dry yeast and cross-linker concentration were incubated at 30°C in YPD-rich medium without agitation (1% yeast extract, 2% peptone, and 2% D-glucose). To measure area and volume changes, three samples for each composition were incubated in 7 ml of rich medium that was changed every 6 hours. Area change was measured every hour for 48 hours using a Mighty Scope 5M digital microscope, and

volume changes were measured every 24 hours for 48 hours using a Canon Rebel T5i camera.

Dry mass change was obtained by weighing samples with varying yeast content before and after cell proliferation. Briefly, one set of living composites that was not exposed to medium was dried at 30°C under vacuum to allow water evaporation. An identical set of living composites was incubated in YPD medium for 48 hours with medium change every 6 hours and then dried under the same conditions. Upon drying, samples were weighed and mass was measured. Data presented are an average of three samples per composition.

2.4.7. Material characterization

Samples (3 mm by 3 mm by 1 mm) were cut from polymerized living composites with varying yeast and cross-linker content after equilibration in dH_2O. Compression testing was performed using a MicroSquisher (CellScale Biomaterials Testing). Briefly, a tungsten beam with a diameter of 1.016 mm was glued to a 6 mm–by–6 mm platen on one end. This compliant beam was attached to an actuator with a cantilever beam grip at the opposite end from the platen. Samples were loaded to the test chamber filled with dH_2O at room temperature. The beam was brought into contact with the sample and then moved at a rate of 0.5 mm/min. Force as a function of displacement was measured along the height (1-mm dimension) of the samples and calculated by the MicroSquisher software using the beam's stiffness, displacement, and length. Strains from 1 to 10% were used to calculate Young's modulus, as the stress-strain response in this region was linear.

2.4.8. Optical images of living composites

Microscopic imaging was carried out using an Olympus FV3000RS confocal laser scanning microscope. To visualize embedded yeast cell budding, living composites with 10% (w/v) acrylamide and 0.1% (w/v) MBAA were synthesized, mixing approximately 1×10^6 cells/ml of the pre-gel solution. Before polymerization, a 0.05% (w/v) aqueous solution of PolyFluor 570 was added at 1% of the total pre-gel solution volume. Cells, after incubation for 48 hours in YPD medium, were further stained by submerging samples in a 0.05% (w/v) aqueous solution of trypan blue for 3 min and then washed two times in dH_2O. Budding of embedded cells and colonies were observed throughout the thickness and area of the imaged samples ($n = 3$).

2.4.9. Macroscopic fluorescence images

For fluorescence imaging, living composites were dyed with a 0.05% (w/v) solution of sulforhodamine B in water. By shining light at a wavelength of 455 nm, fluorescent images of the UV-patterned coatings and free-standing structures were obtained using a DSLR camera (Canon Rebel T5i) fitted with a red filter (Hoya HMC R25A). This filter blocks light below 600 nm, thus allowing visualization of the emitted light.

2.4.10. UV photopatterning of composites with active dried yeast

Living composites covalently bound to methacrylate-functionalized glass molds with a thickness of 500 μm were prepared as described above. Composites were allowed

to equilibrate in water before UV exposure. A shadow mask of the word ALIVE was designed in AutoCAD and laser cut from black polymer sheets. Irradiation with 254-nm UV light with an intensity of 2 mW/cm^2 was performed from one side for 35 min using an UVP UVLink 1000 cross-linker chamber. Samples were placed on a dark background during irradiation.

For UV patterning of free-standing composites, 12-mm-diameter disks were cut from 500-μm-thick films and patterned to induce cell death in a 6-mm-diameter inner circle or a 3-mm-wide ring pattern using aluminum foil as a mask. Irradiation with 254-nm UV light with an intensity of 2 mW/cm^2 was performed from one side for 35 min using the UV chamber.

For cylindrical helix patterning, living composite samples were synthesized with the same composition of monomers as described above and a pre-gel solution (0.9 billion to 1.1 billion cells/ml). Samples were cut into rectangular shapes (length, 40 mm; height, 5 mm; and thickness, 0.5 mm) and patterned to induce cell death in 2.3-mm-wide rectangles separated by 1.1 mm and positioned at 56° angle along the length of the samples (Figure 2-3A). Irradiation was performed with the same wavelength, intensity, and time as described above.

After irradiation, living composites bound to glass were incubated for 36 hours at 30°C with a medium change every 12 hours. Free-standing disks were incubated for 48 hours at 30°C with medium change every 12 hours. These samples were then imaged using a fluorescent dye as described above. Cylindrical helix films were incubated for 48

hours at room temperature with medium change every 6 hours and then imaged using a Mighty Scope 5M digital microscope every 5 min.

2.4.11. Topography measurements of UV photopatterned living composite coatings

Topography (Figure 2-1F) of living composite coatings was imaged using a digital microscope (Keyence VHX-1000). To characterize the change in film thickness after cell proliferation, measurements along the depth profile of the letter "A" were taken. The camera limit points were set by focusing on the highest point of the grown letter and on the coated UV-killed surface. Between these limits, images were taken at ×100 magnification along the surface of the letter. Images were then stitched using the KEYENCE software.

2.4.12. Quantifying shape change in living composites with auxotrophic yeast strain

Before composite synthesis, the auxotrophic yeast strain (CRY with empty vector, denoted as negative control strain) was grown overnight in selective medium [0.7% yeast nitrogen base without amino acids, 2% D-glucose, and appropriate amino acid supplements[234] lacking tryptophan, leucine, and histidine] containing L-histidine. Subsequently, overgrowths were made in 50 ml of YPAD (1% yeast extract, 2% peptone, 0.004% adenine sulfate, and 2% D-glucose) medium at 30°C for 15 hours. Growth was followed by measuring optical density at 660 nm until desired yeast concentration was reached (OD_{660} = 1 to 1.1). Cells were then centrifuged in 50-ml conical tubes and washed twice in distilled water before encapsulation. Composites with encapsulated auxotrophic yeast were synthesized by using 10% (w/v) acrylamide and

0.1% (w/v) MBAA with pre-gel solution (0.9 billion to 1.1 billion cells/ml), as described above. For volume change experiments, living composites were first equilibrated in water for 24 hours and then cut into 10-mm-diameter disks with a thickness of 500 μm. Disks were incubated in selective medium lacking L-histidine with 10 mM 3-AT (*HIS3* gene competitive inhibitor) for 48 hours at 30°C, with a medium change every 12 hours. After this time, composites were incubated in selective medium containing L-histidine and 10 mM 3-AT for another 48 hours, with a medium change every 12 hours. Disks were measured after growth for quantification of volume change.

Identical disks were also exposed to selective medium containing L-histidine, selective medium containing D-histidine, a stereoisomer of the natural amino acid L-histidine, and selective medium without L-histidine. These composites were incubated for 72 hours at 30°C, with a medium change every 12 hours. Data presented are an average of three samples per experiment.

2.4.13. Controlled blockage of microfluidic device

For shape change experiments using a microfluidic device, composites were cast into microfluidic polymer micromolds. These molds were built with 75 mm–by–51 mm glass slides. One of the two slides was functionalized with methacrylate groups by the processes described above. The other slide was coated in Rain-X. Slides were separated with one 250-μm polystyrene spacer on each side, and BPA mixture with 1 wt % I-369 photoinitiator was pipetted into the mold. Using a Vivitek D912HD (B9Creator) projector with the UV filter removed and the optics modified to decrease the focal length, a positive mold of a microfluidic device with a 600-μm-wide inlet channel and

four 400-μm-wide outlet channels was polymerized onto the methacrylate-functionalized glass slide. To remove all unpolymerized BPA, slides were cleaned by multiple washes between acetone and isopropanol. This micromold was then used to create a cell for the polymerization of the living composite. After polymerization, microfluidic devices were allowed to equilibrate in dH_2O for 24 hours. Using UV patterning (254-nm wavelength, 35 min, 2 mW/cm^2 intensity), most of the composite was rendered inviable. Two of the four outlet channels, as indicated in Figure 2-3F, were kept alive by preventing UV exposure on the channel areas with a shadow mask. Selective medium containing L-histidine was then flowed at a rate of 34 μl/min through one set of microfluidic devices (n = 3), and selective medium without L-histidine was flowed through another set of devices (n = 3) at the same rate. Before and after medium flow, channels were injected with a PEG-DA solution mixed with sulforhodamine B aqueous solution at 1% of the total PEG-DA volume. Flowing this solution allowed visualization of the flow through the microchannels before and after growth. Topographical quantification of these samples was performed following the same process described for living composite coatings.

2.4.14. Yeast two-hybrid assays

L40 cells were cotransformed with the appropriate plasmids as described above and in the literature.[235] Cells were plated on selective medium agar plates with 10 mM 3-AT. Two replicate plates were grown in the dark, and two were irradiated with blue light at 455 nm for 2 s every 2 min. Plates were incubated at 30°C for 3 days.

Transformants were grown to saturation in selective medium lacking L-histidine overnight at 30°C. Afterward, aliquots (100 µl) of the saturated cultures were outgrown in 1 ml of fresh minimal medium and incubated at 30°C for 4 hours. Optical density at 660 nm was recorded using a Spark 20 M multimode reader. β-Galactosidase expression was quantified using the Beta-Glo Assay System (Promega). Briefly, 50 µl of cell cultures was added to an equal volume of reagent and allowed to incubate for 45 min before quantification. The luminescence values were normalized to cell densities for each culture.

2.4.15. Optogenetic control of shape change

Control of proliferation by exposure to blue light was achieved by encapsulating experimental yeast strains that express photosensory proteins. Pre-gel solutions with a composition of 10% (w/v) acrylamide and 0.1% (w/v) cross-linker were mixed with 0.9 billion to 1.1 billion transformed cells per milliliter of solution. Positive and negative control strains were encapsulated using the same pre-gel composition and cell concentration. For volume change experiments, composites with each of the three strains were cut into 10-mm-diameter disks with a thickness of 500 µm. Samples were incubated in selective medium lacking L-histidine with 10 mM 3-AT for 72 hours with medium change every 12 hours. Then, samples were irradiated with blue light (455 nm) (Figure 2-4C) or kept in the dark. The intensity of irradiation was measured with a solar power meter (Amprobe SOLAR-100) and set at 2.7 mW/cm^2. For blue light experiments, samples were irradiated for 2 s every 2 min. Volume changes were

measured every 24 hours for all samples before and after incubation. Data presented are an average of three samples per experiment.

For spatiotemporal control of proliferation, free-standing films with encapsulated experimental yeast strain were UV-patterned as shown in fig. S10. Films were kept in dH_2O for 24 hours in the dark before blue light exposure. Films were then incubated in selective medium with 10 mM 3-AT at 30°C in the dark for 72 hours. For the first 48 hours, only the left half of the film was exposed to blue light to induce proliferation of cells. After this time, the right half was irradiated for 24 hours. Images are representative from three trials.

3. 4D PRINTING OF ENGINEERED LIVING MATERIALS*

3.1. Abstract

Herein, a method that uses direct-ink-write printing to fabricate engineering living materials (ELMs) that respond by undergoing a programmed shape change in response to specific molecules is reported. Stimuli-responsiveness is imparted to ELMs by integrating genetically engineered yeast that only proliferate in the presence of specific biomolecules. This proliferation, in turn, leads to a shape change in the ELM in response to that biomolecule. These ELMs are fabricated by co-printing bioinks that contain multiple yeast strains. Locally, cellular proliferation leads to controllable shape change of the material resulting in up to a 370% increase in volume. Globally, the printed 3D structures contain regions of material that increase in volume and regions that do not under a given set of conditions, leading to programmable changes in form in response to target amino acids and nucleotides. Finally, this printing method is applied to design a reservoir-based drug delivery system for the on-demand delivery of a model drug in response to a specific biomolecule.

3.2. Introduction

Stimuli-responsive materials respond to changes in the external environment by self-healing, changing mechanical properties, or morphing from one form to another.[236–

* Reprinted with permission from "4D Printing of Engineered Living Materials" by L.K Rivera-Tarazona, T. Shukla, KA Singh, A.K Gaharwar, Z.T Campbell, and T.H Ware, 2021. Advanced Functional Materials. 10, 2106843. Copyright [2021] by John Wiley & Sons Inc.

[238] The utility of these materials in engineering applications is dictated by the type of stimulus used as well as elicited response. Numerous examples of stimuli-responsive materials that respond to external stimuli, including pH, temperature, light, and electric field, have been described for various biomedical and biotechnological applications.[239] Typically, these stimuli directly modify the material's physical properties, which results in the desired stimulus-response.[240–243] For example, shape-changing materials can be synthesized by engineering hydrogels that swell or shrink in response to changes in pH or temperature.[244,245] These stimuli-responsive materials can be used to generate materials that undergo programmable shape change if the magnitude or anisotropy of the swelling can be varied spatially in the structure. [208,240] For example, half-tone lithography can be used to pattern crosslink density, and four-dimensional (4D) printing can be used to program anisotropic shape change behavior by controlling the local orientation of polymer composites.[220,223,246] These techniques can be used to build sensors, soft robots, biomimetic devices, and drug delivery devices.[173,247–250] Nevertheless, the external stimuli that trigger shape change are often temperature changes, UV light irradiation, or solvent exposures that are often limiting factors in biomedical applications. In general, these types of stimuli may cause deleterious effects to the surrounding tissue if used in the human body. To overcome such limitations, materials that respond to subtle biochemical changes in the environment may be more suitable for biomedical applications.

Some classes of materials respond to weak and poorly differentiated stimuli. Here, we define weak and poorly differentiated stimuli as changes in the external

environment that are too small and subtle to cause a material to traverse a phase transition, dramatically swell, or undergo other physical changes. For example, most hydrogels would not swell dramatically in the presence of one amino acid while resisting swelling in another amino acid. Materials that detect the presence or absence of different biomolecules can be of great advantage in mimicking biomolecular recognition in artificial systems. Typically, biomolecular-responsive materials are engineered with highly specific recognition elements that induce programmed responses when subjected to specific processes, including enzyme-catalyzed reactions and DNA hybridization exchange.[20,21,251] Incorporation of biomolecule-responsive motifs in materials can enable therapeutic applications in the early detection of disease-related biomarkers or the delivery of drugs to target tissue for the treatment of numerous diseases. Shape-changing materials capable of responding to physiologically relevant biomolecules represent one option for the delivery of therapeutics to target tissue. For example, phenylboronic acid-based hydrogels are capable of delivering insulin by responding to physiological glucose concentrations that change the swelling behavior of the hydrogel.[252] Molecularly imprinted hydrogels can swell or shrink in response to specific target proteins, such as thrombin; this thrombin-responsive volume change has been proposed as a method to trigger drug delivery.[253] However, the responses achieved with these types of materials are difficult to generalize to a wide variety of potential biochemical targets as each target should induce a highly specific change to the polymeric material. In contrast, living organisms natively respond with specificity to a wide variety of target biochemicals and can be engineered to induce specific responses in materials.

Engineered living materials (ELMs) integrate living cells and synthetic components and have been used to create stimuli-responsive devices.[26,27,254,255] ELMs can be designed to harness the biological functions of living cells to detect small changes in the environment and respond in a programmed manner. Importantly, genetic manipulation of living cells enables the design of ELMs with engineered responses to a wide range of stimuli.[185,197,201] These stimuli induce a variety of chemical responses in ELMs, including sensing and reporting, drug-producing, self-healing, and self-cleaning.[63,256–259] ELMs comprised of genetically engineered living microorganisms can be programmed to perform desired functions and thrive in a wide range of environmental conditions, from those found in infrastructure to the gastrointestinal tract in the human body.[69,260] In some cases, ELMs can be formed using probiotics, providing a multimodal mechanism of action in biomedical devices.[256] In each of these ELMs, the primary function is derived from the chemical activity of the living cells.

Distinct from chemically active ELMs, we previously described mechanically-active ELMs where encapsulated yeast proliferate and induce shape change in a hydrogel matrix.[197] In these ELMs, however, the spatial distribution of cells and the form of the material were limited by molding techniques used for fabrication. 3D printing techniques have been used to spatially control the distribution of yeast and bacteria in 3D structures used for biocatalytic processes and environmental and biomedical applications.[76,89,94,261,262] In synthetic materials, 4D printing techniques have enabled the design of stimuli-responsive materials that change shape, in which the 3D

fabricated form changes over time to yield 4D printed structures.[8,220,263,264] These 4D architectures have opened new avenues for the design and study of shape-morphing medical devices.

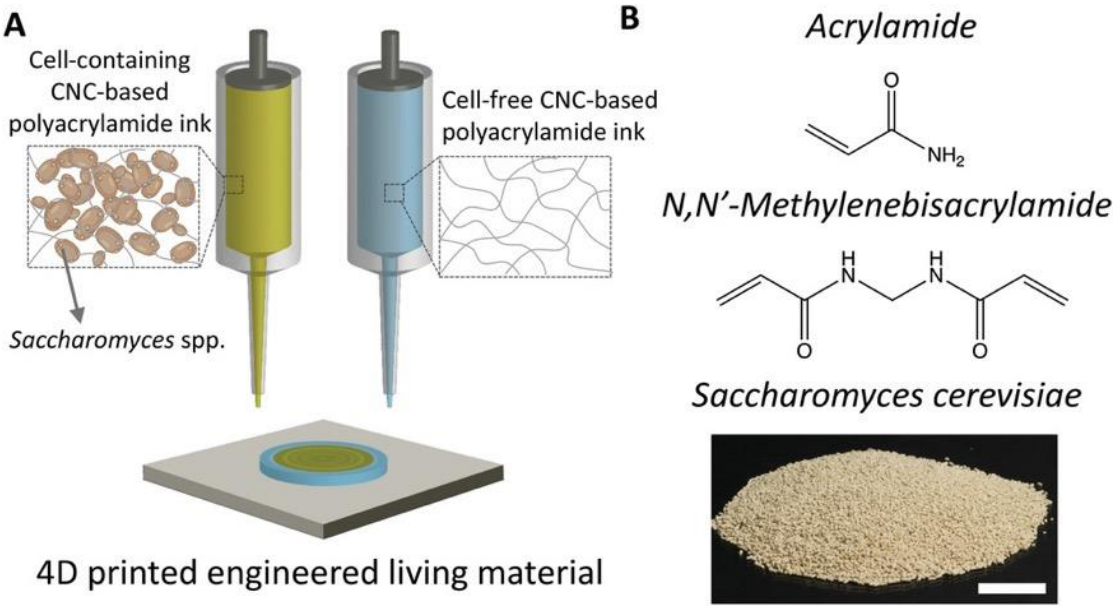

Figure 3-1: Fabrication of shape-morphing engineered living materials. (A) Schematic represents the process of 4D printing a multimaterial shape-changing ELM. (B) Chemical structures of acrylamide monomer and bisacrylamide crosslinker, and picture of active dried yeast (Scale bar: 10 mm). Reprinted with permission from [296]. Copyright (2021) Wiley-VCH.

Here, we report the use of direct-ink-write additive manufacturing to synthesize ELMs capable of shape change in response to small changes in the environment. We investigate the 4D- printing of hydrogels from yeast-containing bioinks and cell-free inks (Figure 3-1A). Importantly, control over the spatial distribution of yeast quantity and type allows for the controlled proliferation of cells within the 3D structure, resulting in structures that morph into complex shapes. These programmable shape transformations can be controlled using genetically engineered yeast probiotics capable

of proliferating only in the presence of specific biogenic amines or nucleotides. Finally, we show that these printed ELMs can be designed into drug delivery devices that change shape and deliver a model drug to the surrounding environment in response to a biochemical cue.

3.3. Results and discussion

In this work, we describe a system of 4D printed ELMs where the strain and concentration of embedded yeast can be controlled in 3D printed objects. The resulting objects respond to the presence of specific biochemicals by undergoing programmed changes in form. We then use this system to create a 4D printed drug delivery device, where the programmed shape change of the ELM ruptures a reservoir in response to a biochemical cue.

3.3.1. Ink characterization

We formulate a series of printable inks that can be crosslinked into hydrogels and study the rheological behavior of both cell-containing and cell-free materials. Cell-containing inks are comprised of yeast (*Saccharomyces cerevisiae* or *Saccharomyces boulardii*), cellulose nanocrystals (CNCs) as a rheological modifier, acrylamide as a linear monomer, bisacrylamide (BIS) as a crosslinker, LAP as a photoinitiator, and water (Figure 3-1B). The presence of both yeast and CNCs affects the rheological properties of the inks. Previously, both have been used to induce shear-thinning behavior and increase the shear modulus of 3D printable hydrogel precursors.[89,265,266] To fabricate cell-containing inks (bioinks), we vary the concentration of CNC (5, 8, 11 wt %) in compositions comprised of a fixed concentration of active dried yeast (*S. cerevisiae* 12

wt % corresponding to approximately 4 x 10^9 cells/mL) dispersed in aqueous solutions containing 8 wt % acrylamide, 0.1 wt % BIS crosslinker, and 0.02 wt % LAP photoinitiator. We observed that each of the bioinks exhibits strong shear thinning behavior. Viscosity at low shear rates slightly increases as CNC concentration increases (Figure 3-2A). Cell-free inks composed of 11, 16, 19, or 22 wt % CNC and the same concentrations of monomer, crosslinker, and photoinitiator as described above were also strongly shear-thinning and showed a slight increase in viscosity as CNC concentration increases (Figure 3-2B). Both bioinks and cell-free inks follow the power-law viscosity model with flow indices of near 0, as shown in the tabulated results in Table A-1. For both bioinks and cell-free inks synthesized in this study, the inclusion of CNCs led to higher shear storage modulus than shear loss modulus (FigureS 3-2C, D), which indicates that, at low shear strains, both types of inks have a solid-like behavior that allows shape retention. This shape retention allows the bioinks and cell-free inks to retain form during photocuring with UV light under a nitrogen environment to form ELMs and cell-free hydrogels, respectively.

3.3.2. Mechanical properties, volume change, and shape change evaluation

The mechanical properties of ELMs and cell-free hydrogels are influenced by CNC concentration.[23,25] We altered the feed ratio of CNC from 5 wt % to 14 wt % in ELMs containing *S. cerevisiae* and from 11 wt % to 22 wt % in cell-free hydrogels. We measured Young's modulus of ELMs and cell-free hydrogels using uniaxial compression testing on samples after synthesis (no growth). As shown in Figure 3A, an

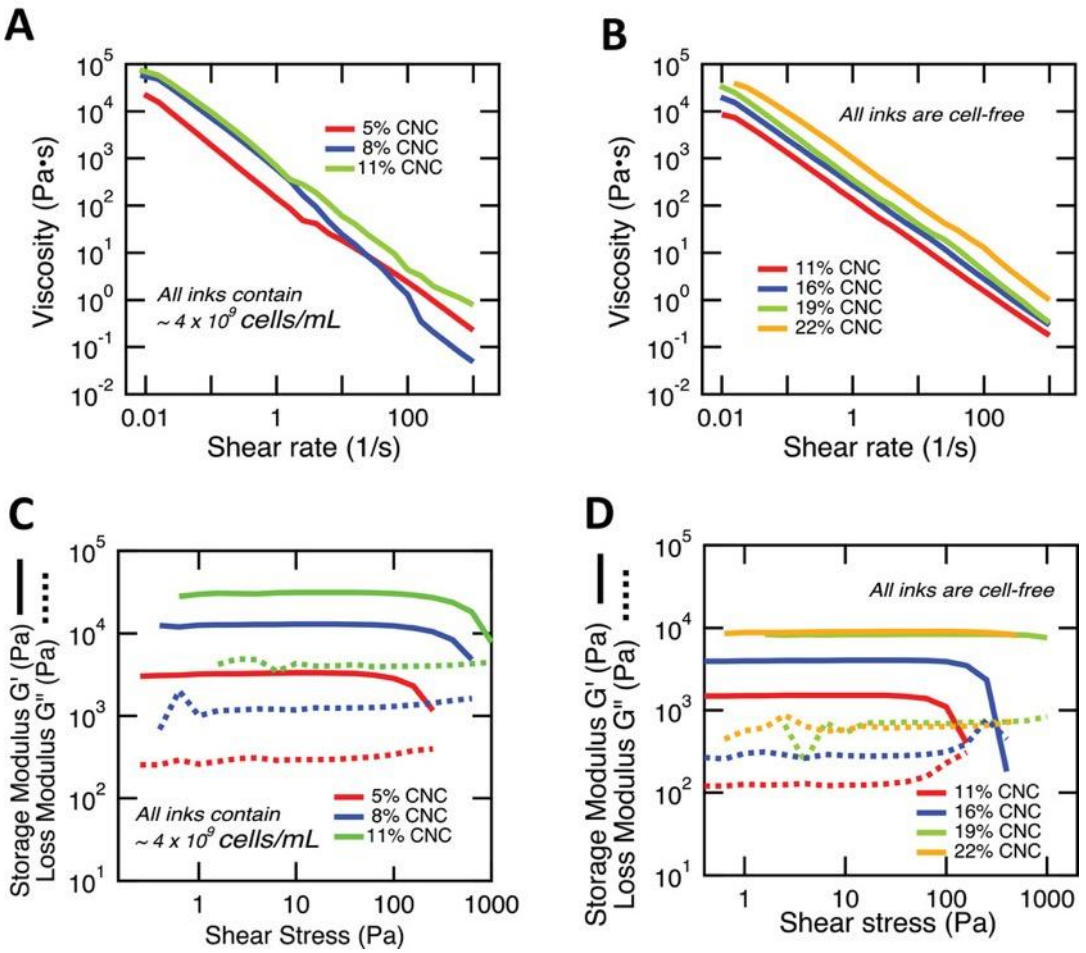

Figure 3-2: Influence of CNC on printability of ELMs and cell-free inks. (A) Log-log plot of viscosity for each bioink composition as a function of shear rate at room temperature. (B) Log-log plot of viscosity for each cell-free ink as a function of shear rate at room temperature. (C) Storage and loss modulus as a function of shear stress for each bioink composition. (D) Storage and loss modulus as a function of shear stress for each cell-free ink composition. Reprinted with permission from [296]. Copyright (2021) Wiley-VCH.

increase in Young's modulus from 13 $\pm$ 2 kPa to 20 $\pm$ 1 kPa, as CNC loading increases up to 11 wt % in ELMs, is observed. After 14 wt % CNC, the Young's modulus of the ELM decreased. This decrease may be attributed to the reduction of the crosslinking density due to the presence of both cells and CNC making up to 26 wt % of the ELM. For cell-free hydrogels, an increase in the overall Young's modulus from 13 $\pm$ 1 kPa to

26 ± 2 kPa, as CNC increases from 11 wt % to 22 wt %, is observed (Figure 3-3A). Similar behavior related to the increase in Young's modulus has been previously reported in polyacrylamide hydrogels containing CNCs. [267]

Each of the ELMs undergoes an increase in volume when exposed to conditions appropriate for growth, while the cell-free hydrogels undergo a decrease in volume in the same growth medium. To quantify the shape change of each of these composites due to cell proliferation, ELMs and cell-free hydrogels (n = 3) were grown in synthetic complete medium at 30 ºC in aerobic conditions. The volume change for both types of materials was measured every 12 h for two days. For each of the ELMs, cell proliferation within the hydrogel leads to an increase in the total biomass within the material. As yeast are substantially stiffer (1-10 MPa)[268] than the surrounding hydrogel (20 ± 1 kPa for 11 wt% CNC), the increase in biomass is accommodated by a macroscopic volume change.[197] We observed that as CNC concentration increases from 5 to 14 wt %, the volume change of ELMs decreases from 370 ± 23 % to 190 ± 13 % (Figure 3B and Figure A-11), likely due to the increase in stiffness of these ELMs. Significant differences between the volume changes at 48 h of ELMs made with 5 wt % CNC and ELMs made with 14 wt % CNC were observed (*t*-test, $P < 0.001$). The macroscopic volume change of an 11 wt % CNC ELM disk is shown in Figure 3C. Cell-free hydrogels were placed in the same culture flasks as the ELMs. As described in the literature, yeast acidifies the external medium due to proton secretion during fermentation, secretion of organic acids, and CO_2 evolution.[269–271] These cell-free hydrogels undergo a minor deswelling due to acidification of the synthetic complete

medium (Figure A-12 and Figure A-13). Previously, CNC/polyacrylamide hydrogels

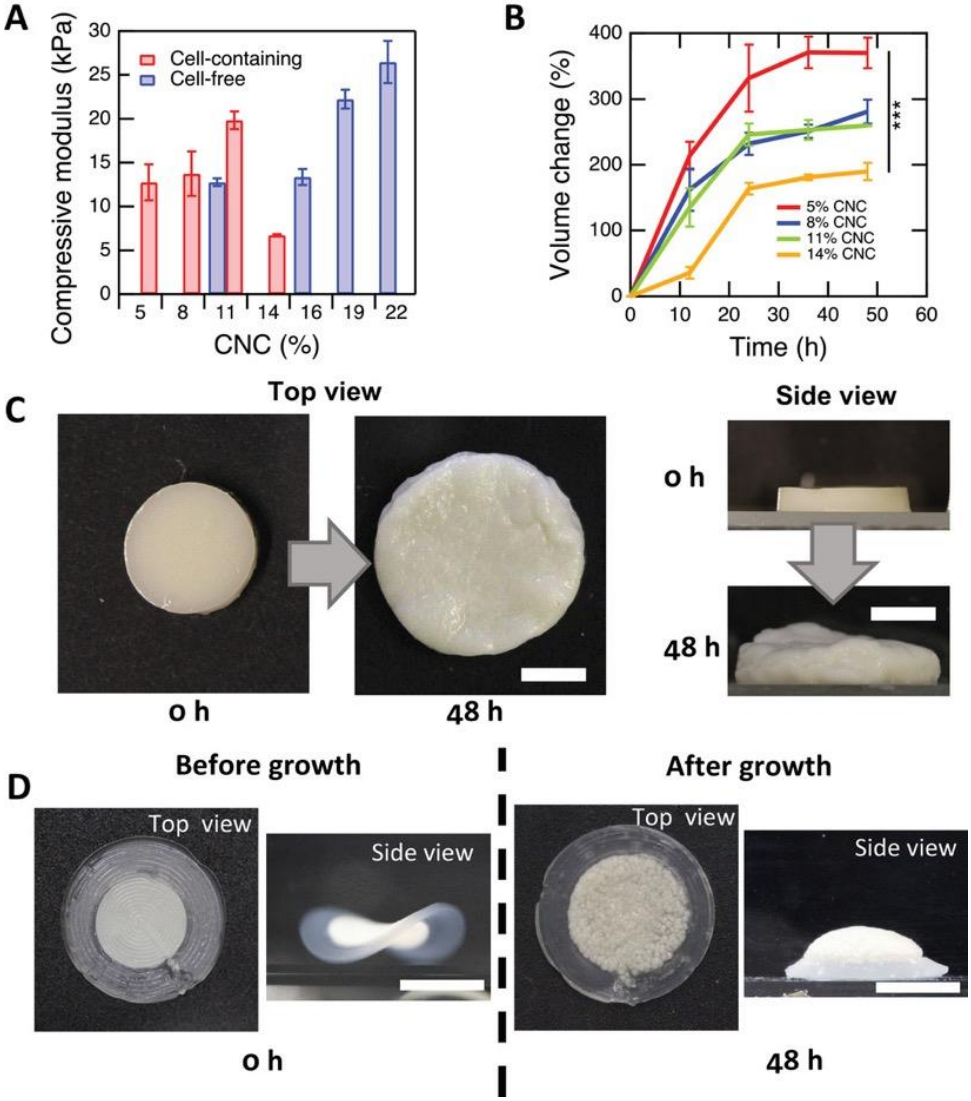

Figure 3-3: Influence of CNC at varying concentrations on mechanical properties and shape change. (A) Compressive modulus as a function of CNC content for cell-containing and cell-free materials. (B) Volume change as a function of time for each ELM composition. (C) ELM disk before and after growth in synthetic complete medium. Top view shown on the left and side view shown on the right (Scale bars: 5 mm). (D) 4D printed ELM in the form of a disk that consists of a cell-free outer ring and a cell-containing inner disk. After 48 h of growth in synthetic complete medium, the structure changes shape from a negative (left) to a positive (right) Gaussian curvature geometry (Scale bars: 10 mm). Each data point represents the mean (n = 3) and error bars represent standard deviation. Trend lines are only intended to guide the eye. Statistical analysis: t-test, *** P-value < 0.001. Reprinted with permission from [296]. Copyright (2021) Wiley-VCH.

have been shown to deswell at low pH.[272,273] In the remaining experiments, we use bioinks with 11 wt % CNC and cell-free inks with 22 wt % CNC to build 4D printed structures.

Using the materials described thus far, we employ direct-ink-write printing to build objects comprised of ELMs and cell-free hydrogels that grow into patterned forms. Using multi-material printing, we fabricate a disk composed of ELM and cell-free material. The 4D printed structure adopts a saddle-like shape after being equilibrated in synthetic medium without glucose (Figure 3-3D, left). This saddle-like shape is obtained due to the differential swelling between the ELM inner disk and the outer ring cell-free material. In this case, the outer cell-free ring gets larger in area as compared to the inner disk due to a slightly higher volume increase after equilibrating in the medium. Thus, the ELM structure minimized its elastic energy by adopting the observed 3D negative Gaussian curvature form.[197,219] After growth in synthetic complete medium for 48 h, cell proliferation within the inner disk induces a 3D transformation into a hat-like structure (Figure 3-3D, right).[219] This positive Gaussian curvature structure is adopted due to the ELM inner disk growth that increases in volume and the slight decrease in volume of the cell-free outer ring after growth. While direct-ink-write printing is used to encapsulate yeast in 3D ELM objects, it is important to note that yeast leak during growth of the ELMs. We expect that yeast found on or near the surface of the 3D printed ELMs are not fully trapped. Due to the same forces that drive shape change, these cells escape from the object and freely proliferate in the growth medium. The printed ELMs, however, remain intact while increasing in volume due to cell proliferation during growth.

3.3.3. Fabrication of genetically engineered ELMs

Having developed a system of 4D printable ELMs that undergo shape change, we now seek to use this system to create 3D structures that respond to specific biochemical stimuli. As we are motivated by the ultimate use of these materials in biomedical applications, such as drug delivery to specific tissues in the gastrointestinal tract, we built ELMs using a probiotic strain of *S. cerevisiae.* This strain, *Saccharomyces boulardii*, is used as a biotherapeutic agent to prevent and treat gastrointestinal disorders.[274,275] In particular, *S. boulardii* is a good candidate for designing ELMs that function in the gastrointestinal tract of the human body, as it can grow at 37º C, is well tolerated *in vivo*, survives transit through the stomach, and is amenable to genetic engineering.[276–278]

Genetic engineering of probiotics enables programming of the conditions required for proliferation of the embedded strains and, therefore, the shape change of the composite. We utilized a series of *S. boulardii* auxotrophic mutants (LEU2, URA3, TRP1, and HIS3) that were previously modified through the clustered regularly interspaced short palindromic repeat (CRISPR)-Cas9 genome editing system (Figure 3-4A).[278] Each mutant used was deficient in either L-leucine, uracil, L-tryptophan, or L-histidine synthesis. As a result, the proliferation of each mutant is minimal unless the specific amino acid or nucleotide is present in the growth environment. The auxotrophic phenotype for each mutant was confirmed after growth in Petri dishes containing synthetic medium agar lacking the corresponding amino acid or nucleotide (Figure 3-4B).

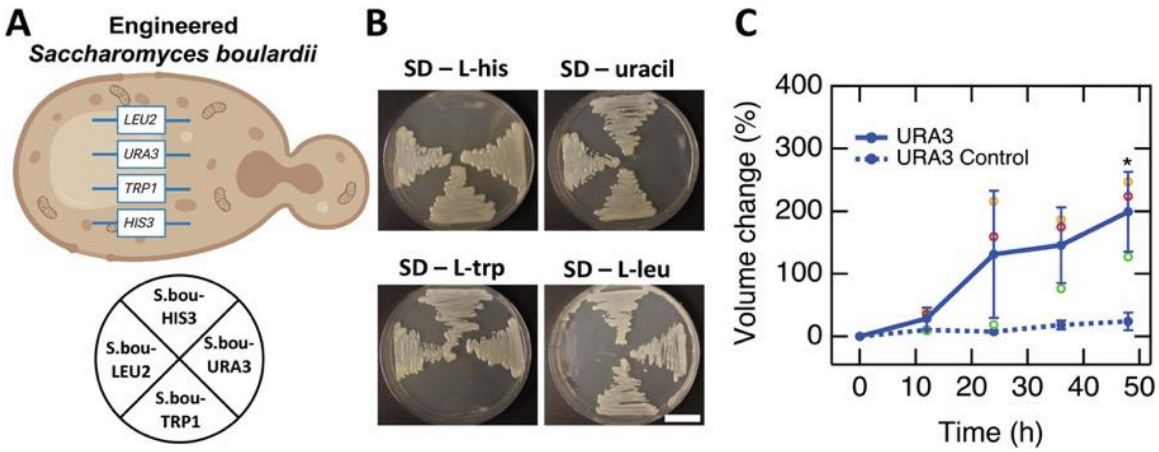

Figure 3-4: Engineered probiotics can form ELMs. (A) Schematic of engineered *Saccharomyces boulardii* probiotic (top). This probiotic has been modified to obtain four different mutants that are each auxotrophic for either L-leucine, L-tryptophan, L-histidine, or uracil. Schematic represents the position of the mutant streaked on synthetic medium agar plates (bottom). (B) Growth behavior of each of the mutants on synthetic medium agar plates that lack each of the amino acids or nucleotide. (C) Volume change over time of ELM disks that contain *S. boulardii*-URA3 grown in the presence of synthetic complete medium and synthetic medium lacking uracil (control). (S.bou: *S. boulardii*; SD: synthetic medium agar; L-his: L-histidine; L-trp: L-tryptophan; L-leu: L-leucine). Each data point represents the mean (n = 3) and error bars represent standard deviation. Trend lines are only intended to guide the eye. To better visualized the data, open dots show the individual data points for ELMs grown in the presence of uracil. Statistical analysis: *t*-test, * *P*-value < 0.05. Reprinted with permission from [296]. Copyright (2021) Wiley-VCH.

The probiotic strains proliferate within and drive volume change of the ELM. Using the same growth conditions as *S. cerevisiae* ELMs, we observed that ELM disks containing *S. boulardii*-URA3 mutant changed in volume up to 191 $\pm$ 60 % after 48 h in synthetic complete medium (Figure 3-4C). This increase in volume is significantly different compared to control samples of these ELMs (*t*-test, P < 0.05) that increased only 24 $\pm$ 14 % in volume after 48 h in synthetic medium lacking uracil (Figure 3-4C). ELMs encapsulating auxotrophic mutants LEU2, TRP1, and HIS3 were also tested in synthetic complete medium and synthetic medium lacking the corresponding amino acid

(Figure A-144 and Figure A-15). Similar behavior as the composites containing the *S. boulardii*-URA3 was observed in these ELMs, where growth is triggered by the presence of all amino acids in the synthetic complete medium and nearly totally absent in the absence of the specific amino acid that the strain cannot synthesize (Figure A-16). Significant differences between the volume changes of these ELMs at 48 h and their corresponding controls were also observed (*t*-test, LEU2, $P < 0.01$; TRP1, $P < 0.01$; HIS3, $P < 0.05$). The use of auxotrophic probiotics enables ELMs that change shape only after detecting small concentrations (e.g., ~ 80 μg/mL of uracil in medium) of specific amino acids or nucleotides.

3.3.4. Multi-probiotic shape-changing ELMs

Direct-ink-write printing allows the spatial distribution of different probiotic mutants within a single ELM structure. Each region of the structure then grows only when then the appropriate biochemical cue is present. ELM bilayers were printed that contained two of the genetically engineered *S. boulardii* mutants (TRP1, URA3), with each layer containing one mutant (Figure 3-5A). The resulting bilayers bent in the presence of synthetic medium with either the amino acid L-tryptophan or the nucleotide uracil. We first measured the change in bending curvature ($k = 1/r$) of an ELM bilayer growing in synthetic medium lacking L-tryptophan. The bilayer underwent a change in curvature that was obtained due to the mismatch strain between the ungrown layer containing the mutant *S. boulardii*-TRP1 and the growing layer of *S.boulardii*-URA3. In Figure 3-5B, we observed that the bilayer underwent a substantial increase in curvature when grown in synthetic medium lacking L-tryptophan for the first 36 h, with the layer

containing the *S. boulardii*-URA3 on the outside of the structure. After changing the bilayer to synthetic medium lacking uracil, the curvature continued to increase during the first 12 h of growth. This continued bending might correspond to the time required to exhaust residual metabolic pools of uracil enabling some residual growth of the cells in the *S.boulardii*-URA3 layer. After 12 h, the bending curvature decreases due to the growth of the *S. boulardii*-TRP1 layer and the absence of growth of the *S.boulardii*-URA3 layer. After 120 h of total growth time, the ELM bilayer returns to a flat shape and has an overall increase in volume. The evolution of the curvature of a representative ELM bilayer is shown in Figure 3-5C and replicates are shown in Figure A-17. This sequential shape change is triggered first by the presence of a specific amino acid and then by a specific nucleotide in medium that contains many other amino acids and nucleotides. In contrast to experiments where hydrogel bilayers sequentially change in bending curvature in response to pH and temperature,[279] these ELM bilayers are capable of sequentially changing in curvature in response to multiple specific biomolecules. Sequential shape change in materials triggered by exposure to low concentrations of poorly differentiated molecules has not been previously demonstrated.

This multi-probiotic material platform can provide a novel way to achieve structures that transform into multiple shapes in response to multiple specific molecules. To create such a structure, we printed ELM structures composed of two *S. boulardii* probiotic mutants (TRP1 and LEU2) arranged in an asymmetric configuration (Figure 3-6A). These structures consisted of patterned bilayers where the bottom was printed as a rectangular continuous structure encapsulating *S. boulardii*-LEU2, and the top layer was

printed as stripes encapsulating *S. boulardii*-TRP1. These ELMs undergo distinct shape transformations in response to two specific stimuli (Figure 3-6A). After 48 h of growth in synthetic medium lacking L-leucine but containing L-tryptophan, the flat structure morphs into a cylindrical tube with normal curvature only along its short axis. This curvature results from the growth in volume of the stripes and the underlying layer maintaining its original form.

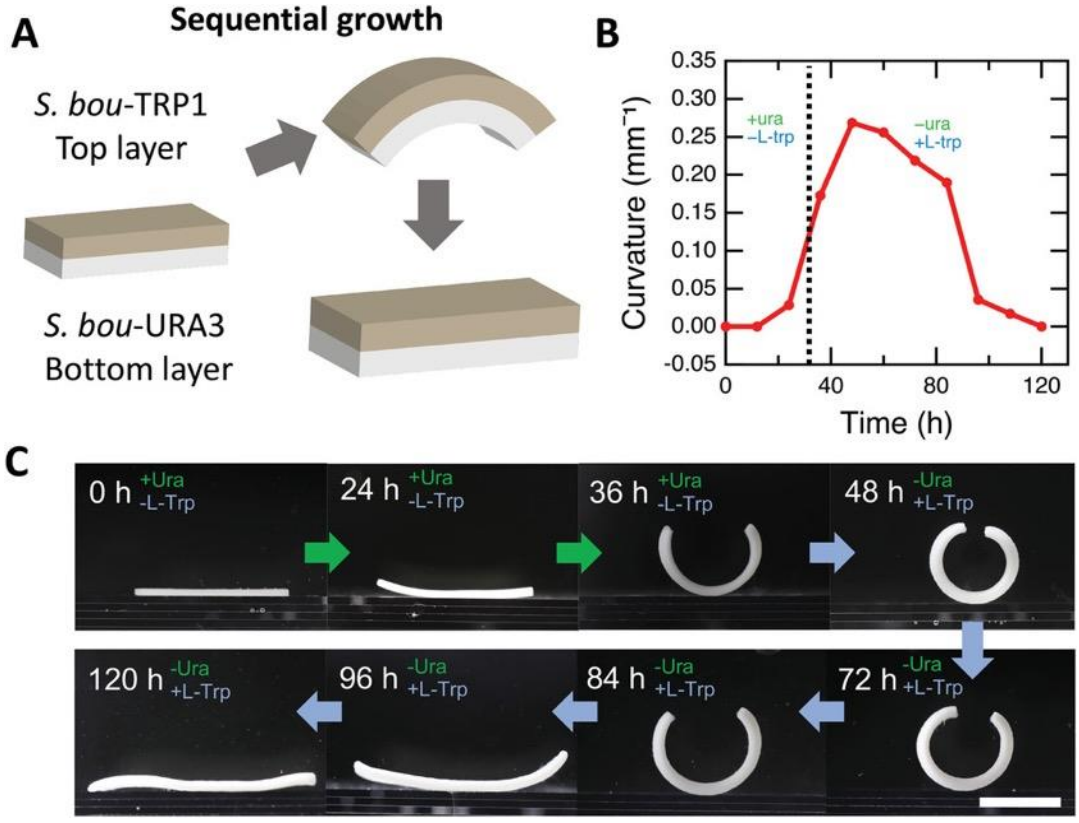

Figure 3-5: 4D printing ELMs capable of sequential shape change. (A) Schematic of a printed bilayer composed of two engineered *S. boulardii* mutants. Bilayer is capable of sequential shape change. (B) Curvature as a function of time of a bilayer that contains *S. boulardii* mutants URA3 and TRP1. Bilayer grows in synthetic medium lacking L-tryptophan for the first 36 h and then it grows in synthetic medium lacking uracil for 96 h. (C) Sequential shape change over time of the ELM bilayer (Scale bar: 10 mm). Reprinted with permission from [296]. Copyright (2021) Wiley-VCH.

The same type of ungrown printed geometry was incubated in synthetic medium lacking L-tryptophan but containing L-leucine. In this case, the continuous bottom layer of the ELM increases in volume due to cell proliferation. As shown in Figure 3-6B, when the bottom layer of the printed film grows in this medium, the ELM changes into a bent tube with normal curvature along both the short and long axes after growing for 48 h. This curvature that develops along the short axis is in the opposite sense as compared to the structures grown in L-tryptophan, as now the continuous bottom layer is larger than the stripes. Either of the grown ELMs can then be incubated in synthetic medium containing the other biochemical stimulus. In both cases, the grown structure partially unbends due cell proliferation of the previously ungrown layer (Figure A-18 and Figure A-19).

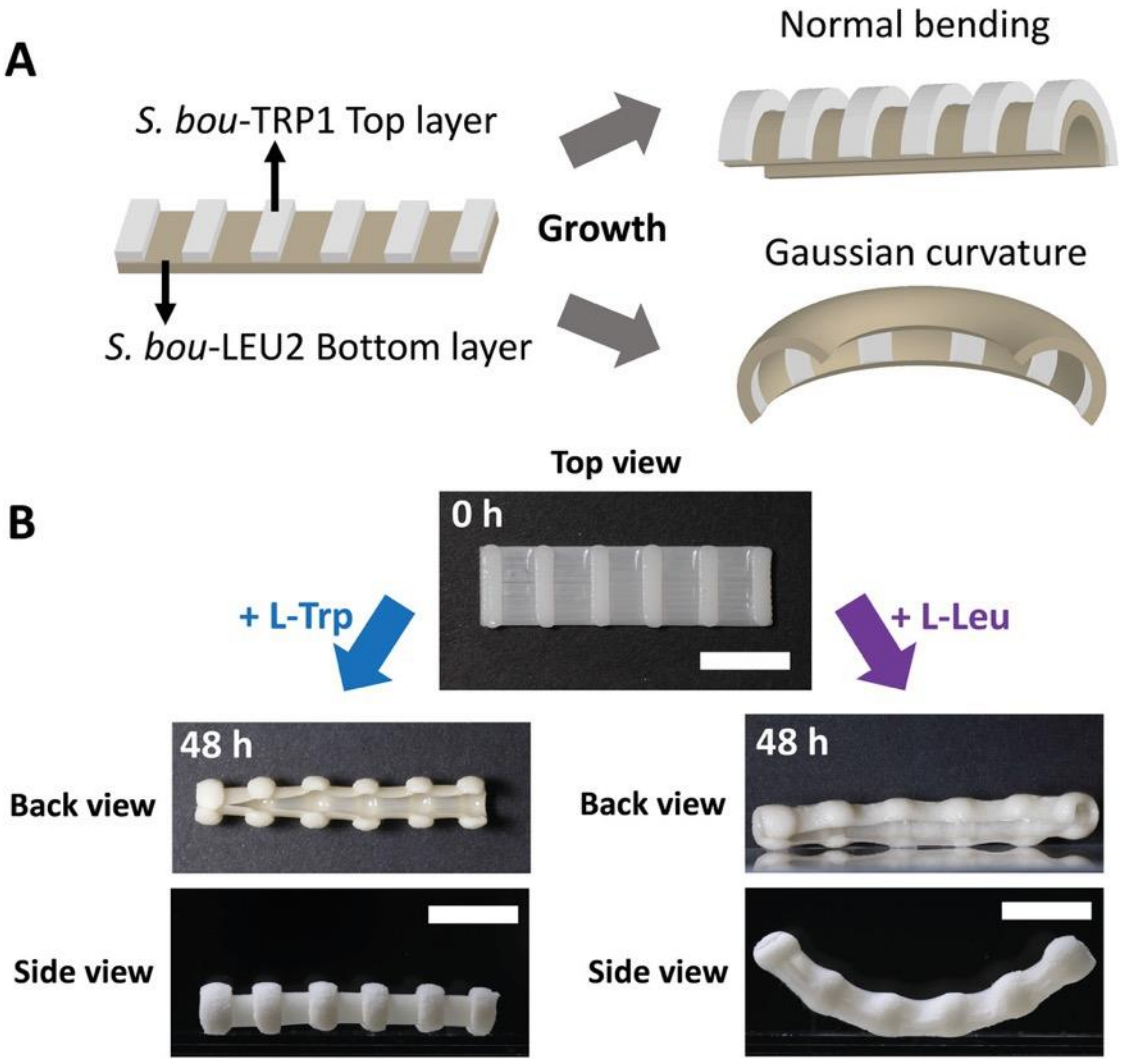

Figure 3-6: 4D printing ELMs capable of multiple shape change. (A) Schematic of a printed bilayer composed of two engineered *S. boulardii* mutants. Top layer is printed as stripes and bottom layer as a flat sheet. (B) Printed structure is capable of changing shape into two different types of geometries. When the bilayer is incubated in synthetic medium lacking L-leucine, it changes shape into a tube-like structure (left). When it is incubated in synthetic medium lacking L-tryptophan, the bilayer adopts a geometry with two types of bending (right) (Scale bars: 10 mm). Reprinted with permission from [296]. Copyright (2021) Wiley-VCH.

3.3.5. 3D-printing shape-changing drug delivery ELMs

Having established that we can fabricate 4D printed ELMs that respond by changing shape in a programmed manner to specific biochemical cues, we hypothesized

that we could harness this shape change to build capsules that deliver a model drug in response to a biochemical cue. By designing a device that can respond to such subtle cues, we ultimately aim to enable the use of ELM drug delivery devices to target specific locations of the body, while noting that the current device only tests the delivery mechanism. We fabricated a model drug delivery device by printing an ELM *S. boulardii*-TRP1 mutant in the base and cell-free material in the body and lid of a capsule (Figure 3-7A). The capsules are fabricated with dimensions that resemble those of common oral pharmaceuticals and are hollow to function as reservoirs of a model drug that cannot diffuse through the hydrogel. The working principle of this device is that growth of the ELM base layer will rupture the capsule and the model drug will be released from the capsule's reservoir in response to a specific amino acid. The ELM capsules are filled during printing by injecting the model drug into the open, hollow structure. This process was done before the printer finished the process of closing the capsule. Micrometer-sized materials that carry drugs have been useful in therapeutic applications via the oral route, such as inflammatory bowel diseases, diabetes, cancer, and anti-inflammatory therapies.[280–283] Our capsules are printed using a concentric path in the shape of a square for each part of the capsule. The use of a concentric path to build the base of the capsule results in a weak point at the center of the base. We hypothesized that the capsules would fail near this weak point to enable the release of the model drug. We fabricated capsules that were grown in synthetic complete medium at 37 ºC to record their shape change and model drug release over time. Due to the base of the capsules being constricted by the cell-free structure, the base expands and eventually ruptures

between the 12 h and 24 h or between the 24 h 36 h timepoints. The evolution of shape change and rupture of a representative capsule is shown in Figure 3-7B. This rupturing was observed to start near the fabricated weak point, which allows the release of the model drug from the reservoir.

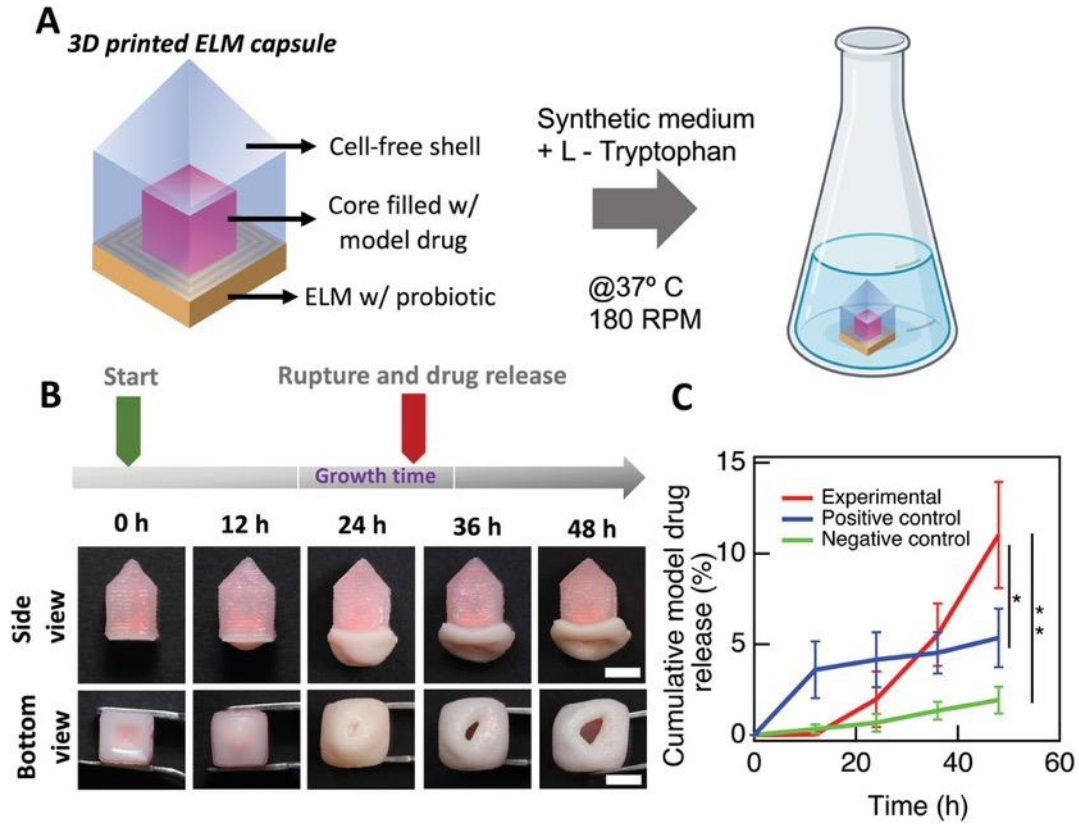

Figure 3-7: 4D printing ELM drug delivery devices. (A) Schematic of a 3D printed ELM capsule with an embedded probiotic mutant at the base. ELM capsules were grown in synthetic complete medium or synthetic medium lacking the corresponding amino acid. (B) Printed capsule containing *S. boulardii*-TRP1 and encapsulating model drug in the reservoir (fluorescent microparticles). The device changes in area at the bottom and eventually ruptures at 24 or 36 h timepoints. (C) Cumulative microparticle release quantification. Experimental capsules rupture and release fluorescent microparticles between 12 and 24 or 24 and 36 h of growth in synthetic complete medium. Positive controls are manually ruptured and release model drug from start to end of growth in synthetic medium lacking L-tryptophan. Negative controls incubated in synthetic medium lacking L-tryptophan do not rupture or release model drug (Scale bars: 5 mm). Each data point represents the mean (n = 3) and error bars represent standard deviation. Trend lines are only intended to guide the eye. Statistical analysis: one-way ANOVA

followed by a post hoc Tukey test, * *P*-value < 0.05, ** *P*-value < 0.01. Reprinted with permission from [296]. Copyright (2021) Wiley-VCH.

The release of the model drug to the surrounding medium is governed by the rupture of the capsule. To monitor model drug release, the medium surrounding the capsule was collected every 12 h for two days, and the contents were quantified by counting the released model drug in the flow cytometer. A single type of capsule was fabricated, and the release of drug was monitored in three conditions. The experimental condition consisted of capsules grown in synthetic medium containing L-tryptophan. The negative control was capsules incubated in synthetic medium without L-tryptophan. The positive control was capsules that were manually ruptured along the base and incubated in synthetic medium without L-tryptophan. In the first 12 h, the experimental and negative control capsules release very few or no model drug fluorescent microparticles, while the positive control capsules release 4 ± 2 % of the total encapsulated model drug. By 36 h, all of the experimental capsules have ruptured and have released 6 ± 2 % of the total encapsulated model drug. Statistical analysis using one-way ANOVA reveals that there is a significant difference between the release of the model drug at 48 h between the experimental and positive control capsules ($P < 0.05$). We relate this higher release of model drug from the experimental capsules to the ruptured point at the base growing larger over the time of growth (Figure 3-7C). This increase at the ruptured point in positive control capsules is not observed because the base of the capsule remains ungrown throughout the total growth time in its corresponding medium (Figure A-20). Importantly, we also tested intact negative control

capsules that were placed in medium lacking L-tryptophan and observed a small apparent release of the model drug to the surrounding environment. On observation, we did not detect any failure in these capsules. As such, it is unclear if a small release was observed or if accumulated noise in the measurements leads to this small apparent release (Figure A-21). There is a significant increase in model drug release ($P < 0.01$) for the experimental capsules with the growing base as compared to the negative control capsules. We note that the experimental capsules were all ruptured by 36 h, however, a great percentage of the model drug was not released. The same behavior was observed in positive control samples. We believe that the retention of model drug within the capsules might be due to some of the model drug adhering to the internal walls of the capsules prior to crosslinking (Figure A-22). To ensure a higher percentage of microparticles are released, future work may require crosslinking strategies that prevent the adherence of microparticles to the material.

In this work, direct-ink-write printing enables spatial-control of the strain and quantity of embedded yeast within synthetic hydrogels. This spatial control enables structures that morph into complex shapes in response to engineered conditions. We note that having such control could enable ELMs that serve as components of active drug delivery devices. We created ELM capsules to provide a proof-of-concept demonstration for the release of drugs driven by material shape change. This demonstration validates the idea that shape-changing ELMs can respond to a biochemical stimulus and release a contained compound. Nonetheless, several important challenges remain before these devices could be used in a delivery device, for example, in the gastrointestinal (GI) tract.

One important challenge is the timescale of shape change after exposure to a stimulus. This timescale of shape change must occur before the device is cleared from the body and ideally would target the released compound to a tissue of interest. ELM delivery strategies may need to be coupled up with other strategies that allow retention in the GI tract, such as microneedles or floating systems.[284–286] Furthermore, while the presence or absence of an amino acid is a convenient laboratory stimulus, it is not necessarily a useful biochemical stimulus in a medical device. Free amino acid content in the GI tract will be controlled by a range of conditions.[287] However, we note that proliferation, which is the key behavior needed to induce delivery, is a behavior seen in all microorganisms. Future advances in synthetic biology where probiotics are engineered to respond to a disease-specific stimulus may be leveraged into ELM delivery devices.

3.4. Conclusion

We demonstrated the 4D printing of ELM objects that undergo programmable shape changes in response to the presence or absence of particular biochemicals in a milieu of biochemicals. The rheological modifier CNC was used to tune the viscosity of bioinks and cell-free inks that are used to direct-ink-write different architectures. Multi-material 4D printing of one or two types of bioinks within the same structure was used to spatially distribute yeast of different strains and spatially control the concentration of yeast. This approach enables the genetics of the encapsulated yeast to control the stimulus needed to induce shape change. This approach is quite distinct from most shape changing materials where physical changes in a synthetic polymer are driven by heat, light, solvents, or other stimuli. This approach may enable new types of bioresponsive

medical devices. Using genetically engineered probiotics, we fabricated proof-of-concept drug delivery capsules that could release a model drug to the surrounding environment only when a particular biochemical cue is present.

3.5. Materials and methods

3.5.1. Materials

Acrylamide, *N*,*N*′-methylenebisacrylamide (BIS), Lithium phenyl-2,4,6-trimethylbenzoylphosphinate (LAP) photoinitiator, L-leucine, uracil, agar, yeast synthetic drop-out medium supplements without histidine, leucine, tryptophan, and uracil (Y2001) were purchased from Sigma-Aldrich. Amino acids L-histidine and L-tryptophan were purchased from Acros Organics. Cellulose nanocrystals (CNC) were purchased from CelluForce. Commercial yeast (*S. cerevisiae*, active dry yeast, Fleischmann's) was purchased from Amazon. Yeast extract, yeast nitrogen base without amino acids, D-(+)-glucose, and Thermo Scientific™ Fluoro-Max red aqueous fluorescent microparticles (R0200) were purchased from Fisher Scientific. Rain-X was purchased from Wal-Mart (College Station, TX). All chemicals were used as received without further purification.

3.5.2. Mold construction

For volume change and mechanical testing experiments, molds were used to create flat sheets of the ELM and cell-free hydrogels. Molds were made of two glass slides (75 mm by 51 mm) treated with Rain-X to avoid material adhesion. The unpolymerized material was sandwiched between the treated glass slides separated by 1-mm thick spacer.

3.5.3. Quantification of cell density for ELMs encapsulating active dried yeast or probiotic yeast

To quantify the number of cells of active dried yeast, cell density was measured with a Genesys 10S UV/visible spectrophotometer by observing the optical density at 660 nm. Briefly, 1.2 g of yeast in was mixed with dH_2O to prepare a 50 mL yeast solution. Then, two-fold serial dilutions from 1:2 to 1:64 were made (n = 3) by mixing 1 mL of the initial yeast solution with 1 mL of dH_2O until the 1:64 dilution. Diluted yeast solutions (1 mL) were pipetted into a 1-mL cuvette for spectrophotometer measurements. Optical densities between 1.6 and 0.8 were measured respectively for 1:16 and 1:64 dilutions. These densities correspond to numbers of cells of 5.22×10^7 and 1.26×10^7 cells, respectively. These results indicate that 1.2 g of active dried yeast contains approximately 4×10^{10} cells.

Saccharomyces boulardii probiotic mutants (leu2, trp1, his3, ura3 – 18 tubes per mutant) were incubated for 12 h in 5 mL of synthetic complete medium [0.67 wt % yeast nitrogen base without amino acids, 0.139 wt % yeast synthetic drop-out medium supplements, 2 wt % D-glucose, 0.038 wt% L-leucine, 0.0076 wt % L-tryptophan, 0.0076 wt % L-tryptophan, and 0.0076 wt % uracil] at 30º C in a shaking incubator at 200 RPM. Subsequently, overgrowths were made using nine flasks containing 2 overnight tubes each with 50 mL of synthetic complete medium that were incubated in the same conditions. Overgrowths were combined and cell density was measured to calculate the volume needed to reach approximately 4×10^{10} cells. This volume of cells

was centrifuged and washed twice in synthetic complete medium to obtain a pellet. Pellet of cells were kept in an incubator at 30º C for one hour before ink preparation.

3.5.4. Ink preparation for ELMs and cell-free hydrogels

To prepare 3D printable hydrogels containing active dried yeast, pregel/CNC solutions containing 8 wt% acrylamide, 0.1 wt% BIS, 0.02 wt% LAP photoinitiator, 11 wt% CNC, and 12 wt% active dried yeast in sterile dH_2O. The mixing process began by mixing acrylamide, BIS, LAP and CNC with 38.88 wt% sterile dH_2O. Before adding the yeast, the solution was mixed in a planetary AR-100 mixer (Thinky, Laguna Hills, CA) for 2 min at 2000 RPM and then hand mixed with a metal spatula. The process was repeated until the solution was well mixed. Then, yeast and remaining sterile dH_2O was added into the pregel solution and mixing process was repeated in the planetary mixer until the ink was homogenous. For inks containing probiotic mutants, the appropriate volume of pelleted cells (4×10^9 cells/mL) was mixed into the pregel/CNC mixture and total ink volume was adjusted with sterile synthetic medium lacking D-glucose.

To prepare cell-free 3D printable inks, we prepared a solution containing 8 wt% acrylamide, 0.1 wt% BIS, 0.02 wt% LAP photoinitiator, and 22 wt% CNC in sterile dH_2O. All ingredients were added in a glass vial and the solution was mixed in a planetary AR-100 mixer (Thinky, Laguna Hills, CA) for 5 min at 2000 RPM and then hand mixed with a metal spatula. The process was repeated until the solution was well mixed.

For volume change experiments, mechanical testing, and rheology of ELMs containing active dried yeast solutions were prepared with 8 wt% acrylamide, 0.1 wt%

BIS, 0.02 wt% LAP photoinitiator, 12 wt% active dried yeast, and different concentrations of CNC (5, 8, 11, 14 wt %). For volume change experiments, mechanical testing, and rheology of cell-free hydrogels solutions were prepared with 8 wt% acrylamide, 0.1 wt% BIS, 0.02 wt% LAP photoinitiator, and different concentrations of CNC (11, 16, 19, 22 wt %).

For volume change experiments of ELMs containing probiotic mutants, solutions were prepared with 8 wt% acrylamide, 0.1 wt% BIS, 0.02 wt% LAP photoinitiator, 11 wt% CNC, and each *S. boulardii* probiotic mutant (4 x 10^9 cells/mL).

3.5.5. Ink rheological measurements and analysis

The rheological behavior of the ELMs containing active dried yeast and cell-free inks using different concentrations of CNC were characterized using a Discovery HR-3 Hybrid Rheometer (TA Instruments, New Castle, DE) using a 40 mm, 2.029° cone plate geometry and a gap of 30 μm. Viscosity measurements were conducted through logarithmic sweeps of shear rates from 0.01 to 1000 s^{-1}. Oscillation sweep tests were conducted at a fixed frequency of 1 Hz and a sweep stress from 0.1 to 500 Pa. All measurements are performed at constant room temperature (22° C). The shear-thinning properties of both bioinks and cell-free inks were determined using the power law viscosity model following the equation: $\eta = K\dot{\gamma}^{n-1}$. In this model, η represents the viscosity, $\dot{\gamma}$ is the shear rate, *K* is the consistency index, and *n* is the flow index. The flow index gives important information regarding the type of material. When $n < 1$, the material is shear thinning, whereas $n > 1$ or $n = 1$ indicate that the material is shear thickening or Newtonian, respectively. For both bioinks (5, 11 wt % CNC) and cell-free

inks (11, 16, 19, 22 wt % CNC), the flow indices were measured using the corresponding viscosity data at shear rates between 10^{-1} and 10^{1} 1/s. For bioinks made of 8 wt% CNC, flow indices were measured using the corresponding viscosity data at shear rates between 10^{-2} and 10^{0} 1/s.

3.5.6. Volume change quantification of ELMs and cell-free hydrogels

To quantify volume changes in ELMs with active dried yeast, cell-free hydrogels, and ELMs with probiotic mutants, all inks were sandwiched between the fabricated molds. Then, the molds were exposed to UV irradiation at 365 nm with an intensity of 28 mW/cm^2 for 35 s on each side. All hydrogels were stored in synthetic complete medium lacking D-glucose for 24 h prior to their corresponding growth test. All hydrogels were cut into 10 mm diameter disks (n = 3 for each type of hydrogel). The dimensions of each disk were measured before growth. ELMs containing active dried yeast and cell-free hydrogels were incubated in the same culture flasks but separately for each CNC composition using 175 mL of synthetic complete medium. ELMs containing each probiotic mutant were grown in 175 mL of synthetic complete medium and in 175 mL of synthetic medium lacking their corresponding amino acid or nucleotide. All disks were incubated in aerobic conditions at 30º C for 48 h with constant agitation (200RPM). Volume changes were measured every 12 hours for 48 hours using a Canon Rebel T7i camera.

3.5.7. Mechanical characterization

ELMs containing active dried yeast with 11 wt% CNC and cell-free hydrogels containing 22 wt% CNC were selected for mechanical characterization. Briefly, samples

(3 mm x 3 mm x 1 mm) were cut from polymerized hydrogels in triplicates after equilibration in synthetic medium lacking D-glucose. Compression testing was performed using a MicroSquisher (CellScale Biomaterials Testing). We utilized tungsten beam with a diameter of 1.016 mm that was glued to a 6 mm–by–6 mm platen on one end. This tungsten beam was attached from the opposite end of the glued platen to the machine's actuator using a cantilever beam grip. Samples were loaded to the test chamber filled with dH_2O at room temperature. The bottom part of the flat platen was brought into contact with the sample before measurements. The actuator was programmed to move at a rate of 0.5 mm/min. Force as a function of displacement was measured along the height (1-mm dimension) of the sample and calculated by the machine's software using the beam's stiffness, beam's length, and the changing height. To calculate compressive modulus, we used strains from 1 to 20% because the stress-strain response in this region was linear.

3.5.8. Probiotic mutant growth on agar plates

All probiotic mutants were plated on synthetic medium agar (15 wt % agar) plates lacking L-leucine, L-tryptophan, L-histidine, or uracil. Growth was recorded after 60 h of incubation at 30º C using a Canon Rebel T7i camera.

3.5.9. Fabrication of 3D printed structures

The ELM and cell-free inks are loaded into 10 mL plastic syringes that are fitted into the SDS-10 print heads (Hyrel 3D, Norcross, GA), attachments of the System 30M 3D printer (Hyrel 3D, Norcross, GA). For all multi-material printed structures, two SDS-10 print heads are loaded in the 3D printer, and the X-Y coordinates between the two

nozzle tips are calibrated using a Mighty Scope 5M digital microscope. G-codes were designed to direct the print path of each print head to obtain the desired structures. During the printing process, the inks are deposited at room temperature (22º C) through a 250 μm conical nozzle onto cleaned glass slides at printing speeds of 1.5 mm s^{-1} and uniform volumetric flow rates.

For disk geometries composed of ELM (*S. cerevisiae*) and cell-free materials, a concentric print path was first printed to form a 1-layer inner ELM disk of 10 mm diameter. Then, an outer ring with a width of 3 mm was printed to fit around the boundaries of the disk. Bilayers composed of two different probiotic mutants (*S. boulardii*-ura3 and *S. boulardii*-trp1) were printed as rectangular prisms (20 mm x 5 mm x 0.5 mm) using a rectilinear print path that moved along the long geometric axis. First, a 1-layer rectangular prism with a 0.25 mm thickness was printed with the first probiotic mutant, and then the 2-layer with a different mutant was printed on top of the first ELM layer.

To form the bilayers that change shape into multiple structures with probiotic mutants *S. boulardii*-TRP1 and *S. boulardii*-LEU2, a rectangular prism (26.5 mm x 7 mm x 0.25 mm) was printed using a rectilinear print path that moved along the long geometric axis. After printing this layer with the first probiotic mutant, the second layer was printed on top and perpendicular to the long geometric axis of the bottom layer with the second probiotic mutant. This layer formed six stripes (7 mm x 1.5 mm x 0.25 mm) with a spacing of 3.5 mm between the stripes.

To print drug delivery capsules, an ELM ink containing the probiotic mutant *S. boulardii*-TRP1 was printed as a 1-layer square prism (5 mm x 5 mm x 0.25 mm) using a concentric print path. Then a hollow rectangular prism (8 mm x 5 mm x 5 mm) with a 0.5 mm thickness using cell-free ink was printed on top of the ELM structure. After printing, the hollow structure was filled with 50 μL of Thermo Scientific™ Fluoro-Max Red Aqueous Fluorescent Particles. To close the capsule geometry, a hollow pyramidal structure (4 mm height and 0.5 mm thick) made of cell-free ink was printed on top of the rectangular prism. This geometry avoided the material collapsing on the open part of the rectangular prism and allowed the fabrication of a sealed capsule.

After printing, all structures were placed in a nitrogen environment and photopolymerized under UV (Omnicure LX500) irradiation at 365 nm with an intensity of 10 mW/cm^2. All geometries were exposed for 35 s to irradiate from the top and then flipped and exposed for another 35 s to irradiate from the bottom.

3.5.10. Shape changes of 3D printed geometries

All shape changes of the 3Dprinted structures in this research study were recorded every 12 h using a Canon Rebel T7i camera. Bilayer structures with one type of shape change were grown at 30º C with constant shaking (200 RPM) in aerobic conditions. Every bilayer was grown in 50 mL of synthetic medium lacking L-tryptophan for 36 h and then in 50 mL of synthetic medium lacking uracil. The medium was changed every 12 h.

Bilayers with multiple shape transformations were grown at 30º C with constant shaking (200 RPM) in aerobic conditions. One set of these bilayers (n = 3) was grown in

synthetic medium lacking L-tryptophan, and another set (n = 3) was grown in synthetic medium lacking L-leucine. The medium was changed every 12 h.

3D printed drug delivery capsules were grown at 37º C with constant shaking (180 RPM) in aerobic conditions. The experimental set of these bilayers (n = 3) was grown in synthetic complete medium. Positive controls (n = 3) were grown in synthetic medium lacking L-tryptophan and were manually ruptured at the bottom ELM layer to allow the release of the model drug throughout the experiment. Negative controls (n = 3) were grown in synthetic medium lacking L-tryptophan. Every capsule was grown separately in 50 mL of their corresponding medium. Medium was collected every 12 h and centrifuged for further experiments using flow cytometry.

3.5.11. Flow cytometry

The number of released fluorescent microparticles was quantified using a BD Accuri C6 flow cytometer. The solution around the devices was centrifuged to collect the released microparticles, which were then resuspended in dH_2O to make a total solution of 5 mL prior to flow cytometry. Dilutions were made by pipetting 100 µL of the 5 mL solution containing microparticles in 900 µL of dH_2O. For each sample, 250 µL of the diluted solution was run through the cytometer, with gating such that particles showing high fluorescence (~10^6, similar to that of the Fluoro-Max Red Aqueous Fluorescent Particles) in the 580 nm emission range being counted. All samples were run in triplicate.

3.5.12. Statistical analysis

Statistical comparisons were determined using Student's *t*-test or one-way ANOVA followed by a *post-hoc* Tukey test (GraphPad Prism 9). Data are shown as the mean $\pm$ standard deviation. For all tests, a $P < 0.05$ was used to consider the results statistically significant.

4. CONTROLLING CELL RELEASE IN SHAPE MORPHING LIVING MATERIALS

4.1. Abstract

Here, an approach that uses shape changing prokaryotic ELMs to deliver cells to the surroundings is investigated. We fabricate ELMs comprised of different loadings of prokaryotes and control material's chemistry to understand better the delivery behavior of cells from these encapsulating matrices. Cell viability of ELMs is studied to quantify the approximate number of viable cells capable of driving mechanical transformations. The combination of materials properties and the control of ELM chemistry enables materials with controlled cell delivery. ELMs that change volume up to 100% can deliver 3× the number of cells after 24 h of incubation compared to 2 h of incubation. These prokaryotic ELMs could potentially be used in biomedical applications for the long-term controlled delivery of bacteria probiotics within the human body.

4.2. Introduction

Engineered living materials (ELMs) are a class of materials that use living organisms incorporated into biomaterial matrices. The biological activity of living cells, such as bacteria and yeast, and their ability to be genetically engineered, is crucial to impart multifunctionality in materials.[255] Matrices, such as biofilms can also be produced by living cells to engineer the living material itself.[288,289] ELMs with functionalities for biomedical applications have been implemented to create devices for biomedical applications. For example, wearable sensors that encapsulate engineered microbes and respond by expressing fluorescent proteins have been designed.[76] Drug delivery engineered biofilms have been created to elute growth factors for stem cell

differentiation.[161] Bacterial matrices have been fabricated with adhesive properties for potential treatments in chronic inflammation.[290] ELMs that use biomaterial matrices are typically hydrogels that are soft and porous to maintain the survival of the living microorganisms by facilitating the diffusion of water, nutrients, gases, and biomolecules and protecting the cells from harsh conditions.[291] Natural and synthetic hydrogels, which provide the bulk of the materials, are generally used for the synthesis of ELMs.[257,292,293] All these biomaterial matrices provide a protective habitat for the cells to allow cell growth and proliferation. Their properties can be tuned to best suit desired functionalities for diverse applications.

Biomaterial matrices with tunable mechanical and chemical properties can control the growth of cells and modulate interactions with the surrounding environment.[294] Such control is usually difficult to obtain by simply using traditional culture techniques of cells growing in suspension. ELMs with controlled growth and activity of cells within soft matrices can be used to fabricate biosensing, therapeutic, self-healing, and shape-morphing devices.[128,258,295,296] For example, a tough hydrogel material was designed as a biocontainment platform to lower the escape to the surroundings of genetically engineered bacteria capable of sensing and responding to specific biomolecules.[256] In another example, *Staphylococcus epidermis* encapsulated within a membrane-in-gel patch was fabricated to secrete beneficial factors that act against skin pathogens.[297] In these approaches, the engineering of a matrix capable of reducing cell escape was necessary to avoid the unwanted release of genetically modified cells. Many other ELMs do not fully retain cells within the encapsulating

matrix during cultivation, and cells that escape can proliferate within the surrounding media.

We have previously reported that yeast proliferation within polyacrylamide hydrogels can be controlled to drive complex shape transformations in materials, but it was observed that cells are able to escape from the composites and freely proliferate.[197] The same behavior was observed in another of our reports, where ELM bioinks encapsulating yeast probiotics were designed to create 3D objects that delivered a model drug by using this yeast proliferation-driven shape change.[296] For these studies, we took advantage of the mechanical properties of yeast, which have stiff cell walls with Young's modulus of approximately 110 MPa.[298] As these cells are stiffer than the soft biomaterial matrices, they are able to proliferate and cause ELM volumetric expansions. Nevertheless, the use of yeast for delivery applications within the body is reduced to one type of probiotic yeast strain, *Saccharomyces boulardii*.[299] For the purpose of using ELMs as future delivery platforms in the human body, bacteria probiotics are a primary candidate, as these cells are used in many food products or dietary supplements and are extensively studied in synthetic biology approaches.[300,301] For example, *Escherichia coli* also has a stiff cell envelope with Young's modulus between 50-150 MPa and has also been found in probiotic forms.[302] In the present study, we seek to understand the behavior of prokaryotic strains embedded in hydrogel matrices to create ELMs that change shape and deliver the cells themselves.

Approaches that utilize bacterial release from the ELM itself could provide novel ways to use ELMs for applications that require cells to be continuously delivered. For

example, ELMs could deliver probiotics to places in the body for therapeutic purposes, like treating infections. For example, ELMs could be placed within the bladder to inhibit the growth and persistence of uropathogenic strains that cause urinary tract infections. These approaches could be used in future preventative care or treatments in patients that suffer from recurrent urinary tract infections.

Here, we introduce a method to controllably deliver bacteria from ELM hydrogels of different stiffnesses and cell densities. This cell delivery occurs from shape changing composites, which will potentially enable multifunctional medical devices. Bacteria, *Escherichia coli*, embedded within synthetic hydrogel matrices, form prokaryotic ELMs that change shape due to cell proliferation (Figure 4-1A). Due to the forces that drive these shape changes, and the cells found on or near the surface of the ELMs, cells can be delivered from the object and freely proliferate in the surrounding growth media (Figure 4-1A). We seek to quantify this cell delivery over time by performing a series of experiments that will help us understand the control needed to deliver cells by modulating the stiffness and initial cell loading of ELMs. By controlling the number of cells released from ELMs, we foresee applications where ELMs could be

used in the continuous delivery of bacteria probiotics that are not capable of colonizing the human body.

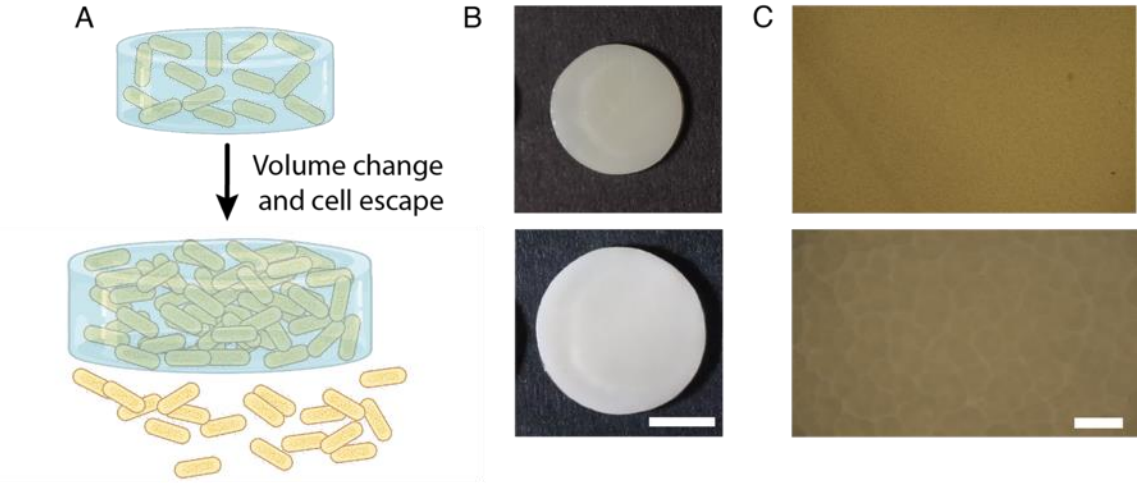

Figure 4-1: Prokaryotic ELM volume change
(A) Schematic represents an ELM encapsulating *E. coli*. The ELM is capable of changing in volume and deliver cells to the surroundings during incubation. (B) Prokaryotic ELM change in volume. Before incubation (Top) and after incubation (Bottom) (Scale bar: 5 mm). (C) Microscopic image of prokaryotic ELM before incubation (Top) and after incubation (Bottom) (Scale bar: 200μm).

4.3. Results and discussion

4.3.1. Fabrication and characterization of prokaryotic ELMs

A series of prokaryotic ELMs embedding *E. coli* were fabricated and their physical properties characterized. Prokaryotic ELMs are comprised of *E. coli* DH5α strain modified with an ampicillin resistant plasmid. These bacteria are encapsulated within hydrogels made of 2-hydroxyethylacrylate (HEA) crosslinked with *N*, *N*'-methylenebisacrylamide (BIS). ELMs with varying stiffnesses were fabricated by changing the monomer and crosslinker contents and by loading with high cell concentrations (3 x 10^{11} cells/mL). These formulations were comprised of 10% HEA with 0.1% BIS (10H/0.1B), 10% HEA with 0.4% BIS (10H/0.4B), and 15% HEA with

0.4% BIS (15H/0.4B). ELMs with different cell densities were also fabricated by loading high (3 x 10^{11} cells/mL), medium (1 x 10^{11} cells/mL), and low (3 x 10^{10} cells/mL) cell densities within the 10H/0.1B formulation. For all formulations, ELMs with a thickness of 250 μm cut into 10 mm diameter disks were grown in Lysogeny Broth (LB) media containing the antibiotic ampicillin at 37ºC under shaking and aerobic conditions. Due to the mechanical properties of the loaded bacteria,[302] cells are capable of proliferating within the soft acrylic matrices and changing the global shape of the ELM (Figure 4-1B). By observing the in-situ proliferation of cells within the matrices under the optical microscope, colony formation is observed during 24 h of incubation and is found throughout the composite's thickness and along the surface (Figure 4-1C).

The presence of viable cells within biomaterial matrices is key to designing shape changing ELMs. It has been reported that encapsulation of microorganisms within acrylic hydrogels can result in a loss in the number of cells that are viable.[303] We performed experiments to study the cell viability of bacteria after being exposed to monomer solutions (10H/0.1B, 10H/0.4B, 15H/0.4B, and 20H/0.4B) for 2 min and 10 min using a plate counting technique. It is important to note that, when crosslinking ELMs, gelation for all formulations happens within 2 min, but the total polymerization time, meaning the time before the hydrogels are demolded and washed, was set to 10 min. We selected this method to measure cell viability because determining cell viability directly in polymerized ELMs is difficult. A direct assessment of cell viability cannot be performed by plate counting because of the insoluble nature of the acrylic hydrogel.

Direct staining and imaging assessments cannot give accurate information about which cells are viable when large number of cells are encapsulated and clustered together.

Mixing bacteria in monomer solutions of varying monomer and crosslinker concentrations help us evaluate which formulations are best suited to fabricate shape changing prokaryotic ELMs to deliver cells to the surroundings. Cell viability was compared between control samples of cells exposed to LB-amp media and samples that were exposed to monomer solutions used to make ELMs with different stiffnesses. Cell viability of control samples was significantly higher when comparing the viability of all monomer solutions with the control sample after the cells were exposed for 2 min (one-way ANOVA, $P < 0.0001$ for 10H/0.1B, 15H/0.4B, 20H/0.4B and $P < 0.05$ for 10H/0.4B) (Figure 4-2). After 10 min exposure, there was no significant difference between the cell viability of formulations 10H/0.1B and 10H/0.4B compared to the control (one-way ANOVA, $P > 0.05$), but viability was significantly higher in control samples compared to formulations 15H/0.4B and 20H/0.4B (one-way ANOVA, $P < 0.0001$) (Figure 4-3). Cell viability for the formulation 20H/0.4B compared to the rest of the formulations was significantly lower (unpaired *t*-test, $P < 0.0001$) (Figure 4-3). This latter result implies that exposing bacteria to high monomer concentrations can critically decrease cell viability. Future studies should focus on evaluating viable cells within polymerized ELMs. These studies can help us understand the number of viable cells responsible for colony formation within ELMs.

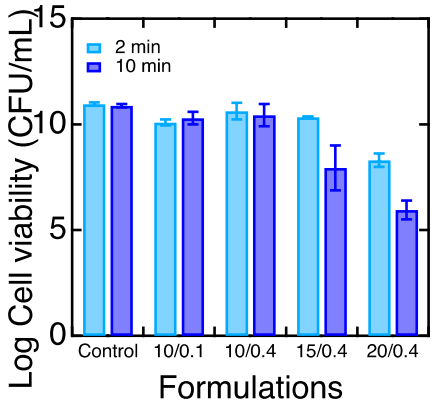

Figure 4-2: Cell viability of bacteria after exposure to pre-gel solutions
Log cell viability as a function of the formulation that cells were exposed to. Bacteria was exposed to these pre-gel solutions for 2 min and 10 min.

Bacterial colony formation within synthetic matrices can be tuned by controlling the initial composition of the ELM. By varying the initial cell loading of bacteria from medium cell loading to high cell loading in 10H/0.1B formulations, the volume change of the ELMs increases significantly from 56.1 % ± 11.7% to 92.9 % ± 14.8 % after 24 h of incubation (*t*-test, $P < 0.05$) (Figure 4-3A). After 48 h of incubation, there was no significant difference observed between the volume changes of these ELMs (82.9 % ± 24.9 % vs. 115.7 % ± 11.7%, *t*-test, $P > 0.05$) (Figure 4-3A). Finally, after 72 h of incubation, ELMs made with high cell concentrations had a significantly greater change in volume compared to the change in volume of ELMs with medium cell concentration (105.9 % ± 11.9% vs. 174.1 % ± 16.7 %, *t*-test, $P < 0.01$) (Figure 4-3A). From these results, we observe that all volume changes of ELMs with medium cell loading were lower compared to ELMs with high cell loading. These results denote that bacterial

proliferation changes the global shape of the ELMs, and these changes can be controlled by modulating the initial cell loading within synthetic matrices.

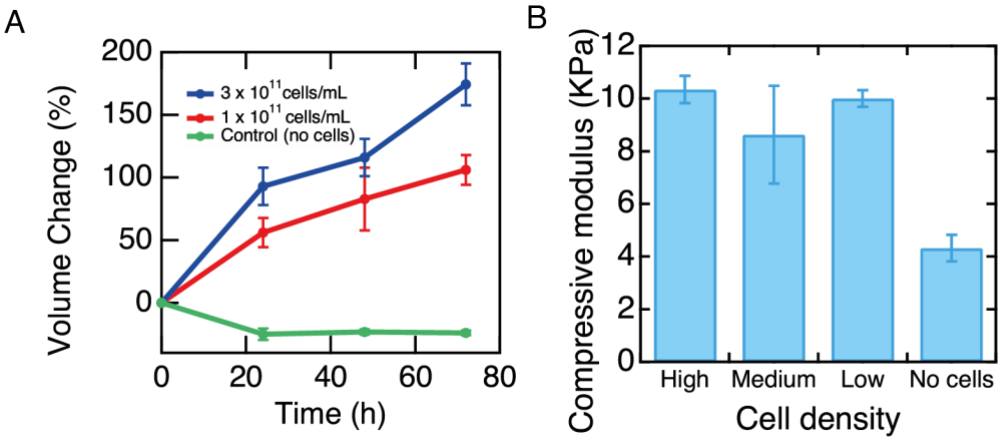

Figure 4-3: Volume change of prokaryotic ELMs can be controlled
(A) Volume change of ELMs with varying cell densities as a function of time. (B) Compressive modulus as a function of cell density.

Mechanical studies of ELMs with varying cell loadings suggest that the presence of cells within hydrogels increases the stiffness of the biomaterial matrix. The Young's modulus of the materials was assessed, and results indicate that there is no significant difference between the compressive modulus of ELMs made with high, medium, and low cell loadings (one-way analysis of variance (ANOVA), $P > 0.05$) (Figure 4-3B). However, there was a significant difference between the compressive modulus of all these ELMs and the modulus of hydrogels fabricated without cells (one-way ANOVA, $P < 0.01$) (Figure 4-3B). Further studies using low cell loadings within ELMs will provide us with a better understanding of the number of cells needed to design ELMs with shape changing capabilities.

The mechanical transformations of prokaryotic ELMs are influenced by the composition of the biomaterial matrix. As formulations with different concentrations of HEA and BIS were synthesized, ELMs varied in stiffness. These materials undergo volumetric changes after 72 h of incubation that decrease from 174 % ± 16 % to 95% ± 45% (Figure 4-3A) as the encapsulating matrix increases in stiffness from 10 kPa ± 1 kPa to 39 kPa ± 16 kPa for 10H/0.1B and 15H/0.4B formulations respectively (Figure 4-4A, B). This decrease in volume change can be attributed to an increase in the elastic resistance to the expanding bacterial colonies that could result in limited colony formation. It could also be attributed to a certain loss in cell viability of the total number of bacteria.

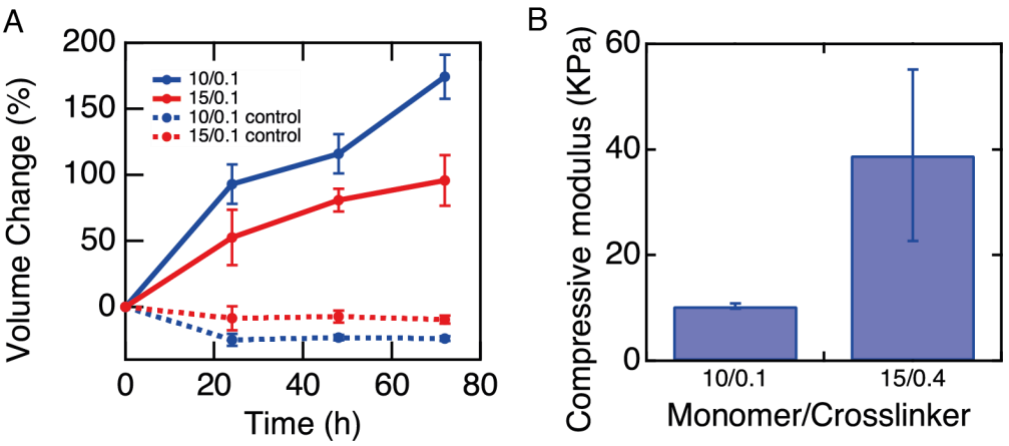

Figure 4-4: Volume change of prokaryotic ELMs can be controlled
(A) Volume change of ELMs with varying crosslinking densities as a function of time. (B) Compressive modulus as a function of crosslinking density of gels before incubation.

4.3.2. Bacterial release and quantification

We hypothesize that the mechanical properties and the initial number of cells loaded into the ELMs affect cell delivery to the surrounding media. As we described in

the previous section, the mechanical properties and volume changes can be controlled by changing the concentrations of monomer and crosslinker and by adjusting the number of cells loaded. We have previously shown that delivery of a model drug from a reservoir in ELMs is driven by mechanical changes of the ELM.[296] Within the scope of this research, we set out to use prokaryotes that proliferate within hydrogels, and that can be delivered to the surrounding media. These ELMs could potentially be used to deliver the living component itself, for example, by delivering probiotics.

The control that we have over the mechanical and physical properties of ELMs can be utilized to adjust the number of cells delivered to the surrounding media. We quantified the number of cells delivered into the media (CFU/mL) from ELMs with varying stiffnesses and with a high and medium number of cells loaded using traditional plating techniques. ELMs were grown in LB-amp media for a total of 30 h where aliquots (100 μL) of the growth media were collected at 2 h, 4 h, 24 h incubation + 2 h, and 24 h incubation + 4 h. It is important to note that after 24 h of incubation, ELMs were washed in PBS and then placed in fresh LB-amp to collect aliquots of the media after an additional 2 h and 4 h of incubation. Before 24 h of incubation, during the first 2 h and 4 h of incubation, all ELMs delivered cells to the surrounding media (Figure 4-5, Figure 4-6).

We hypothesize that delivered cells to the surrounding media come from the ELM itself and that this release is due to the ability of the ELMs to change shape. For ELMs with varying stiffness, cell delivery in formulations made with 10H/0.1B were significantly lower as compared to 10H/0.4B (one-way ANOVA, $P < 0.01$) and

significantly higher as compared to 15H/0.4B (one-way ANOVA, $P < 0.0001$) for the first 2 h of incubation (Figure 4-5A). This low cell delivery in 15H/0.4B formulations can be attributed to the stiffness of the material, where it is observed that the encapsulated cells find it challenging to proliferate within stiff matrices, as these materials have lower volumetric changes (Figure 4-4). After 4 h of incubation, the higher number of cells compared to 2 h could be a combination of both cells that come from the ELM itself and cells that are replicating within the media (Figure 4-5A). During the first 2 h of incubation, we note that cell delivery is relatively low compared to the cell delivery in ELMs that are incubated for 24 h + 2 h.

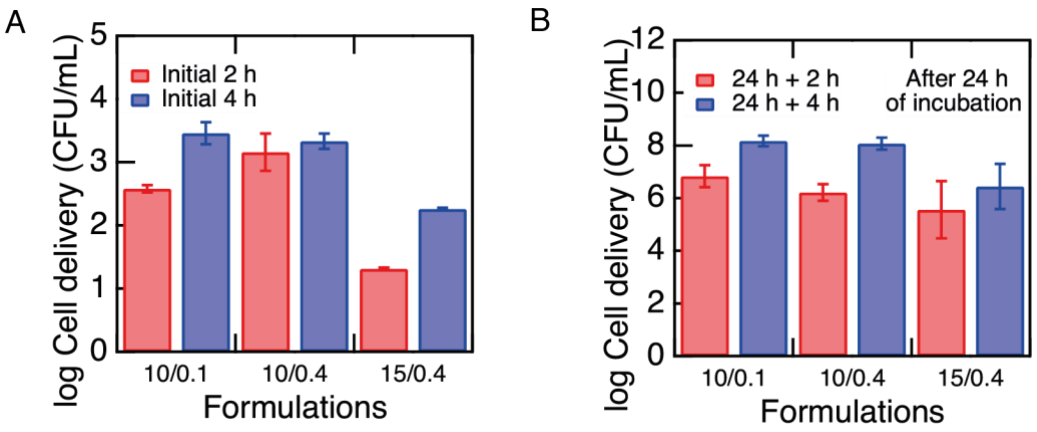

Figure 4-5: Cell delivery as a function of ELMs with varying crosslinking density (A) Log cell delivery as a function of ELM crosslinking formulations at the first 2 h and 4 h of incubation. (B) Log cell delivery as a function of ELM crosslinking formulations after growing for 24 h. Cell delivery was measured at 24 h + 2 h and 24 h + 4 h.

After 24 h of incubation, cell delivery measured at 24 h + 2 h was significantly higher in all formulations with varying stiffnesses as compared to the release at the initial 2 h of incubation (one-way ANOVA, $P < 0.0001$) (Figure 4-5B). There is no significant difference between the delivery of 10H/0.1B and 10H/0.4B or 10H/0.4B and

15H/0.4B formulations at 24 h + 2 h (one-way ANOVA, $P > 0.05$). Between 10H/0.1B and15H/0.4B, there was a significantly higher cell delivery from 10H/0.1B ELMs, also thought to be due to the difference in material stiffness (Figure 4-5B). A more extensive range of materials synthesized with higher stiffness was thought to better the control of delivered cells, but polymerization in stiffer matrices can affect the viability of the cells, as shown in our previous experiments. Moreover, at these incubation time points, cells are delivered at a higher rate, which corresponds to the materials getting larger in volume and, at the same time, to the higher presence of cells found within colonies formed in one day. Nevertheless, because of these observations, it is unclear how many cells that were encapsulated are, in fact, released from the material at any time point. Further studies could focus on evaluating the number of cells released at shorter collection times and in both LB-amp media and PBS as a control.

Next, we hypothesize that initial cell loading within ELMs controls the number of delivered cells. For formulations with high and medium cell loading, higher cell delivery was observed at 24 h + 2 h as compared to the initial 2 h because of the same observations discussed above (Figure 4-6B). Nevertheless, cell delivery at either the initial 2 h or 24 h + 2 h was not significantly different between both cell loadings. This information tells us that, over these ranges of loaded cell densities, no control can be obtained as no large differences between cell delivery are recorded. In the future, we will further characterize these materials by further varying the initial loading of cells. The results described within both sections give us information that, after 24 h of incubation, ELMs capable of having volume changes of 100% can deliver at least 3× the number of

cells compared to the number of cells delivered within the first 2 h of incubation. Ultimately, by further characterizing the cell delivery behavior of ELMs, we expect to modulate the stiffness and initial cell loading further to obtain better control of cell delivery to the surrounding environment. We envision that a multifunctional materials platform could be designed for biomedical applications by coupling shape change, prokaryotic delivery, and fabrication techniques. This platform could enable the release of encapsulated therapeutics from a reservoir in addition to the controlled delivery of probiotics to specific places in the body.

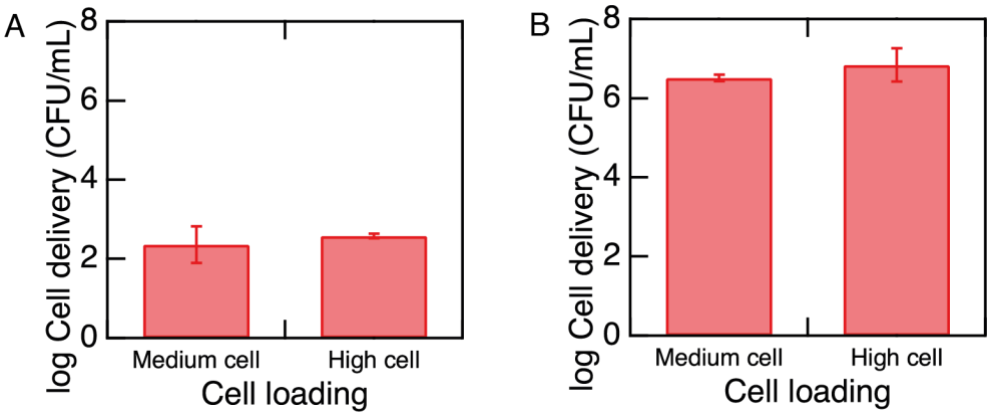

Figure 4-6: Cell delivery as a function of ELMs with varying cell density
(A) Log cell delivery as a function of ELM cell density formulations at the initial 2 h of incubation (B) Log cell delivery as a function of ELM cell density formulations after growing for 24 h. Cell delivery was measured at 24 h of incubation + additional 2 h.

4.4. Conclusions

We studied the ability of shape changing prokaryotic ELMs to delivery cells to the surrounding media. We tuned the mechanical and physical properties of these materials to understand how we can further control the number of delivered cells. Prokaryotic ELM fabrication using acrylic hydrogels significantly affect the viability of the total number of encapsulated cells when using monomer solutions of high monomer

and crosslinker concentrations. Nevertheless, ELMs have large deformations, indicating that a relatively high quantity of cells that remain viable form colonies that contribute to the large changes in volumes obtained. By increasing the stiffness of ELMs, we observed that materials decrease in deformation due to lower cell proliferation and that the delivered number of cells can be significantly lowered. However, the ability of ELMs to change shape allows cells to be delivered in high quantities to the surroundings after long periods of incubation, in a continuous fashion. Further studies need to be conducted to understand how other formulations of ELMs and the initial cell loading affects cell delivery. These prokaryotic ELMs could potentially be used in the controlled delivery of bacteria probiotics. Furthermore, encapsulating bacteria probiotics in ELMs could be used in approaches to achieve continuous cell release to the surrounding tissue. For example, a cell delivery device could be designed to deliver probiotics to outcompete pathogenic strains that colonize the gastrointestinal tract or the bladder and that cause infections.

4.5. Materials and methods

4.5.1. Materials

2-Hydroxyethylacrylate (HEA), *N*,*N*′-methylenebisacrylamide (BIS), ammonium persulfate (APS), *N*,*N*,*N*′,*N*′-tetramethylethylenediamine (TEMED), sodium chloride, and agar were purchased from Sigma-Aldrich. Yeast extract, tryptone, ampicillin sodium salt, and PBS tablets were purchased from Fisher Scientific. All chemicals were used as received without further purification.

4.5.2. Bacterial growth and quantification for encapsulation in ELMs

To grow bacteria to a high density, *Escherichia coli* DH5α (transformed with pAAV-Syn-GFP plasmid) were first incubated for 7 h in culture tubes containing 7 mL of Lysogeny Broth (LB) media [0.5 wt % yeast extract, 1 wt % tryptopne, 1 wt % sodium chloride, and 50 μg of ampicillin per mL of media] at 37^{o} C in a shaking incubator at 200 RPM. Subsequently, bacteria overgrowths were made using twelve flasks containing 2 overnight tubes each with 50 mL of LB. Overgrowths were combined and cell density was measured to calculate the volume needed to reach approximately 5.7×10^{11} cells (High cell concentration). This number of cells was centrifuged, washed three times in PBS, and then centrifuged to obtain a pellet. For ELMs with medium and low cell concentration, pellets with 2.8×10^{11} cells and 5.7×10^{10} cells were collected respectively.

To quantify the number of bacteria, cell density was measured with a Genesys 10S UV/visible spectrophotometer by observing the optical density at 600 nm. Each of the pellets collected was suspended in 25 mL of PBS. Then, ten-fold serial dilutions from 1:10 to 1:1000 were made (n = 3) by mixing 0.1 mL of the initial suspension with 0.9 mL of PBS. Diluted bacteria solutions were pipetted into a 1-mL cuvette for spectrophotometer measurements. Optical densities between 1.6 and 0.03 were measured for these dilutions.

4.5.3. Mold construction

For volume change and cell release experiments, molds were used to create flat sheets of the prokaryotic ELMs. Molds were made of two glass slides (75 mm by 51

mm) sterilized with heat. The unpolymerized material was sandwiched between the glass slides separated by 0.25-mm thick spacer. For mechanical testing, the unpolymerized material was sandwiched between the glass slides separated by 1-mm thick spacer.

4.5.4. Preparation of prokaryiotic ELMs

ELM prokaryotics were prepared at room temperature by free radical polymerization of HEA monomer and BIS crosslinker. HEA was filtered sterilized prior to ELM preparation. Stock solutions of BIS (0.02 g/ml) were prepared in dH_2O and filter sterilized. All ELMs with varying crosslinking densities were prepared with high cell densities and using 10 wt % HEA with 0.1 wt% BIS or 0.4 wt% BIS and 15 wt% HEA with 0.4 wt% BIS. ELMs with varying cell density were prepared using 10 wt% HEA and 0.1 wt% BIS with cell loadings of 3×10^{11} cells and 1×10^{11} cells. To polymerize ELMs with varying crosslinker density, a 10 wt% APS stock solution was added at 1% of the total solution volume, and TEMED was added at a ratio of 0.1% of total solution volume. To polymerize ELMs with medium cell density, APS was added at 1.3% of the total solution volume, and TEMED was added at a ratio of 0.13% of total solution volume. To polymerize ELMs with low cell density, APS was added at 1.5% of the total solution volume, and TEMED was added at a ratio of 0.15% of total solution volume After adding APS and TEMED to all pre-gel solution, they were vortexed for 3 s and quickle pipetted into the molds. Filled molds were flipped every 45 s, while polymerization occurred to avoid bacteria settling. After 10 min, polymerized ELMs were demolded and rinsed three times with LB-amp media to remove unpolymerized

HEA residues. ELMs were stored in LB-amp at 4ºC for 24 hours before mechanical testing, volume change, and cell release experiments.

4.5.5. Volume change quantification

To quantify volume changes in prokaryotic ELMs, samples were molded in 0.25-mm thick molds. All ELMs were stored in LB-amp for 24 h prior to growth test. All ELMs were cut with a biopsy punch of 10 mm diameter to make ELM disks (n = 3 for each type of formulation). The dimensions of each disk were measured before growth. All ELM formulations (n = 3) were grown in 250 mL flasks with 150 mL of LB-amp (3 gels per flask) for 72 h at 37ºC in aerobic conditions with constant agitation (200 RPM). (200RPM). Volume changes were measured every 24 hours using a Canon Rebel T7i camera.

4.5.6. Cell release quantification

All ELM formulations were molded and stored as described in the volume change quantification section. After storage, ELMs were punched (n = 3), washed three times in PBS, and each sample was placed in 50 mL of LB-amp media. Before incubation, an aliquot (100 μL) of media for all formulations was plated on LB-amp agar plates (1.5 wt% agar) using sterile glass beads that are shaken back and forth on the plate for around one minute. All samples were incubated at 37ºC under constantig shaking (200 RPM) and aerobic conditions. After 2 h and 4 h, an aliquot (100 μL) of growth media was diluted (10-fold dilutions depending on the concentration of cells) and plated using sterile glass beads. The same procedure was followed after ELM formulations are

incubated for 24 h, 48 h, or 72 h. Plates were incubated at 37ºC and colony forming units (CFU) were counted after one day of incubation.

4.5.7. Cell viability quantification

To quantify cell viability for each formulation, we prepared all ELM formulations as described in section 4.5.4 without crosslinking the ELMs using APS and TEMED. A control sample was also prepared by replacing the volume of monomer and crosslinker used in the solution with LB-amp media. All formulations were prepared and after 2 min and 10 min of exposure, an aliquot of the formulation was pipetted, diluted (10-fold dilutions) and plated on LB-amp agar plates using the glass bead plating technique. Plates were incubated at 37ºC and colony forming units (CFU) were counted after one day of incubation.

4.5.8. Mechanical characterization

All ELM samples for mechanical testing (6 mm diameter, 1 mm thickness) were cut from polymerized formulations. Samples were equilibrated in LB-amp media prior to testing. Compression testing was performed using a TA RSA-G2 instrument at room temperature. Briefly, flat plates attached to the instrument were brought into contact with the sample and a bath attachment was placed to run the testing under immersion in LB-amp media. The plates were then set to move at a rate of 0.05 mm/s. Strains between 0.2 % and 5% were used to calculate the Young's modulus, as the stress-strain response in this region was linear.

4.5.9. Optical images of living composites

Microscopic imaging was carried out using a Nikon optical microscope. To visualize embedded bacteria and cell proliferation, samples were observed under bright field and dark field at 10X magnification. Bright field (transmission) was used to observe cell distribution and colony formation throughout the thickness of the sample. Dark field (reflection) was used visualize the surface of the samples (n = 3).

4.5.10. Statistical analysis

Statistical comparisons were studied using Student's *t*-test (paired or unpaired) or one-way ANOVA (followed by a post hoc Tukey test) (GraphPad Prism 9). Data are shown as the mean $\pm$ standard deviation. For all studied, a $P < 0.05$ was utilized to consider the results significantly different.

5. CONCLUSIONS

We have described engineered living materials with programmed functions governed by living microorganisms. ELMs capable of responding to external cues have enabled shape changing materials where cell activity and cell proliferation within the encapsulating biomaterial matrix were key to the overall function of the ELM. We presented a series of studies to understand the fundamental mechanisms that drive these shape changes and performed a series of experiments to understand the potential use of these ELMs in biomedical applications. Importantly, using different approaches of synthetic biology and fabrication techniques, stimuli-responsive ELMs were fabricated that responded to small changes in the environment, enabling materials capable of mechanical transformation in response to single or multiple biochemical or physical cues.

Controlling the necessary parameters that drive cell proliferation within our stimuli-responsive ELMs is of importance when selecting ELM formulations for biomedical applications. As described in chapter 2, baker's yeast, *S. cerevisiae*, was a key model organism used to understand how these cells expand the volume of synthetic materials that do not respond to small changes in external conditions. The addition of these cells to polyacrylamide hydrogels enabled materials with the ability to respond to biochemical cues, such as L-histidine, and physical cues, like low-power blue light. As these cells are stiffer than the encapsulating matrices, high concentration of cells can form colonies that, together, are responsible for driving the large volumetric changes of the whole composite. Controlling the viability of these cells within the thickness and

area of the ELMs enabled materials that undergo complex shape transformations. Although, these transformations were only controlled within 2D materials, we could obtain spatio-temporal control of growth by using an optogenetic switch transformed in yeast that respond to pulses of blue light. The study of these materials addressed a critical need for materials that are capable of sensing highly specific biochemical or physical cues and respond in a mechanical way in a controlled manner.

In chapter 3, we described a fabrication method to 4D print ELMs, where control over the distribution of yeast within 3D structures enabled materials capable of complex shape changes. These shape changes were obtained without compromising the viability of the cells throughout the thickness and area of the composite. Instead, yeast were spatially distributed within 3D objects that were made by using formulations with shear-thinning behavior. The ability to induce shear-thinning characteristics to the formulations described in chapter 2, enabled a way to fabricate ELMs that contained multiple yeast strains within the same structure. These ELMs were capable of responding to the presence of multiple biochemical cues and enabled materials with multiple programmed shape changes. Further, as yeast is also found in probiotic forms, such as *Saccharomyces boulardii*, these ELMs opened a potential direction to build shape-changing devices that could be used within the human body. These devices could be used to detect specific biochemical cues or biomarkers related to disease and act as biosensors or drug delivery devices with the potential to have a control release of therapeutics at the right location and at the right time. As such, with this fabrication technique we enabled the design of a drug-delivery device concept that was capable of

rupturing and releasing a model drug to the surrounding environment when detecting a specific biochemical cue. This 3D printing fabrication technique is a versatile way that can be used in a variety of model organisms such as genetically engineered or probiotic prokaryotes.

In chapter 4, we studied the ability of prokaryotes to drive ELM shape change and controlled the ability to release these cells to the surroundings for the understanding of future probiotic delivery platforms. The fundamental understandings from the work achieved in chapters 2 and 3, opened the path to study the potential use of prokaryotes in the control of the mechanical deformation of ELMs. Control of this mechanical deformation, as well as the mechanical properties and composition of ELMs, is of essential importance to potentially use probiotic prokaryotes that can target pathogenic strains of bacteria or fungi within the human body. We take advantage of a general issue observed in ELMs, where biocontainment of cells is an issue that needs to be targeted. We harness the ability of cells to escape from ELMs during growth to potentially use these materials in probiotic delivery within the gastrointestinal tract or the bladder. Such probiotics could target pathogens related to infectious diseases, such as urinary tract infections, by continuously delivering probiotics to the site of infection and targeting the growth of pathogens that colonize the human body and persist, generally causing recurrent infections.

These works present a significant advancement in the field of engineered living materials, where living cells can be used as sensing components that drive mechanical transformations for future biomedical devices. Future directions should focus on the

study of the local behavior of microorganisms within these matrices, to understand the general forces that cells use to cause volumetric expansion of the materials. Further, cell viability experiments within the encapsulating matrices should be carried out to make sense of the real number of viable cells that contribute to the local and global mechanical transformations of these composites. Approaches that use cell staining techniques, cell tracking, as well as imaging techniques, could be utilized to understand how viable cells form colonies within confined these matrices and how different strains of bacteria or yeast behave when encapsulated.

6. REFERENCES

1. Lendlein A, Langer R. Biodegradable, Elastic Shape-Memory Polymers for Potential Biomedical Applications. *Science*. 2002;296(5573):1673-1676. doi:10.1126/science.1066102

2. Malachowski K, Breger J, Kwag HR, Wang MO, Fisher JP, Selaru FM, Gracias DH. Stimuli-Responsive Theragrippers for Chemomechanical Controlled Release. *Angewandte Chemie Int Ed*. 2014;53(31):8045-8049. doi:10.1002/anie.201311047

3. Choe A, Yeom J, Shanker R, Kim MP, Kang S, Ko H. Stretchable and wearable colorimetric patches based on thermoresponsive plasmonic microgels embedded in a hydrogel film. *Npg Asia Mater*. 2018;10(9):912-922. doi:10.1038/s41427-018-0086-6

4. Yi H, Lee S, Ko H, Lee D, Bae W, Kim T, Hwang DS, Jeong HE. Ultra-Adaptable and Wearable Photonic Skin Based on a Shape-Memory, Responsive Cellulose Derivative. *Adv Funct Mater*. 2019;29(34):1902720. doi:10.1002/adfm.201902720

5. Deng Z, Hu T, Lei Q, He J, Ma PX, Guo B. Stimuli-Responsive Conductive Nanocomposite Hydrogels with High Stretchability, Self-Healing, Adhesiveness, and 3D Printability for Human Motion Sensing. *Acs Appl Mater Inter*. 2019;11(7):6796-6808. doi:10.1021/acsami.8b20178

6. Zhao Y, Shi C, Yang X, Shen B, Sun Y, Chen Y, Xu X, Sun H, Yu K, Yang B, Lin Q. pH- and Temperature-Sensitive Hydrogel Nanoparticles with Dual Photoluminescence for Bioprobes. *Acs Nano*. 2016;10(6):5856-5863. doi:10.1021/acsnano.6b00770

7. Ma C, Lu W, Yang X, He J, Le X, Wang L, Zhang J, Serpe MJ, Huang Y, Chen T. Bioinspired Anisotropic Hydrogel Actuators with On–Off Switchable and Color-Tunable Fluorescence Behaviors. *Adv Funct Mater*. 2018;28(7):1704568. doi:10.1002/adfm.201704568

8. Saed MO, Ambulo CP, Kim H, De R, Raval V, Searles K, Siddiqui DA, Cue JMO, Stefan MC, Shankar MR, Ware TH. Molecularly-Engineered, 4D-Printed Liquid Crystal Elastomer Actuators. *Adv Funct Mater*. 2019;29(3):1806412. doi:10.1002/adfm.201806412

9. Yoon C, Xiao R, Park J, Cha J, Nguyen TD, Gracias DH. Functional stimuli responsive hydrogel devices by self-folding. *Smart Mater Struct*. 2014;23(9):094008. doi:10.1088/0964-1726/23/9/094008

10. Zarek M, Layani M, Cooperstein I, Sachyani E, Cohn D, Magdassi S. 3D Printing of Shape Memory Polymers for Flexible Electronic Devices. *Adv Mater*. 2016;28(22):4449-4454. doi:10.1002/adma.201503132

11. He Q, Wang Z, Wang Y, Minori A, Tolley MT, Cai S. Electrically controlled liquid crystal elastomer–based soft tubular actuator with multimodal actuation. *Sci Adv*. 2019;5(10):eaax5746. doi:10.1126/sciadv.aax5746

12. Ware TH, McConney ME, Wie JJ, Tondiglia VP, White TJ. Voxelated liquid crystal elastomers. *Science*. 2015;347(6225):982-984. doi:10.1126/science.1261019

13. Jeon SJ, Hauser AW, Hayward RC. Shape-Morphing Materials from Stimuli-Responsive Hydrogel Hybrids. *Accounts Chem Res*. 2017;50(2):161-169. doi:10.1021/acs.accounts.6b00570

14. Espinosa LM de, Meesorn W, Moatsou D, Weder C. Bioinspired Polymer Systems with Stimuli-Responsive Mechanical Properties. *Chem Rev*. 2017;117(20):12851-12892. doi:10.1021/acs.chemrev.7b00168

15. Herzer N, Guneysu H, Davies DJD, Yildirim D, Vaccaro AR, Broer DJ, Bastiaansen CWM, Schenning APHJ. Printable Optical Sensors Based on H-Bonded Supramolecular Cholesteric Liquid Crystal Networks. *J Am Chem Soc*. 2012;134(18):7608-7611. doi:10.1021/ja301845n

16. Deng Z, Guo Y, Zhao X, Ma PX, Guo B. Multifunctional Stimuli-Responsive Hydrogels with Self-Healing, High Conductivity, and Rapid Recovery through Host–Guest Interactions. *Chem Mater*. 2018;30(5):1729-1742. doi:10.1021/acs.chemmater.8b00008

17. Zhang S, Bellinger AM, Glettig DL, Barman R, Lee YAL, Zhu J, Cleveland C, Montgomery VA, Gu L, Nash LD, Maitland DJ, Langer R, Traverso G. A pH-responsive supramolecular polymer gel as an enteric elastomer for use in gastric devices. *Nat Mater*. 2015;14(10):1065-1071. doi:10.1038/nmat4355

18. Raman R, Hua T, Gwynne D, Collins J, Tamang S, Zhou J, Esfandiary T, Soares V, Pajovic S, Hayward A, Langer R, Traverso G. Light-degradable hydrogels as dynamic triggers for gastrointestinal applications. *Sci Adv*. 2020;6(3):eaay0065. doi:10.1126/sciadv.aay0065

19. Bozuyuk U, Yasa O, Yasa IC, Ceylan H, Kizilel S, Sitti M. Light-Triggered Drug Release from 3D-Printed Magnetic Chitosan Microswimmers. *Acs Nano*. 2018;12(9):9617-9625. doi:10.1021/acsnano.8b05997

20. Cangialosi A, Yoon C, Liu J, Huang Q, Guo J, Nguyen TD, Gracias DH, Schulman R. DNA sequence–directed shape change of photopatterned hydrogels via high-degree swelling. *Science*. 2017;357(6356):1126-1130. doi:10.1126/science.aan3925

21. Culver HR, Clegg JR, Peppas NA. Analyte-Responsive Hydrogels: Intelligent Materials for Biosensing and Drug Delivery. *Accounts Chem Res*. 2017;50(2):170-178. doi:10.1021/acs.accounts.6b00533

22. Zhang X, Chen L, Lim KH, Gonuguntla S, Lim KW, Pranantyo D, Yong WP, Yam WJT, Low Z, Teo WJ, Nien HP, Loh QW, Soh S. The Pathway to Intelligence: Using Stimuli-Responsive Materials as Building Blocks for Constructing Smart and Functional Systems. *Adv Mater*. 2019;31(11):1804540. doi:10.1002/adma.201804540

23. Zhang H, Zeng H, Priimagi A, Ikkala O. Viewpoint: Pavlovian Materials—Functional Biomimetics Inspired by Classical Conditioning. *Adv Mater*. 2020;32(20):1906619. doi:10.1002/adma.201906619

24. Chen AY, Zhong C, Lu TK. Engineering Living Functional Materials. *Acs Synth Biol*. 2015;4(1):8-11. doi:10.1021/sb500113b

25. Nguyen PQ, Courchesne NMD, Duraj-Thatte A, Praveschotinunt P, Joshi NS. Engineered Living Materials: Prospects and Challenges for Using Biological Systems to Direct the Assembly of Smart Materials. *Adv Mater*. 2018;30(19):1704847. doi:10.1002/adma.201704847

26. Gilbert C, Ellis T. Biological Engineered Living Materials - growing functional materials with genetically-programmable properties. *Acs Synth Biol*. 2018;8(1):1-15. doi:10.1021/acssynbio.8b00423

27. Liu S, Xu W. Engineered Living Materials-Based Sensing and Actuation. *Frontiers Sensors*. 2020;1:586300. doi:10.3389/fsens.2020.586300

28. Huang J, Liu S, Zhang C, Wang X, Pu J, Ba F, Xue S, Ye H, Zhao T, Li K, Wang Y, Zhang J, Wang L, Fan C, Lu TK, Zhong C. Programmable and printable Bacillus subtilis biofilms as engineered living materials. *Nat Chem Biol*. 2018;15(1):34-41. doi:10.1038/s41589-018-0169-2

29. Duraj-Thatte AM, Courchesne ND, Praveschotinunt P, Rutledge J, Lee Y, Karp JM, Joshi NS. Genetically Programmable Self-Regenerating Bacterial Hydrogels. *Adv Mater*. 2019;31(40):1901826. doi:10.1002/adma.201901826

30. Zhang C, Huang J, Zhang J, Liu S, Cui M, An B, Wang X, Pu J, Zhao T, Fan C, Lu TK, Zhong C. Engineered Bacillus subtilis biofilms as living glues. *Mater Today*. 2019;28:40-48. doi:10.1016/j.mattod.2018.12.039

31. Florea M, Hagemann H, Santosa G, Abbott J, Micklem CN, Spencer-Milnes X, Garcia L de A, Paschou D, Lazenbatt C, Kong D, Chughtai H, Jensen K, Freemont PS, Kitney R, Reeve B, Ellis T. Engineering control of bacterial cellulose production using a genetic toolkit and a new cellulose-producing strain. *Proc National Acad Sci*. 2016;113(24):E3431-E3440. doi:10.1073/pnas.1522985113

32. Fang J, Kawano S, Tajima K, Kondo T. In Vivo Curdlan/Cellulose Bionanocomposite Synthesis by Genetically Modified Gluconacetobacter xylinus. *Biomacromolecules*. 2015;16(10):3154-3160. doi:10.1021/acs.biomac.5b01075

33. Vos P de, Faas MM, Spasojevic M, Sikkema J. Encapsulation for preservation of functionality and targeted delivery of bioactive food components. *Int Dairy J*. 2010;20(4):292-302. doi:10.1016/j.idairyj.2009.11.008

34. Mainardi JC, Rezwan K, Maas M. Embedding live bacteria in porous hydrogel/ceramic nanocomposites for bioprocessing applications. *Bioproc Biosyst Eng*. 2019;42(7):1215-1224. doi:10.1007/s00449-019-02119-4

35. Desimone MF, Hélary C, Mosser G, Giraud-Guille MM, Livage J, Coradin T. Fibroblast encapsulation in hybrid silica–collagen hydrogels. *J Mater Chem*. 2010;20(4):666-668. doi:10.1039/b921572g

36. Demirci U, Khademhosseini A, Chen P, Wang S, Inci F, Güven S, Tasoglu S, Demirci U. Cell-Encapsulating Hydrogels for Biosensing. Published online 2016:327-356. doi:10.1142/9789813140417_0012

37. Zujur D, Kanke K, Lichtler AC, Hojo H, Chung U il, Ohba S. Three-dimensional system enabling the maintenance and directed differentiation of pluripotent stem cells under defined conditions. *Sci Adv*. 2017;3(5):e1602875. doi:10.1126/sciadv.1602875

38. Gu Q, Tomaskovic-Crook E, Wallace GG, Crook JM. 3D Bioprinting Human Induced Pluripotent Stem Cell Constructs for In Situ Cell Proliferation and Successive Multilineage Differentiation. *Adv Healthc Mater*. 2017;6(17):1700175. doi:10.1002/adhm.201700175

39. Jones KA, Zinkus-Boltz J, Dickinson BC. Recent advances in developing and applying biosensors for synthetic biology. *Nano Futur*. 2019;3(4):042002. doi:10.1088/2399-1984/ab4b78

40. Inda ME, Lu TK. Microbes as Biosensors. *Annu Rev Microbiol*. 2020;74(1):1-23. doi:10.1146/annurev-micro-022620-081059

41. Hill SJ, Baker JG, Rees S. Reporter-gene systems for the study of G-protein-coupled receptors. *Curr Opin Pharmacol*. 2001;1(5):526-532. doi:10.1016/s1471-4892(01)00091-1

42. Khalil AS, Collins JJ. Synthetic biology: applications come of age. *Nat Rev Genet*. 2010;11(5):367-379. doi:10.1038/nrg2775

43. Hossain GS, Saini M, Miyake R, Ling H, Chang MW. Genetic Biosensor Design for Natural Product Biosynthesis in Microorganisms. *Trends Biotechnol*. 2020;38(7):797-810. doi:10.1016/j.tibtech.2020.03.013

44. Charbonneau MR, Isabella VM, Li N, Kurtz CB. Developing a new class of engineered live bacterial therapeutics to treat human diseases. *Nat Commun*. 2020;11(1):1738. doi:10.1038/s41467-020-15508-1

45. Martin-Yken H. Yeast-Based Biosensors: Current Applications and New Developments. *Biosensors*. 2020;10(5):51. doi:10.3390/bios10050051

46. Struss AK, Pasini P, Daunert S. Recognition Receptors in Biosensors. Published online 2009:565-598. doi:10.1007/978-1-4419-0919-0_14

47. Jiang T, Xing B, Rao J. Recent Developments of Biological Reporter Technology for Detecting Gene Expression. *Biotechnology Genetic Eng Rev*. 2008;25(1):41-76. doi:10.5661/bger-25-41

48. Walhout AJM, Vidal M. High-Throughput Yeast Two-Hybrid Assays for Large-Scale Protein Interaction Mapping. *Methods*. 2001;24(3):297-306. doi:10.1006/meth.2001.1190

49. Davis MP, Sparks JS, Smith WL. Repeated and Widespread Evolution of Bioluminescence in Marine Fishes. *Plos One*. 2016;11(6):e0155154. doi:10.1371/journal.pone.0155154

50. Meighen EA. Molecular biology of bacterial bioluminescence. *Microbiol Rev*. 1991;55(1):123-142. doi:10.1128/mmbr.55.1.123-142.1991

51. Campbell ZT, Weichsel A, Montfort WR, Baldwin TO. Crystal Structure of the Bacterial Luciferase/Flavin Complex Provides Insight into the Function of the β Subunit. *Biochemistry-us*. 2009;48(26):6085-6094. doi:10.1021/bi900003t

52. Daunert S, Barrett G, Feliciano JS, Shetty RS, Shrestha S, Smith-Spencer W. Genetically Engineered Whole-Cell Sensing Systems: Coupling Biological Recognition with Reporter Genes. *Chem Rev*. 2000;100(7):2705-2738. doi:10.1021/cr990115p

53. Gui Q, Lawson T, Shan S, Yan L, Liu Y. The Application of Whole Cell-Based Biosensors for Use in Environmental Analysis and in Medical Diagnostics. *Sensors Basel Switz*. 2017;17(7):1623. doi:10.3390/s17071623

54. Tolle F, Stücheli P, Fussenegger M. Genetic circuitry for personalized human cell therapy. *Curr Opin Biotech*. 2019;59:31-38. doi:10.1016/j.copbio.2019.02.003

55. McCarty NS, Ledesma-Amaro R. Synthetic Biology Tools to Engineer Microbial Communities for Biotechnology. *Trends Biotechnol*. 2018;37(2):181-197. doi:10.1016/j.tibtech.2018.11.002

56. Liu X, Tang TC, Tham E, Yuk H, Lin S, Lu TK, Zhao X. Stretchable living materials and devices with hydrogel–elastomer hybrids hosting programmed cells. *Proc National Acad Sci*. 2017;114(9):2200-2205. doi:10.1073/pnas.1618307114

57. Li P, Müller M, Chang MW, Frettlöh M, Schönherr H. Encapsulation of Autoinducer Sensing Reporter Bacteria in Reinforced Alginate-Based Microbeads. *Acs Appl Mater Inter*. 2017;9(27):22321-22331. doi:10.1021/acsami.7b07166

58. Liu Z, Zhang J, Jin J, Geng Z, Qi Q, Liang Q. Programming Bacteria With Light—Sensors and Applications in Synthetic Biology. *Front Microbiol*. 2018;9:2692. doi:10.3389/fmicb.2018.02692

59. Zhao EM, Zhang Y, Mehl J, Park H, Lalwani MA, Toettcher JE, Avalos JL. Optogenetic regulation of engineered cellular metabolism for microbial chemical production. *Nature*. 2018;555(7698):683-687. doi:10.1038/nature26141

60. Inglés-Prieto Á, Reichhart E, Muellner MK, Nowak M, Nijman SMB, Grusch M, Janovjak H. Light-assisted small-molecule screening against protein kinases. *Nat Chem Biol*. 2015;11(12):952-954. doi:10.1038/nchembio.1933

61. Salinas F, Rojas V, Delgado V, Agosin E, Larrondo LF. Optogenetic switches for light-controlled gene expression in yeast. *Appl Microbiol Biot*. 2017;101(7):2629-2640. doi:10.1007/s00253-017-8178-8

62. Sakar MS, Neal D, Boudou T, Borochin MA, Li Y, Weiss R, Kamm RD, Chen CS, Asada HH. Formation and optogenetic control of engineered 3D skeletal muscle bioactuators. *Lab Chip*. 2012;12(23):4976-4985. doi:10.1039/c2lc40338b

63. Sankaran S, Becker J, Wittmann C, Campo AD. Optoregulated Drug Release from an Engineered Living Material: Self-Replenishing Drug Depots for Long-Term, Light-Regulated Delivery. *Small Weinheim Der Bergstrasse Ger*. 2018;15(5):e1804717. doi:10.1002/smll.201804717

64. Piraner DI, Abedi MH, Moser BA, Lee-Gosselin A, Shapiro MG. Tunable thermal bioswitches for in vivo control of microbial therapeutics. *Nat Chem Biol*. 2017;13(1):75-80. doi:10.1038/nchembio.2233

65. Bañares AB, Valdehuesa KNG, Ramos KRM, Nisola GM, Lee WK, Chung WJ. A pH-responsive genetic sensor for the dynamic regulation of D-xylonic acid accumulation in Escherichia coli. *Appl Microbiol Biot*. 2020;104(5):2097-2108. doi:10.1007/s00253-019-10297-0

66. Mora K de, Millar A, Davidson B, Kozma-Bognar L, Ma H, French C, Bizzari F, Elfick A, Wilson J, Cai Y, Aleksic J, Seshasayee SL, Nicholson J, Ivakhno S. Development of a novel biosensor for the detection of arsenic in drinking water. *Iet Synthetic Biology*. 2007;1(1):87-90. doi:10.1049/iet-stb:20060002

67. Ravikumar S, Ganesh I, Yoo I keun, Hong SH. Construction of a bacterial biosensor for zinc and copper and its application to the development of multifunctional heavy metal adsorption bacteria. *Process Biochem*. 2012;47(5):758-765. doi:10.1016/j.procbio.2012.02.007

68. Zhang J, Barajas JF, Burdu M, Ruegg TL, Dias B, Keasling JD. Development of a Transcription Factor-Based Lactam Biosensor. *Acs Synth Biol*. 2017;6(3):439-445. doi:10.1021/acssynbio.6b00136

69. Daeffler KN, Galley JD, Sheth RU, Ortiz-Velez LC, Bibb CO, Shroyer NF, Britton RA, Tabor JJ. Engineering bacterial thiosulfate and tetrathionate sensors for detecting gut inflammation. *Mol Syst Biol*. 2017;13(4):923. doi:10.15252/msb.20167416

70. Hicks M, Bachmann TT, Wang B. Synthetic Biology Enables Programmable Cell-Based Biosensors. *Chemphyschem*. 2019;21(2):132-144. doi:10.1002/cphc.201900739

71. Brophy JAN, Voigt CA. Principles of genetic circuit design. *Nat Methods*. 2014;11(5):508-520. doi:10.1038/nmeth.2926

72. Courbet A, Endy D, Renard E, Molina F, Bonnet J. Detection of pathological biomarkers in human clinical samples via amplifying genetic switches and logic gates. *Sci Transl Med*. 2015;7(289):289ra83-289ra83. doi:10.1126/scitranslmed.aaa3601

73. Moon TS, Lou C, Tamsir A, Stanton BC, Voigt CA. Genetic programs constructed from layered logic gates in single cells. *Nature*. 2012;491(7423):249-253. doi:10.1038/nature11516

74. Saltepe B, Kehribar EŞ, Yirmibeşoğlu SSS, Şeker UÖŞ. Cellular Biosensors with Engineered Genetic Circuits. *Acs Sensors*. 2017;3(1):13-26. doi:10.1021/acssensors.7b00728

75. Hoynes-O'Connor A, Shopera T, Hinman K, Creamer JP, Moon TS. Enabling complex genetic circuits to respond to extrinsic environmental signals. *Biotechnol Bioeng*. 2017;114(7):1626-1631. doi:10.1002/bit.26279

76. Liu X, Yuk H, Lin S, Parada GA, Tang TC, Tham E, Fuente-Nunez C de la, Lu TK, Zhao X. 3D Printing of Living Responsive Materials and Devices. *Adv Mater*. 2017;30(4):1704821. doi:10.1002/adma.201704821

77. Wang B, Barahona M, Buck M. Engineering modular and tunable genetic amplifiers for scaling transcriptional signals in cascaded gene networks. *Nucleic Acids Res*. 2014;42(14):9484-9492. doi:10.1093/nar/gku593

78. Cassidy MB, Lee H, Trevors JT. Environmental applications of immobilized microbial cells: A review. *J Ind Microbiol*. 1996;16(2):79-101. doi:10.1007/bf01570068

79. de-Bashan LE, Bashan Y. Immobilized microalgae for removing pollutants: Review of practical aspects. *Bioresource Technol*. 2010;101(6):1611-1627. doi:10.1016/j.biortech.2009.09.043

80. Alkayyali T, Cameron T, Haltli B, Kerr R, Ahmadi A. Microfluidic and Cross-Linking Methods for Encapsulation of Living Cells and Bacteria - A Review. *Anal Chim Acta*. 2019;1053:1-21. doi:10.1016/j.aca.2018.12.056

81. Chimene D, Lennox KK, Kaunas RR, Gaharwar AK. Advanced Bioinks for 3D Printing: A Materials Science Perspective. *Ann Biomed Eng*. 2016;44(6):2090-2102. doi:10.1007/s10439-016-1638-y

82. Gopinathan J, Noh I. Recent trends in bioinks for 3D printing. *Biomaterials Res*. 2018;22(1):11. doi:10.1186/s40824-018-0122-1

83. Donderwinkel I, Hest JCM van, Cameron NR. Bio-inks for 3D bioprinting: recent advances and future prospects. *Polym Chem-uk*. 2017;8(31):4451-4471. doi:10.1039/c7py00826k

84. Li YC, Zhang YS, Akpek A, Shin SR, Khademhosseini A. 4D bioprinting: the next-generation technology for biofabrication enabled by stimuli-responsive materials. *Biofabrication*. 2016;9(1):012001. doi:10.1088/1758-5090/9/1/012001

85. Chimene D, Kaunas R, Gaharwar AK. Hydrogel Bioink Reinforcement for Additive Manufacturing: A Focused Review of Emerging Strategies. *Adv Mater*. 2020;32(1):1902026. doi:10.1002/adma.201902026

86. Ji S, Guvendiren M. Recent Advances in Bioink Design for 3D Bioprinting of Tissues and Organs. *Frontiers Bioeng Biotechnology*. 2017;5:23. doi:10.3389/fbioe.2017.00023

87. Deo KA, Singh KA, Peak CW, Alge DL, Gaharwar AK. Bioprinting 101: Design, Fabrication, and Evaluation of Cell-Laden 3D Bioprinted Scaffolds. *Tissue Eng Pt A*. 2020;26(5-6):318-338. doi:10.1089/ten.tea.2019.0298

88. Johnston TG, Fellin CR, Carignano A, Nelson A. Additive manufacturing of catalytically active living material hydrogels. 2019;10982:10. doi:10.1117/12.2518653

89. Qian F, Zhu C, Knipe JM, Ruelas S, Stolaroff JK, DeOtte JR, Duoss EB, Spadaccini CM, Henard CA, Guarnieri MT, Baker SE. Direct Writing of Tunable Living Inks for Bioprocess Intensification. *Nano Lett*. 2019;19(9):5829-5835. doi:10.1021/acs.nanolett.9b00066

90. Connell JL, Ritschdorff ET, Whiteley M, Shear JB. 3D printing of microscopic bacterial communities. *P Natl Acad Sci Usa*. 2013;110(46):18380-18385. doi:10.1073/pnas.1309729110

91. González LM, Mukhitov N, Voigt CA. Resilient living materials built by printing bacterial spores. *Nat Chem Biol*. 2019;16(2):126-133. doi:10.1038/s41589-019-0412-5

92. Smith RSH, Bader C, Sharma S, Kolb D, Tang T, Hosny A, Moser F, Weaver JC, Voigt CA, Oxman N. Hybrid Living Materials: Digital Design and Fabrication of 3D Multimaterial Structures with Programmable Biohybrid Surfaces. *Adv Funct Mater*. 2019;30(7):1907401. doi:10.1002/adfm.201907401

93. Lehner BAE, Schmieden DT, Meyer AS. A Straightforward Approach for 3D Bacterial Printing. *Acs Synth Biol*. 2017;6(7):1124-1130. doi:10.1021/acssynbio.6b00395

94. Schaffner M, Rühs PA, Coulter F, Kilcher S, Studart AR. 3D printing of bacteria into functional complex materials. *Sci Adv*. 2017;3(12):eaao6804. doi:10.1126/sciadv.aao6804

95. Kyle S. 3D Printing of Bacteria: The Next Frontier in Biofabrication. *Trends Biotechnol*. 2018;36(4):340-341. doi:10.1016/j.tibtech.2018.01.010

96. Malik S, Hagopian J, Mohite S, Lintong C, Stoffels L, Giannakopoulos S, Beckett R, Leung C, Ruiz J, Cruz M, Parker B. Robotic Extrusion of Algae-Laden Hydrogels for Large-Scale Applications. *Global Challenges Hoboken Nj*. 2019;4(1):1900064. doi:10.1002/gch2.201900064

97. Johnston TG, Fillman JP, Priks H, Butelmann T, Tamm T, Kumar R, Lahtvee PJ, Nelson A. Cell-Laden Hydrogels for Multikingdom 3D Printing. *Macromol Biosci*. Published online 2020:e2000121. doi:10.1002/mabi.202000121

98. Stojanov S, Berlec A. Electrospun Nanofibers as Carriers of Microorganisms, Stem Cells, Proteins, and Nucleic Acids in Therapeutic and Other Applications. *Frontiers Bioeng Biotechnology*. 2020;8:130. doi:10.3389/fbioe.2020.00130

99. Sarioglu OF, Keskin NOS, Celebioglu A, Tekinay T, Uyar T. Bacteria encapsulated electrospun nanofibrous webs for remediation of methylene blue dye in water. *Colloids Surfaces B Biointerfaces*. 2017;152:245-251. doi:10.1016/j.colsurfb.2017.01.034

100. Letnik I, Avrahami R, Rokem JS, Greiner A, Zussman E, Greenblatt C. Living Composites of Electrospun Yeast Cells for Bioremediation and Ethanol Production. *Biomacromolecules*. 2015;16(10):3322-3328. doi:10.1021/acs.biomac.5b00970

101. Zupančič Š, Škrlec K, Kocbek P, Kristl J, Berlec A. Effects of Electrospinning on the Viability of Ten Species of Lactic Acid Bacteria in Poly(Ethylene Oxide) Nanofibers. *Pharm*. 2019;11(9):483. doi:10.3390/pharmaceutics11090483

102. Moustafa M, Tarek T, Elnouby M, El-Deeb N, Hamad G, Abu-Saied MA, Alrumman S. Potential detoxification of aflatoxin B2 using Kluyveromyces lactis and Saccharomyces cerevisiae integrated nanofibers. *Biocell*. 2018;41(2):67-73. doi:10.32604/biocell.2017.00067

103. Dutta S, Cohn D. Temperature and pH responsive 3D printed scaffolds. *J Mater Chem B*. 2017;5(48):9514-9521. doi:10.1039/c7tb02368e

104. Knierim C, Enzeroth M, Kaiser P, Dams C, Nette D, Seubert A, Klingl A, Greenblatt CL, Jérôme V, Agarwal S, Freitag R, Greiner A. Living Composites of Bacteria and Polymers as Biomimetic Films for Metal Sequestration and Bioremediation. *Macromol Biosci*. 2015;15(8):1052-1059. doi:10.1002/mabi.201400538

105. Schulz-Schönhagen K, Lobsiger N, Stark WJ. Continuous Production of a Shelf-Stable Living Material as a Biosensor Platform. *Adv Mater Technologies*. 2019;4(8):1900266. doi:10.1002/admt.201900266

106. Wang YF, Sekine T, Takeda Y, Yokosawa K, Matsui H, Kumaki D, Shiba T, Nishikawa T, Tokito S. Fully Printed PEDOT:PSS-based Temperature Sensor with High Humidity Stability for Wireless Healthcare Monitoring. *Sci Rep-uk*. 2020;10(1):2467. doi:10.1038/s41598-020-59432-2

107. Zhang YZ, Lee KH, Anjum DH, Sougrat R, Jiang Q, Kim H, Alshareef HN. MXenes stretch hydrogel sensor performance to new limits. *Sci Adv*. 2018;4(6):eaat0098. doi:10.1126/sciadv.aat0098

108. Lei Z, Wang Q, Sun S, Zhu W, Wu P. A Bioinspired Mineral Hydrogel as a Self-Healable, Mechanically Adaptable Ionic Skin for Highly Sensitive Pressure Sensing. *Adv Mater*. 2017;29(22):1700321. doi:10.1002/adma.201700321

109. Gao W, Emaminejad S, Nyein HYY, Challa S, Chen K, Peck A, Fahad HM, Ota H, Shiraki H, Kiriya D, Lien DH, Brooks GA, Davis RW, Javey A. Fully integrated wearable sensor arrays for multiplexed in situ perspiration analysis. *Nature*. 2016;529(7587):509-514. doi:10.1038/nature16521

110. Koh A, Kang D, Xue Y, Lee S, Pielak RM, Kim J, Hwang T, Min S, Banks A, Bastien P, Manco MC, Wang L, Ammann KR, Jang KI, Won P, Han S, Ghaffari R, Paik U, Slepian MJ, Balooch G, Huang Y, Rogers JA. A soft, wearable microfluidic device for the capture, storage, and colorimetric sensing of sweat. *Sci Transl Med*. 2016;8(366):366ra165-366ra165. doi:10.1126/scitranslmed.aaf2593

111. Jin H, Abu-Raya YS, Haick H. Advanced Materials for Health Monitoring with Skin-Based Wearable Devices. *Adv Healthc Mater*. 2017;6(11):1700024. doi:10.1002/adhm.201700024

112. Guk K, Han G, Lim J, Jeong K, Kang T, Lim EK, Jung J. Evolution of Wearable Devices with Real-Time Disease Monitoring for Personalized Healthcare. *Nanomaterials-basel*. 2019;9(6):813. doi:10.3390/nano9060813

113. Moser F, Tham E, González LM, Lu TK, Voigt CA. Light-Controlled, High-Resolution Patterning of Living Engineered Bacteria Onto Textiles, Ceramics, and Plastic. *Adv Funct Mater*. 2019;29(30):1901788. doi:10.1002/adfm.201901788

114. Wang W, Yao L, Cheng CY, Zhang T, Atsumi H, Wang L, Wang G, Anilionyte O, Steiner H, Ou J, Zhou K, Wawrousek C, Petrecca K, Belcher AM, Karnik R, Zhao X, Wang DIC, Ishii H. Harnessing the hygroscopic and biofluorescent behaviors of genetically tractable microbial cells to design biohybrid wearables. *Sci Adv*. 2017;3(5):e1601984. doi:10.1126/sciadv.1601984

115. Elsherif M, Hassan MU, Yetisen AK, Butt H. Wearable Contact Lens Biosensors for Continuous Glucose Monitoring Using Smartphones. *Acs Nano*. 2018;12(6):5452-5462. doi:10.1021/acsnano.8b00829

116. Ding S, Cao S, Liu Y, Lian Y, Zhu A, Shi G. Rational Design of a Stimuli-Responsive Polymer Electrode Interface Coupled with in Vivo Microdialysis for

Measurement of Sialic Acid in Live Mouse Brain in Alzheimer's Disease. *Acs Sensors*. 2017;2(3):394-400. doi:10.1021/acssensors.6b00772

117. Jurado-Sánchez B, Pacheco M, Rojo J, Escarpa A. Magnetocatalytic Graphene Quantum Dots Janus Micromotors for Bacterial Endotoxin Detection. *Angewandte Chemie Int Ed*. 2017;56(24):6957-6961. doi:10.1002/anie.201701396

118. Noh K, Park S. Biosensor Array of Interpenetrating Polymer Network with Photonic Film Templated from Reactive Cholesteric Liquid Crystal and Enzyme-Immobilized Hydrogel Polymer. *Adv Funct Mater*. 2018;28(22):1707562. doi:10.1002/adfm.201707562

119. Hussain S, Park SY. Optical Glucose Biosensor Based on Photonic Interpenetrating Polymer Network with Solid-State Cholesteric Liquid Crystal and Cationic Polyelectrolyte. *Sensors Actuators B Chem*. 2020;316:128099. doi:10.1016/j.snb.2020.128099

120. Oh SY, Hong SY, Jeong YR, Yun J, Park H, Jin SW, Lee G, Oh JH, Lee H, Lee SS, Ha JS. Skin-Attachable, Stretchable Electrochemical Sweat Sensor for Glucose and pH Detection. *Acs Appl Mater Inter*. 2018;10(16):13729-13740. doi:10.1021/acsami.8b03342

121. Hu L, Zhang Q, Li X, Serpe MJ. Stimuli-responsive polymers for sensing and actuation. *Mater Horizons*. 2019;6(9):1774-1793. doi:10.1039/c9mh00490d

122. Jang K, Horne WS, Asher SA. Human Serum Phenylpyruvate Quantification Using Responsive 2D Photonic Crystal Hydrogels via Chemoselective Oxime Ligation: Progress toward Developing Phenylalanine-Sensing Elements. *Acs Appl Mater Inter*. 2020;12(35):39612-39619. doi:10.1021/acsami.0c08787

123. Rizvi AS, Murtaza G, Yan D, Irfan M, Xue M, Meng ZH, Qu F. Development of molecularly imprinted 2D photonic crystal hydrogel sensor for detection of L-Kynurenine in human serum. *Talanta*. 2019;208:120403. doi:10.1016/j.talanta.2019.120403

124. Yu X, Zeng H, Wan J, Cao X. Computational design of a molecularly imprinted polymer compatible with an aqueous environment for solid phase extraction of chenodeoxycholic acid. *J Chromatogr A*. 2019;1609:460490. doi:10.1016/j.chroma.2019.460490

125. Weaver AA, Halweg S, Joyce M, Lieberman M, Goodson HV. Incorporating yeast biosensors into paper-based analytical tools for pharmaceutical analysis. *Anal Bioanal Chem*. 2015;407(2):615-619. doi:10.1007/s00216-014-8280-z

126. Miller RA, Brown G, Barron E, Luther JL, Lieberman M, Goodson HV. Development of a paper-immobilized yeast biosensor for the detection of physiological concentrations of doxycycline in technology-limited settings. *Anal Methods-uk*. 2020;12(16):2123-2132. doi:10.1039/d0ay00001a

127. Tang TC, Tham E, Liu X, Yehl K, Rovner AJ, Yuk H, Isaacs FJ, Zhao X, Lu TK. Tough Hydrogel-Based Biocontainment of Engineered Organisms for Continuous, Self-Powered Sensing and Computation. *Biorxiv*. Published online 2020:2020.02.11.941120. doi:10.1101/2020.02.11.941120

128. Mimee M, Nadeau P, Hayward A, Carim S, Flanagan S, Jerger L, Collins J, McDonnell S, Swartwout R, Citorik RJ, Bulović V, Langer R, Traverso G, Chandrakasan AP, Lu TK. An ingestible bacterial-electronic system to monitor gastrointestinal health. *Science*. 2018;360(6391):915-918. doi:10.1126/science.aas9315

129. Mohammadifar M, Tahernia M, Yang JH, Koh A, Choi S. Biopower-on-Skin: Electricity generation from sweat-eating bacteria for self-powered E-Skins. *Nano Energy*. 2020;75:104994. doi:10.1016/j.nanoen.2020.104994

130. Lantigua D, Kelly YN, Unal B, Camci-Unal G. Engineered Paper-Based Cell Culture Platforms. *Adv Healthc Mater*. 2017;6(22):1700619. doi:10.1002/adhm.201700619

131. Landry BP, Tabor JJ. Bugs as Drugs. *Microbiol Spectr*. 2018;5(5):333-361. doi:10.1128/microbiolspec.bad-0020-2017

132. Chang H, Voyvodic PL, Zúñiga A, Bonnet J. Microbially derived biosensors for diagnosis, monitoring and epidemiology. *Microb Biotechnol*. 2017;10(5):1031-1035. doi:10.1111/1751-7915.12791

133. Beardslee LA, Banis GE, Chu S, Liu S, Chapin AA, Stine JM, Pasricha PJ, Ghodssi R. Ingestible Sensors and Sensing Systems for Minimally Invasive Diagnosis and Monitoring: The Next Frontier in Minimally Invasive Screening. *Acs Sensors*. 2020;5(4):891-910. doi:10.1021/acssensors.9b02263

134. Tanna T, Ramachanderan R, Platt RJ. Engineered bacteria to report gut function: technologies and implementation. *Curr Opin Microbiol*. 2021;59:24-33. doi:10.1016/j.mib.2020.07.014

135. Alvarez-Lorenzo C, Concheiro A. Smart drug delivery systems: from fundamentals to the clinic. *Chem Commun Camb Engl*. 2014;50(58):7743-7765. doi:10.1039/c4cc01429d

136. Mitragotri S, Burke PA, Langer R. Overcoming the challenges in administering biopharmaceuticals: formulation and delivery strategies. *Nat Rev Drug Discov*. 2014;13(9):655-672. doi:10.1038/nrd4363

137. Wells CM, Harris M, Choi L, Murali VP, Guerra FD, Jennings JA. Stimuli-Responsive Drug Release from Smart Polymers. *J Funct Biomaterials*. 2019;10(3):34. doi:10.3390/jfb10030034

138. Yang J, Zhai S, Qin H, Yan H, Xing D, Hu X. NIR-controlled morphology transformation and pulsatile drug delivery based on multifunctional phototheranostic nanoparticles for photoacoustic imaging-guided photothermal-chemotherapy. *Biomaterials*. 2018;176:1-12. doi:10.1016/j.biomaterials.2018.05.033

139. Qu J, Zhao X, Ma PX, Guo B. pH-responsive self-healing injectable hydrogel based on N-carboxyethyl chitosan for hepatocellular carcinoma therapy. *Acta Biomater*. 2017;58:168-180. doi:10.1016/j.actbio.2017.06.001

140. Mohapatra A, Harris MA, LeVine D, Ghimire M, Jennings JA, Morshed BI, Haggard WO, Bumgardner JD, Mishra SR, Fujiwara T. Magnetic stimulus responsive vancomycin drug delivery system based on chitosan microbeads embedded with magnetic nanoparticles. *J Biomed Mater Res Part B Appl Biomaterials*. 2018;106(6):2169-2176. doi:10.1002/jbm.b.34015

141. Yang P, Li D, Jin S, Ding J, Guo J, Shi W, Wang C. Stimuli-responsive biodegradable poly(methacrylic acid) based nanocapsules for ultrasound traced and triggered drug delivery system. *Biomaterials*. 2014;35(6):2079-2088. doi:10.1016/j.biomaterials.2013.11.057

142. Bai S, Ma X, Shi X, Shao J, Zhang T, Wang Y, Cheng Y, Xue P, Kang Y, Xu Z. Smart Unimolecular Micelle-Based Polyprodrug with Dual-Redox Stimuli Response for Tumor Microenvironment: Enhanced in Vivo Delivery Efficiency and Tumor Penetration. *Acs Appl Mater Inter*. 2019;11(39):36130-36140. doi:10.1021/acsami.9b13214

143. Wang B, Liu H, Sun L, Jin Y, Ding X, Li L, Ji J, Chen H. Construction of High Drug Loading and Enzymatic Degradable Multilayer Films for Self-Defense Drug Release and Long-Term Biofilm Inhibition. *Biomacromolecules*. 2017;19(1):85-93. doi:10.1021/acs.biomac.7b01268

144. Bueso YF, Lehouritis P, Tangney M. In situ biomolecule production by bacteria; a synthetic biology approach to medicine. *J Control Release Official J Control Release Soc*. 2018;275:217-228. doi:10.1016/j.jconrel.2018.02.023

145. Maxmen A. Living therapeutics: Scientists genetically modify bacteria to deliver drugs. *Nat Med*. 2017;23(1):5-7. doi:10.1038/nm0117-5

146. Chen Z, He A, Liu Y, Huang W, Cai Z. Recent development on synthetic biological devices treating bladder cancer. *Synthetic Syst Biotechnology*. 2016;1(4):216-220. doi:10.1016/j.synbio.2016.08.001

147. Chien T, Doshi A, Danino T. Advances in bacterial cancer therapies using synthetic biology. *Curr Opin Syst Biology*. 2017;5:1-8. doi:10.1016/j.coisb.2017.05.009

148. Chakravarti D, Wong WW. Synthetic biology in cell-based cancer immunotherapy. *Trends Biotechnol*. 2015;33(8):449-461. doi:10.1016/j.tibtech.2015.05.001

149. Din MO, Danino T, Prindle A, Skalak M, Selimkhanov J, Allen K, Julio E, Atolia E, Tsimring LS, Bhatia SN, Hasty J. Synchronized cycles of bacterial lysis for in vivo delivery. *Nature*. 2016;536(7614):81-85. doi:10.1038/nature18930

150. Isabella VM, Ha BN, Castillo MJ, Lubkowicz DJ, Rowe SE, Millet YA, Anderson CL, Li N, Fisher AB, West KA, Reeder PJ, Momin MM, Bergeron CG, Guilmain SE, Miller PF, Kurtz CB, Falb D. Development of a synthetic live bacterial therapeutic for the human metabolic disease phenylketonuria. *Nat Biotechnol*. 2018;36(9):857-864. doi:10.1038/nbt.4222

151. Bhattarai SR, Yoo SY, Lee SW, Dean D. Engineered phage-based therapeutic materials inhibit Chlamydia trachomatis intracellular infection. *Biomaterials*. 2012;33(20):5166-5174. doi:10.1016/j.biomaterials.2012.03.054

152. Vandenbroucke K, Haard H de, Beirnaert E, Dreier T, Lauwereys M, Huyck L, Huysse JV, Demetter P, Steidler L, Remaut E, Cuvelier C, Rottiers P. Orally administered L. lactis secreting an anti-TNF Nanobody demonstrate efficacy in chronic colitis. *Mucosal Immunol*. 2009;3(1):49-56. doi:10.1038/mi.2009.116

153. Nassif N, Roux C, Coradin T, Bouvet OMM, Livage J. Bacteria quorum sensing in silica matrices. *J Mater Chem*. 2004;14(14):2264. doi:10.1039/b403958k

154. Darshan N, Manonmani HK. Prodigiosin and its potential applications. *J Food Sci Technology*. 2015;52(9):5393-5407. doi:10.1007/s13197-015-1740-4

155. Xie S, Tai S, Song H, Luo X, Zhang H, Li X. Genetically engineering of Escherichia coli and immobilization on electrospun fibers for drug delivery purposes. *J Mater Chem B*. 2016;4(42):6820-6829. doi:10.1039/c6tb01165a

156. Wang H, Wang F, Zhu X, Yan Y, Yu X, Jiang P, Xing XH. Biosynthesis and characterization of violacein, deoxyviolacein and oxyviolacein in heterologous host, and

their antimicrobial activities. *Biochem Eng J*. 2012;67:148-155. doi:10.1016/j.bej.2012.06.005

157. Bilsland E, Tavella TA, Krogh R, Stokes JE, Roberts A, Ajioka J, Spring DR, Andricopulo AD, Costa FTM, Oliver SG. Antiplasmodial and trypanocidal activity of violacein and deoxyviolacein produced from synthetic operons. *Bmc Biotechnol*. 2018;18(1):22. doi:10.1186/s12896-018-0428-z

158. Sankaran S, Campo A del. Optoregulated Protein Release from an Engineered Living Material. *Adv Biosyst*. 2019;3(2):1800312. doi:10.1002/adbi.201800312

159. Sankaran S, Zhao S, Muth C, Paez J, Campo A del. Toward Light-Regulated Living Biomaterials. *Adv Sci*. 2018;5(8):1800383. doi:10.1002/advs.201800383

160. Gerber LC, Koehler FM, Grass RN, Stark WJ. Incorporation of Penicillin-Producing Fungi into Living Materials to Provide Chemically Active and Antibiotic-Releasing Surfaces. *Angewandte Chemie Int Ed*. 2012;51(45):11293-11296. doi:10.1002/anie.201204337

161. Hay JJ, Rodrigo-Navarro A, Petaroudi M, Bryksin AV, García AJ, Barker TH, Dalby MJ, Salmeron-Sanchez M. Bacteria-Based Materials for Stem Cell Engineering. *Adv Mater*. 2018;30(43):1804310. doi:10.1002/adma.201804310

162. Witte K, Rodrigo-Navarro A, Salmeron-Sanchez M, Witte K, Rodrigo-Navarro A, Salmeron-Sanchez M. Bacteria laden microgels as autonomous 3D environments for stem cell engineering. *Mater Today Bio*. 2019;2:100011. doi:10.1016/j.mtbio.2019.100011

163. Dai Z, Lee AJ, Roberts S, Sysoeva TA, Huang S, Dzuricky M, Yang X, Zhang X, Liu Z, Chilkoti A, You L. Versatile biomanufacturing through stimulus-responsive cell–material feedback. *Nat Chem Biol*. 2019;15(10):1017-1024. doi:10.1038/s41589-019-0357-8

164. Guo S, Dubuc E, Rave Y, Verhagen M, Twisk SAE, Hek T van der, Oerlemans GJM, Oetelaar MCM van den, Hazendonk LS van, Brüls M, Eijkens BV, Joostens PL, Keij SR, Xing W, Nijs M, Stalpers J, Sharma M, Gerth M, Boonen RJEA, Verduin K, Merkx M, Voets IK, Greef TFA de. Engineered Living Materials Based on Adhesin-Mediated Trapping of Programmable Cells. *Acs Synth Biol*. 2020;9(3):475-485. doi:10.1021/acssynbio.9b00404

165. Majidi C. Soft-Matter Engineering for Soft Robotics. *Adv Mater Technologies*. 2019;4(2):1800477. doi:10.1002/admt.201800477

166. Cianchetti M, Laschi C, Menciassi A, Dario P. Biomedical applications of soft robotics. *Nat Rev Mater*. 2018;3(6):143-153. doi:10.1038/s41578-018-0022-y

167. Kim O, Kim SJ, Park MJ. Low-voltage-driven soft actuators. *Chem Commun*. 2018;54(39):4895-4904. doi:10.1039/c8cc01670d

168. Martinez RV, Branch JL, Fish CR, Jin L, Shepherd RF, Nunes RMD, Suo Z, Whitesides GM. Robotic Tentacles with Three-Dimensional Mobility Based on Flexible Elastomers. *Adv Mater*. 2013;25(2):205-212. doi:10.1002/adma.201203002

169. Jin B, Song H, Jiang R, Song J, Zhao Q, Xie T. Programming a crystalline shape memory polymer network with thermo- and photo-reversible bonds toward a single-component soft robot. *Sci Adv*. 2018;4(1):eaao3865. doi:10.1126/sciadv.aao3865

170. Scalet G. Two-Way and Multiple-Way Shape Memory Polymers for Soft Robotics: An Overview. *Actuators*. 2020;9(1):10. doi:10.3390/act9010010

171. Zeng H, Wasylczyk P, Parmeggiani C, Martella D, Burresi M, Wiersma DS. Light-Fueled Microscopic Walkers. *Adv Mater*. 2015;27(26):3883-3887. doi:10.1002/adma.201501446

172. Cunha MP da, Debije MG, Schenning APHJ. Bioinspired light-driven soft robots based on liquid crystal polymers. *Chem Soc Rev*. Published online 2020. doi:10.1039/d0cs00363h

173. Cheng Y, Chan KH, Wang XQ, Ding T, Li T, Lu X, Ho GW. Direct-Ink-Write 3D Printing of Hydrogels into Biomimetic Soft Robots. *Acs Nano*. 2019;13(11):13176-13184. doi:10.1021/acsnano.9b06144

174. Francis W, Dunne A, Delaney C, Florea L, Diamond D. Spiropyran based hydrogels actuators—Walking in the light. *Sensors Actuators B Chem*. 2017;250:608-616. doi:10.1016/j.snb.2017.05.005

175. Ricotti L, Trimmer B, Feinberg AW, Raman R, Parker KK, Bashir R, Sitti M, Martel S, Dario P, Menciassi A. Biohybrid actuators for robotics: A review of devices actuated by living cells. *Sci Robotics*. 2017;2(12):eaaq0495. doi:10.1126/scirobotics.aaq0495

176. Won P, Ko SH, Majidi C, Feinberg AW, Webster-Wood VA. Biohybrid Actuators for Soft Robotics: Challenges in Scaling Up. *Actuators*. 2020;9(4):96. doi:10.3390/act9040096

177. Feinberg AW, Feigel A, Shevkoplyas SS, Sheehy S, Whitesides GM, Parker KK. Muscular Thin Films for Building Actuators and Powering Devices. *Science*. 2007;317(5843):1366-1370. doi:10.1126/science.1146885

178. Nawroth JC, Lee H, Feinberg AW, Ripplinger CM, McCain ML, Grosberg A, Dabiri JO, Parker KK. A tissue-engineered jellyfish with biomimetic propulsion. *Nat Biotechnol*. 2012;30(8):792-797. doi:10.1038/nbt.2269

179. Alford PW, Feinberg AW, Sheehy SP, Parker KK. Biohybrid thin films for measuring contractility in engineered cardiovascular muscle. *Biomaterials*. 2010;31(13):3613-3621. doi:10.1016/j.biomaterials.2010.01.079

180. Sun Y, Duffy R, Lee A, Feinberg AW. Optimizing the structure and contractility of engineered skeletal muscle thin films. *Acta Biomater*. 2013;9(8):7885-7894. doi:10.1016/j.actbio.2013.04.036

181. Feinberg AW, Ripplinger CM, van der Meer P, Sheehy SP, Domian I, Chien KR, Parker KK. Functional Differences in Engineered Myocardium from Embryonic Stem Cell-Derived versus Neonatal Cardiomyocytes. *Stem Cell Rep*. 2013;1(5):387-396. doi:10.1016/j.stemcr.2013.10.004

182. Alford PW, Nesmith AP, Seywerd JN, Grosberg A, Parker KK. Vascular smooth muscle contractility depends on cell shape. *Integr Biol*. 2011;3(11):1063-1070. doi:10.1039/c1ib00061f

183. Fu F, Shang L, Chen Z, Yu Y, Zhao Y. Bioinspired living structural color hydrogels. *Sci Robotics*. 2018;3(16):eaar8580. doi:10.1126/scirobotics.aar8580

184. Chen Z, Fu F, Yu Y, Wang H, Shang Y, Zhao Y. Cardiomyocytes-Actuated Morpho Butterfly Wings. *Adv Mater*. 2019;31(8):1805431. doi:10.1002/adma.201805431

185. Park SJ, Gazzola M, Park KS, Park S, Santo VD, Blevins EL, Lind JU, Campbell PH, Dauth S, Capulli AK, Pasqualini FS, Ahn S, Cho A, Yuan H, Maoz BM, Vijaykumar R, Choi JW, Deisseroth K, Lauder GV, Mahadevan L, Parker KK. Phototactic guidance of a tissue-engineered soft-robotic ray. *Science*. 2016;353(6295):158-162. doi:10.1126/science.aaf4292

186. Raman R, Cvetkovic C, Uzel SGM, Platt RJ, Sengupta P, Kamm RD, Bashir R. Optogenetic skeletal muscle-powered adaptive biological machines. *Proc National Acad Sci*. 2016;113(13):3497-3502. doi:10.1073/pnas.1516139113

187. Raman R, Grant L, Seo Y, Cvetkovic C, Gapinske M, Palasz A, Dabbous H, Kong H, Pinera PP, Bashir R. Damage, Healing, and Remodeling in Optogenetic Skeletal

Muscle Bioactuators. *Adv Healthc Mater*. 2017;6(12):1700030. doi:10.1002/adhm.201700030

188. Morimoto Y, Onoe H, Takeuchi S. Biohybrid robot with skeletal muscle tissue covered with a collagen structure for moving in air. *Apl Bioeng*. 2020;4(2):026101. doi:10.1063/1.5127204

189. Akiyama Y, Sakuma T, Funakoshi K, Hoshino T, Iwabuchi K, Morishima K. Atmospheric-operable bioactuator powered by insect muscle packaged with medium. *Lab Chip*. 2013;13(24):4870-4880. doi:10.1039/c3lc50490e

190. Akiyama Y, Odaira K, Sakiyama K, Hoshino T, Iwabuchi K, Morishima K. Rapidly-moving insect muscle-powered microrobot and its chemical acceleration. *Biomed Microdevices*. 2012;14(6):979-986. doi:10.1007/s10544-012-9700-5

191. Alapan Y, Yasa O, Yigit B, Yasa IC, Erkoc P, Sitti M. Microrobotics and Microorganisms: Biohybrid Autonomous Cellular Robots. *Annu Rev Control Robotics Autonomous Syst*. 2019;2(1):205-230. doi:10.1146/annurev-control-053018-023803

192. Singh AV, Ansari MHD, Mahajan M, Srivastava S, Kashyap S, Dwivedi P, Pandit V, Katha U. Sperm Cell Driven Microrobots—Emerging Opportunities and Challenges for Biologically Inspired Robotic Design. *Micromachines-basel*. 2020;11(4):448. doi:10.3390/mi11040448

193. Sun L, Yu Y, Chen Z, Bian F, Ye F, Sun L, Zhao Y. Biohybrid robotics with living cell actuation. *Chem Soc Rev*. 2020;49(12):4043-4069. doi:10.1039/d0cs00120a

194. Chen X, Mahadevan L, Driks A, Sahin O. Bacillus spores as building blocks for stimuli-responsive materials and nanogenerators. *Nat Nanotechnol*. 2014;9(2):137-141. doi:10.1038/nnano.2013.290

195. Yao L, Ou J, Wang G, Cheng CY, Wang W, Steiner H, Ishii H. bioPrint: A Liquid Deposition Printing System for Natural Actuators. *3d Print Addit Manuf*. 2015;2(4):168-179. doi:10.1089/3dp.2015.0033

196. Cakmak O, Tinay HOE, Chen X, Sahin O. Spore-Based Water-Resistant Water-Responsive Actuators with High Power Density. *Adv Mater Technologies*. 2019;4(8):1800596. doi:10.1002/admt.201800596

197. Rivera-Tarazona LK, Bhat VD, Kim H, Campbell ZT, Ware TH. Shape-morphing living composites. *Sci Adv*. 2020;6(3):eaax8582. doi:10.1126/sciadv.aax8582

198. Oosten CL van, Bastiaansen CWM, Broer DJ. Printed artificial cilia from liquid-crystal network actuators modularly driven by light. *Nat Mater*. 2009;8(8):677-682. doi:10.1038/nmat2487

199. Kim H, Lee JA, Ambulo CP, Lee HB, Kim SH, Naik VV, Haines CS, Aliev AE, Ovalle-Robles R, Baughman RH, Ware TH. Intelligently Actuating Liquid Crystal Elastomer-Carbon Nanotube Composites. *Adv Funct Mater*. 2019;29(48):1905063. doi:10.1002/adfm.201905063

200. Zein R, Selting W, Hamblin MR. Review of light parameters and photobiomodulation efficacy: dive into complexity. *J Biomed Opt*. 2018;23(12):120901. doi:10.1117/1.jbo.23.12.120901

201. Justus KB, Hellebrekers T, Lewis DD, Wood A, Ingham C, Majidi C, LeDuc PR, Tan C. A biosensing soft robot: Autonomous parsing of chemical signals through integrated organic and inorganic interfaces. *Sci Robotics*. 2019;4(31):eaax0765. doi:10.1126/scirobotics.aax0765

202. Xu W, Kwok KS, Gracias DH. Ultrathin Shape Change Smart Materials. *Accounts Chem Res*. 2018;51(2):436-444. doi:10.1021/acs.accounts.7b00468

203. Hilber W. Stimulus-active polymer actuators for next-generation microfluidic devices. *Appl Phys*. 2016;122(8):751. doi:10.1007/s00339-016-0258-6

204. Haines CS, Lima MD, Li N, Spinks GM, Foroughi J, Madden JDW, Kim SH, Fang S, Andrade MJ de, Göktepe F, Göktepe Ö, Mirvakili SM, Naficy S, Lepró X, Oh J, Kozlov ME, Kim SJ, Xu X, Swedlove BJ, Wallace GG, Baughman RH. Artificial Muscles from Fishing Line and Sewing Thread. *Science*. 2014;343(6173):868-872. doi:10.1126/science.1246906

205. Pelrine R, Kornbluh R, Kofod G. High-Strain Actuator Materials Based on Dielectric Elastomers. *Adv Mater*. 2000;12(16):1223-1225. doi:10.1002/1521-4095(200008)12:16<1223::aid-adma1223>3.0.co;2-2

206. Thomsen DL, Keller P, Naciri J, Pink R, Jeon H, Shenoy D, Ratna BR. Liquid Crystal Elastomers with Mechanical Properties of a Muscle. *Macromolecules*. 2001;34(17):5868-5875. doi:10.1021/ma001639q

207. Chung T, Romo-Uribe A, Mather PT. Two-Way Reversible Shape Memory in a Semicrystalline Network. *Macromolecules*. 2008;41(1):184-192. doi:10.1021/ma071517z

208. Jeon SJ, Hauser AW, Hayward RC. Shape-Morphing Materials from Stimuli-Responsive Hydrogel Hybrids. *Accounts Chem Res*. 2017;50(2):161-169. doi:10.1021/acs.accounts.6b00570

209. Lendlein A, Kelch S. Shape-Memory Polymers. *Angewandte Chemie Int Ed*. 2002;41(12):2034-2057. doi:10.1002/1521-3773(20020617)41:12<2034::aid-anie2034>3.0.co;2-m

210. Jonkers HM. Bacteria-based self-healing concrete. *Heron*. 2011;56(1):1-12.

211. Saha A, Johnston TG, Shafranek RT, Goodman CJ, Zalatan JG, Storti DW, Ganter MA, Nelson A. Additive Manufacturing of Catalytically Active Living Materials. *Acs Appl Mater Inter*. 2018;10(16):13373-13380. doi:10.1021/acsami.8b02719

212. Kwak S, Giraldo JP, Lew TTS, Wong MH, Liu P, Yang YJ, Koman VB, McGee MK, Olsen BD, Strano MS. Polymethacrylamide and Carbon Composites that Grow, Strengthen, and Self-Repair using Ambient Carbon Dioxide Fixation. *Adv Mater*. 2018;30(46):1804037. doi:10.1002/adma.201804037

213. Hughes AJ, Miyazaki H, Coyle MC, Zhang J, Laurie MT, Chu D, Vavrušová Z, Schneider RA, Klein OD, Gartner ZJ. Engineered Tissue Folding by Mechanical Compaction of the Mesenchyme. *Dev Cell*. 2018;44(2):165-178.e6. doi:10.1016/j.devcel.2017.12.004

214. Streichan SJ, Hoerner CR, Schneidt T, Holzer D, Hufnagel L. Spatial constraints control cell proliferation in tissues. *Proc National Acad Sci*. 2014;111(15):5586-5591. doi:10.1073/pnas.1323016111

215. Minc N, Boudaoud A, Chang F. Mechanical Forces of Fission Yeast Growth. *Curr Biol*. 2009;19(13):1096-1101. doi:10.1016/j.cub.2009.05.031

216. Calvert P. Hydrogels for Soft Machines. *Adv Mater*. 2009;21(7):743-756. doi:10.1002/adma.200800534

217. Zhao XQ, Bai FW. Mechanisms of yeast stress tolerance and its manipulation for efficient fuel ethanol production. *J Biotechnol*. 2009;144(1):23-30. doi:10.1016/j.jbiotec.2009.05.001

218. Tang YQ, Koike Y, Liu K, An MZ, Morimura S, Wu XL, Kida K. Ethanol production from kitchen waste using the flocculating yeast Saccharomyces cerevisiae strain KF-7. *Biomass Bioenergy*. 2008;32(11):1037-1045. doi:10.1016/j.biombioe.2008.01.027

219. Klein Y, Efrati E, Sharon E. Shaping of Elastic Sheets by Prescription of Non-Euclidean Metrics. *Science*. 2007;315(5815):1116-1120. doi:10.1126/science.1135994

220. Gladman AS, Matsumoto EA, Nuzzo RG, Mahadevan L, Lewis JA. Biomimetic 4D printing. *Nat Mater*. 2016;15(4):413-418. doi:10.1038/nmat4544

221. Sharon E, Efrati E. The mechanics of non-Euclidean plates. *Soft Matter*. 2010;6(22):5693-5704. doi:10.1039/c0sm00479k

222. Nojoomi A, Arslan H, Lee K, Yum K. Bioinspired 3D structures with programmable morphologies and motions. *Nat Commun*. 2018;9(1):3705. doi:10.1038/s41467-018-05569-8

223. Kim J, Hanna JA, Byun M, Santangelo CD, Hayward RC. Designing Responsive Buckled Surfaces by Halftone Gel Lithography. *Science*. 2012;335(6073):1201-1205. doi:10.1126/science.1215309

224. Fields S, Song O kyu. A novel genetic system to detect protein–protein interactions. *Nature*. 1989;340(6230):245-246. doi:10.1038/340245a0

225. Romanos MA, Scorer CA, Clare JJ. Foreign gene expression in yeast: a review. *Yeast*. 1992;8(6):423-488. doi:10.1002/yea.320080602

226. Ross MJ. Recombinant DNA products: Insulin, interferon and growth hormone edited by Arthur P. Bollon, CRC Press, 1984. $70.00 in USA ($80.00 elsewhere) (191 pages) ISBN 0 8493 5542 2. *Trends Biotechnol*. 1985;3(9):246. doi:10.1016/0167-7799(85)90020-4

227. Hu X, An Q, Li G, Tao S, Liu J. Imprinted Photonic Polymers for Chiral Recognition. *Angewandte Chemie Int Ed*. 2006;45(48):8145-8148. doi:10.1002/anie.200601849

228. Kennedy MJ, Hughes RM, Peteya LA, Schwartz JW, Ehlers MD, Tucker CL. Rapid blue-light–mediated induction of protein interactions in living cells. *Nat Methods*. 2010;7(12):973-975. doi:10.1038/nmeth.1524

229. Campbell ZT, Menichelli E, Friend K, Wu J, Kimble J, Williamson JR, Wickens M. Identification of a Conserved Interface between PUF and CPEB Proteins. *J Biol Chem*. 2012;287(22):18854-18862. doi:10.1074/jbc.m112.352815

230. Yamada M, Kondo M, Mamiya J, Yu Y, Kinoshita M, Barrett CJ, Ikeda T. Photomobile Polymer Materials: Towards Light-Driven Plastic Motors. *Angewandte Chemie Int Ed*. 2008;47(27):4986-4988. doi:10.1002/anie.200800760

231. Vojtek AB, Hollenberg SM, Cooper JA. Mammalian Ras interacts directly with the serine/threonine kinase raf. *Cell*. 1993;74(1):205-214. doi:10.1016/0092-8674(93)90307-c

232. Luitjens C, Gallegos M, Kraemer B, Kimble J, Wickens M. CPEB proteins control two key steps in spermatogenesis in C. elegans. *Gene Dev*. 2000;14(20):2596-2609. doi:10.1101/gad.831700

233. Karnaushenko D, Münzenrieder N, Karnaushenko DD, Koch B, Meyer AK, Baunack S, Petti L, Tröster G, Makarov D, Schmidt OG. Biomimetic Microelectronics for Regenerative Neuronal Cuff Implants. *Adv Mater*. 2015;27(43):6797-6805. doi:10.1002/adma.201503696

234. Tuite MF. W. Xiao (Ed.). Yeast Protocols, Molecular Biology, second ed., Humana Press, New Jersey, 2006, p. 392 ISBN: 1-59259-958-3. *Phytochemistry*. 2006;67(9):938. doi:10.1016/j.phytochem.2006.02.013

235. Ulitzur S. Methods in Enzymology. *Methods Enzymol*. 1986;133:264-274. doi:10.1016/0076-6879(86)33072-6

236. Jiang Z, Diggle B, Shackleford ICG, Connal LA. Tough, Self-Healing Hydrogels Capable of Ultrafast Shape Changing. *Adv Mater*. 2019;31(48):1904956. doi:10.1002/adma.201904956

237. Chen H, Yang F, Chen Q, Zheng J. A Novel Design of Multi-Mechanoresponsive and Mechanically Strong Hydrogels. *Adv Mater*. 2017;29(21):1606900. doi:10.1002/adma.201606900

238. Kotikian A, Truby RL, Boley JW, White TJ, Lewis JA. 3D Printing of Liquid Crystal Elastomeric Actuators with Spatially Programed Nematic Order. *Adv Mater*. 2018;30(10):1706164. doi:10.1002/adma.201706164

239. Roy D, Cambre JN, Sumerlin BS. Future perspectives and recent advances in stimuli-responsive materials. *Prog Polym Sci*. 2010;35(1-2):278-301. doi:10.1016/j.progpolymsci.2009.10.008

240. Thérien-Aubin H, Wu ZL, Nie Z, Kumacheva E. Multiple Shape Transformations of Composite Hydrogel Sheets. *J Am Chem Soc*. 2013;135(12):4834-4839. doi:10.1021/ja400518c

241. D'Eramo L, Chollet B, Leman M, Martwong E, Li M, Geisler H, Dupire J, Kerdraon M, Vergne C, Monti F, Tran Y, Tabeling P. Microfluidic actuators based on temperature-responsive hydrogels. *Microsystems Nanoeng*. 2018;4(1):17069. doi:10.1038/micronano.2017.69

242. Lu X, Ambulo CP, Wang S, Rivera-Tarazona LK, Kim H, Searles K, Ware TH. 4D-Printing of Photoswitchable Actuators. *Angewandte Chemie Int Ed*. 2021;60(10):5536-5543. doi:10.1002/anie.202012618

243. Xu W, Gao Y, Serpe MJ. Electrochemically color tunable poly(N - isopropylacrylamide) microgel-based etalons. *J Mater Chem C*. 2014;2(20):3873-3878. doi:10.1039/c4tc00271g

244. Ma C, Li T, Zhao Q, Yang X, Wu J, Luo Y, Xie T. Supramolecular Lego Assembly Towards Three-Dimensional Multi-Responsive Hydrogels. *Adv Mater*. 2014;26(32):5665-5669. doi:10.1002/adma.201402026

245. Jeon SJ, Hayward RC. Simultaneous control of Gaussian curvature and buckling direction by swelling of asymmetric trilayer hydrogel hybrids. *Soft Matter*. 2019;16(3):688-694. doi:10.1039/c9sm01922g

246. Ambulo CP, Ford MJ, Searles K, Majidi C, Ware TH. 4D-Printable Liquid Metal–Liquid Crystal Elastomer Composites. *Acs Appl Mater Inter*. 2020;13(11):12805-12813. doi:10.1021/acsami.0c19051

247. Ghosh A, Li L, Xu L, Dash RP, Gupta N, Lam J, Jin Q, Akshintala V, Pahapale G, Liu W, Sarkar A, Rais R, Gracias DH, Selaru FM. Gastrointestinal-resident, shape-changing microdevices extend drug release in vivo. *Sci Adv*. 2020;6(44):eabb4133. doi:10.1126/sciadv.abb4133

248. Mao Y, Ding Z, Yuan C, Ai S, Isakov M, Wu J, Wang T, Dunn ML, Qi HJ. 3D Printed Reversible Shape Changing Components with Stimuli Responsive Materials. *Sci Rep-uk*. 2016;6(1):24761. doi:10.1038/srep24761

249. Hua D, Zhang X, Ji Z, Yan C, Yu B, Li Y, Wang X, Zhou F. 3D printing of shape changing composites for constructing flexible paper-based photothermal bilayer actuators. *J Mater Chem C*. 2018;6(8):2123-2131. doi:10.1039/c7tc05710e

250. Zeng H, Wani OM, Wasylczyk P, Kaczmarek R, Priimagi A. Self-Regulating Iris Based on Light-Actuated Liquid Crystal Elastomer. *Adv Mater*. 2017;29(30):1701814. doi:10.1002/adma.201701814

251. Purcell BP, Lobb D, Charati MB, Dorsey SM, Wade RJ, Zellars KN, Doviak H, Pettaway S, Logdon CB, Shuman JA, Freels PD, III JHG, Gorman RC, Spinale FG, Burdick JA. Injectable and bioresponsive hydrogels for on-demand matrix metalloproteinase inhibition. *Nat Mater*. 2014;13(6):653-661. doi:10.1038/nmat3922

252. Ancla C, Lapeyre V, Gosse I, Catargi B, Ravaine V. Designed Glucose-Responsive Microgels with Selective Shrinking Behavior. *Langmuir*. 2011;27(20):12693-12701. doi:10.1021/la202910k

253. Bai W, Gariano NA, Spivak DA. Macromolecular Amplification of Binding Response in Superaptamer Hydrogels. *J Am Chem Soc*. 2013;135(18):6977-6984. doi:10.1021/ja400576p

254. Nguyen PQ, Courchesne NMD, Duraj-Thatte A, Praveschotinunt P, Joshi NS. Engineered Living Materials: Prospects and Challenges for Using Biological Systems to Direct the Assembly of Smart Materials. *Adv Mater*. 2018;30(19):1704847. doi:10.1002/adma.201704847

255. Rivera-Tarazona LK, Campbell ZT, Ware TH. Stimuli-responsive engineered living materials. *Soft Matter*. 2021;17(4):785-809. doi:10.1039/d0sm01905d

256. Tang TC, Tham E, Liu X, Yehl K, Rovner AJ, Yuk H, Fuente-Nunez C de la, Isaacs FJ, Zhao X, Lu TK. Hydrogel-based biocontainment of bacteria for continuous sensing and computation. *Nat Chem Biol*. Published online 2021:1-8. doi:10.1038/s41589-021-00779-6

257. Gilbert C, Tang TC, Ott W, Dorr BA, Shaw WM, Sun GL, Lu TK, Ellis T. Living materials with programmable functionalities grown from engineered microbial co-cultures. *Nat Mater*. 2021;20(5):691-700. doi:10.1038/s41563-020-00857-5

258. Guo S, Dubuc E, Rave Y, Verhagen M, Twisk SAE, Hek T van der, Oerlemans GJM, Oetelaar MCM van den, Hazendonk LS van, Brüls M, Eijkens BV, Joostens PL, Keij SR, Xing W, Nijs M, Stalpers J, Sharma M, Gerth M, Boonen RJEA, Verduin K, Merkx M, Voets IK, Greef TFA de. Engineered Living Materials Based on Adhesin-Mediated Trapping of Programmable Cells. *Acs Synth Biol*. 2020;9(3):475-485. doi:10.1021/acssynbio.9b00404

259. Heveran CM, Williams SL, Qiu J, Artier J, Hubler MH, Cook SM, Cameron JC, Srubar WV. Biomineralization and Successive Regeneration of Engineered Living Building Materials. *Matter*. 2020;2(2):481-494. doi:10.1016/j.matt.2019.11.016

260. Tziviloglou E, Wiktor V, Jonkers HM, Schlangen E. Bacteria-based self-healing concrete to increase liquid tightness of cracks. *Constr Build Mater*. 2016;122:118-125. doi:10.1016/j.conbuildmat.2016.06.080

261. Johnston TG, Yuan SF, Wagner JM, Yi X, Saha A, Smith P, Nelson A, Alper HS. Compartmentalized microbes and co-cultures in hydrogels for on-demand bioproduction and preservation. *Nat Commun*. 2020;11(1):563. doi:10.1038/s41467-020-14371-4

262. González LM, Mukhitov N, Voigt CA. Resilient living materials built by printing bacterial spores. *Nat Chem Biol*. 2019;16(2):126-133. doi:10.1038/s41589-019-0412-5

263. Wei H, Zhang Q, Yao Y, Liu L, Liu Y, Leng J. Direct-Write Fabrication of 4D Active Shape-Changing Structures Based on a Shape Memory Polymer and Its Nanocomposite. *Acs Appl Mater Inter*. 2016;9(1):876-883. doi:10.1021/acsami.6b12824

264. Kirillova A, Maxson R, Stoychev G, Gomillion CT, Ionov L. 4D Biofabrication Using Shape-Morphing Hydrogels. *Adv Mater*. 2017;29(46):1703443. doi:10.1002/adma.201703443

265. Siqueira G, Kokkinis D, Libanori R, Hausmann MK, Gladman AS, Neels A, Tingaut P, Zimmermann T, Lewis JA, Studart AR. Cellulose Nanocrystal Inks for 3D Printing of Textured Cellular Architectures. *Adv Funct Mater*. 2017;27(12):1604619. doi:10.1002/adfm.201604619

266. Sultan S, Mathew AP. 3D printed scaffolds with gradient porosity based on a cellulose nanocrystal hydrogel. *Nanoscale*. 2018;10(9):4421-4431. doi:10.1039/c7nr08966j

267. Voronova MI, Surov OV, Afineevskii AV, Zakharov AG. Properties of polyacrylamide composites reinforced by cellulose nanocrystals. *Heliyon*. 2020;6(11):e05529. doi:10.1016/j.heliyon.2020.e05529

268. Minc N, Boudaoud A, Chang F. Mechanical Forces of Fission Yeast Growth. *Curr Biol*. 2009;19(13):1096-1101. doi:10.1016/j.cub.2009.05.031

269. Hensing MCM, Bangma KA, Raamsdonk LM, Hulster E de, Dijken JP van, Pronk JT. Effects of cultivation conditions on the production of heterologous α-galactosidase by Kluyveromyces lactis. *Appl Microbiol Biot*. 1995;43(1):58-64. doi:10.1007/bf00170623

270. Thomas KC, Hynes SH, Ingledew WM. Influence of Medium Buffering Capacity on Inhibition of Saccharomyces cerevisiae Growth by Acetic and Lactic Acids. *Appl Environ Microb*. 2002;68(4):1616-1623. doi:10.1128/aem.68.4.1616-1623.2002

271. Hahn-Hägerdal B, Karhumaa K, Larsson CU, Gorwa-Grauslund M, Görgens J, Zyl WH van. Role of cultivation media in the development of yeast strains for large scale industrial use. *Microb Cell Fact*. 2005;4(1):31. doi:10.1186/1475-2859-4-31

272. Yang J, Han CR, Duan JF, Ma MG, Zhang XM, Xu F, Sun RC. Synthesis and characterization of mechanically flexible and tough cellulose nanocrystals–polyacrylamide nanocomposite hydrogels. *Cellulose*. 2013;20(1):227-237. doi:10.1007/s10570-012-9841-y

273. Jayaramudu T, Ko HU, Kim HC, Kim JW, Kim J. Swelling Behavior of Polyacrylamide–Cellulose Nanocrystal Hydrogels: Swelling Kinetics, Temperature, and pH Effects. *Materials*. 2019;12(13):2080. doi:10.3390/ma12132080

274. Kelesidis T, Pothoulakis C. Efficacy and safety of the probiotic Saccharomyces boulardii for the prevention and therapy of gastrointestinal disorders. *Ther Adv Gastroenter*. 2012;5(2):111-125. doi:10.1177/1756283x11428502

275. Terciolo C, Dapoigny M, Andre F. Beneficial effects of Saccharomyces boulardii CNCM I-745 on clinical disorders associated with intestinal barrier disruption. *Clin Exp Gastroenterology*. 2019;12:67-82. doi:10.2147/ceg.s181590

276. Douradinha B, Reis VC, Rogers MB, Torres FA, Evans JD, Jr ETM. Novel insights in genetic transformation of the probiotic yeast Saccharomyces boulardii. *Bioengineered*. 2013;5(1):21-29. doi:10.4161/bioe.26271

277. Palma ML, Zamith-Miranda D, Martins FS, Bozza FA, Nimrichter L, Montero-Lomeli M, Marques ETA, Douradinha B. Probiotic Saccharomyces cerevisiae strains as biotherapeutic tools: is there room for improvement? *Appl Microbiol Biot*. 2015;99(16):6563-6570. doi:10.1007/s00253-015-6776-x

278. Liu JJ, Kong II, Zhang GC, Jayakody LN, Kim H, Xia PF, Kwak S, Sung BH, Sohn JH, Walukiewicz HE, Rao CV, Jin YS. Metabolic Engineering of Probiotic Saccharomyces boulardii. *Appl Environ Microb*. 2016;82(8):2280-2287. doi:10.1128/aem.00057-16

279. Li X, Cai X, Gao Y, Serpe MJ. Reversible bidirectional bending of hydrogel-based bilayer actuators. *J Mater Chem B*. 2017;5(15):2804-2812. doi:10.1039/c7tb00426e

280. Li DX, Oh YK, Lim SJ, Kim JO, Yang HJ, Sung JH, Yong CS, Choi HG. Novel gelatin microcapsule with bioavailability enhancement of ibuprofen using spray-drying technique. *Int J Pharmaceut*. 2008;355(1-2):277-284. doi:10.1016/j.ijpharm.2007.12.020

281. Crcarevska MS, Dodov MG, Petrusevska G, Gjorgoski I, Goracinova K. Bioefficacy of budesonide loaded crosslinked polyeletrolyte microparticles in rat model of induced colitis. *J Drug Target*. 2009;17(10):788-802. doi:10.3109/10611860903161310

282. Chablani L, Tawde SA, Akalkotkar A, D'Souza C, Selvaraj P, D'Souza MJ. Formulation and evaluation of a particulate oral breast cancer vaccine. *J Pharm Sci*. 2012;101(10):3661-3671. doi:10.1002/jps.23275

283. Sander C, Madsen KD, Hyrup B, Nielsen HM, Rantanen J, Jacobsen J. Characterization of spray dried bioadhesive metformin microparticles for oromucosal

administration. *Eur J Pharm Biopharm*. 2013;85(3):682-688. doi:10.1016/j.ejpb.2013.05.017

284. Traverso G, Schoellhammer CM, Schroeder A, Maa R, Lauwers GY, Polat BE, Anderson DG, Blankschtein D, Langer R. Microneedles for Drug Delivery via the Gastrointestinal Tract. *J Pharm Sci*. 2015;104(2):362-367. doi:10.1002/jps.24182

285. Zhu G, Zhang Y, Wang K, Zhao X, Lian H, Wang W, Wang H, Wu J, Hu Y, Guo H. Visualized intravesical floating hydrogel encapsulating vaporized perfluoropentane for controlled drug release. *Drug Deliv*. 2015;23(8):1-7. doi:10.3109/10717544.2015.1101791

286. Babaee S, Pajovic S, Kirtane AR, Shi J, Caffarel-Salvador E, Hess K, Collins JE, Tamang S, Wahane AV, Hayward AM, Mazdiyasni H, Langer R, Traverso G. Temperature-responsive biometamaterials for gastrointestinal applications. *Sci Transl Med*. 2019;11(488):eaau8581. doi:10.1126/scitranslmed.aau8581

287. Gabriel AS, Uneyama H. Amino acid sensing in the gastrointestinal tract. *Amino Acids*. 2013;45(3):451-461. doi:10.1007/s00726-012-1371-2

288. Huang J, Liu S, Zhang C, Wang X, Pu J, Ba F, Xue S, Ye H, Zhao T, Li K, Wang Y, Zhang J, Wang L, Fan C, Lu TK, Zhong C. Programmable and printable Bacillus subtilis biofilms as engineered living materials. *Nat Chem Biol*. 2018;15(1):34-41. doi:10.1038/s41589-018-0169-2

289. Duraj-Thatte AM, Manjula-Basavanna A, Courchesne NMD, Cannici GI, Sánchez-Ferrer A, Frank BP, Hag L van't, Cotts SK, Fairbrother DH, Mezzenga R, Joshi NS. Water-processable, biodegradable and coatable aquaplastic from engineered biofilms. *Nat Chem Biol*. Published online 2021:1-7. doi:10.1038/s41589-021-00773-y

290. Praveschotinunt P, Duraj-Thatte AM, Gelfat I, Bahl F, Chou DB, Joshi NS. Engineered E. coli Nissle 1917 for the delivery of matrix-tethered therapeutic domains to the gut. *Nat Commun*. 2019;10(1):5580. doi:10.1038/s41467-019-13336-6

291. Rodrigo-Navarro A, Sankaran S, Dalby MJ, Campo A del, Salmeron-Sanchez M. Engineered living biomaterials. *Nat Rev Mater*. 2021;6(12):1175-1190. doi:10.1038/s41578-021-00350-8

292. Liu X, Yang Y, Inda ME, Lin S, Wu J, Kim Y, Chen X, Ma D, Lu TK, Zhao X. Magnetic Living Hydrogels for Intestinal Localization, Retention, and Diagnosis. *Adv Funct Mater*. Published online 2021:2010918. doi:10.1002/adfm.202010918

293. Xu L, Wang X, Sun F, Cao Y, Zhong C, Zhang WB. Harnessing proteins for engineered living materials. *Curr Opin Solid State Mater Sci*. 2021;25(1):100896. doi:10.1016/j.cossms.2020.100896

294. Kandemir N, Vollmer W, Jakubovics NS, Chen J. Mechanical interactions between bacteria and hydrogels. *Sci Rep-uk*. 2018;8(1):10893. doi:10.1038/s41598-018-29269-x

295. Han S, Choi EK, Park W, Yi C, Chung N. Effectiveness of expanded clay as a bacteria carrier for self-healing concrete. *Appl Biol Chem*. 2019;62(1):19. doi:10.1186/s13765-019-0426-4

296. Rivera-Tarazona LK, Shukla T, Singh KA, Gaharwar AK, Campbell ZT, Ware TH. 4D Printing of Engineered Living Materials. *Adv Funct Mater*. Published online 2021:2106843. doi:10.1002/adfm.202106843

297. Xu W, Nouri PMM, Demoustier-Champagne S, Glinel K, Jonas AM. Encapsulation of Commensal Skin Bacteria within Membrane-in-Gel Patches. *Adv Mater Interfaces*. Published online 2022:2102261. doi:10.1002/admi.202102261

298. Smith AE, Zhang Z, Thomas CR, Moxham KE, Middelberg APJ. The mechanical properties of Saccharomyces cerevisiae. *Proc National Acad Sci*. 2000;97(18):9871-9874. doi:10.1073/pnas.97.18.9871

299. CZERUCKA D, PICHE T, RAMPAL P. Review article: yeast as probiotics – Saccharomyces boulardii. *Aliment Pharm Therap*. 2007;26(6):767-778. doi:10.1111/j.1365-2036.2007.03442.x

300. Tang TC, An B, Huang Y, Vasikaran S, Wang Y, Jiang X, Lu TK, Zhong C. Materials design by synthetic biology. *Nat Rev Mater*. 2020;6(4):332-350. doi:10.1038/s41578-020-00265-w

301. Bober JR, Beisel CL, Nair NU. Synthetic Biology Approaches to Engineer Probiotics and Members of the Human Microbiota for Biomedical Applications. *Annu Rev Biomed Eng*. 2018;20(1):1-24. doi:10.1146/annurev-bioeng-062117-121019

302. Tuson HH, Auer GK, Renner LD, Hasebe M, Tropini C, Salick M, Crone WC, Gopinathan A, Huang KC, Weibel DB. Measuring the stiffness of bacterial cells from growth rates in hydrogels of tunable elasticity. *Mol Microbiol*. 2012;84(5):874-891. doi:10.1111/j.1365-2958.2012.08063.x

303. Burrill HN, Bell LE, Greenfield PF, Do DD. Analysis of Distributed Growth of Saccharomyces cerevisiae Cells Immobilized in Polyacrylamide Gel. *Appl Environ Microb*. 1983;46(3):716-721. doi:10.1128/aem.46.3.716-721.1983

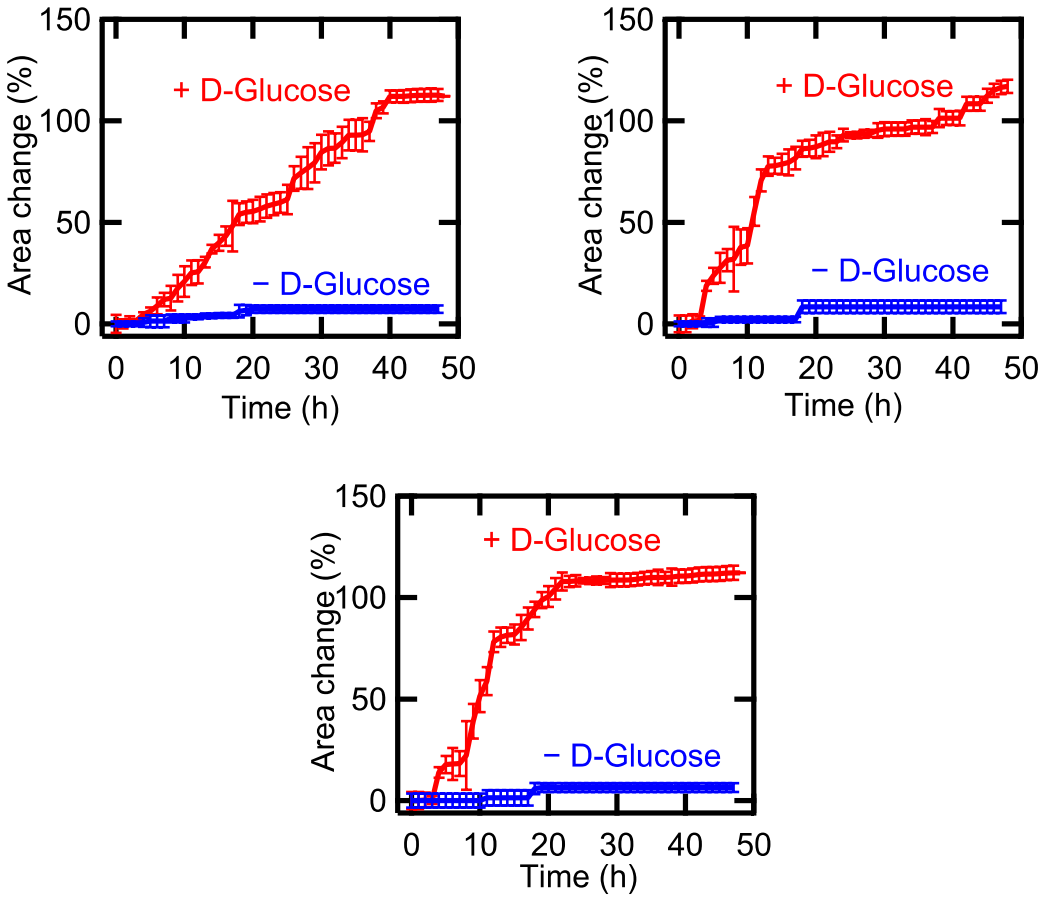

Figure A-1: Change in area depends on initial cell loading. Area change over time for composites with 1 wt% (A), 12 wt% (B) and 18 wt% (C) dry yeast in the presence of media with and without D-glucose. Each data point represents the mean (n=3), and error bars represent standard deviation. Trend lines are only intended to guide the eye. Reprinted with permission from [197]. Copyright (2020) exclusive licensee American Association for the Advancement of Science. Distributed under a Creative Commons Attribution License 4.0 (CC BY).

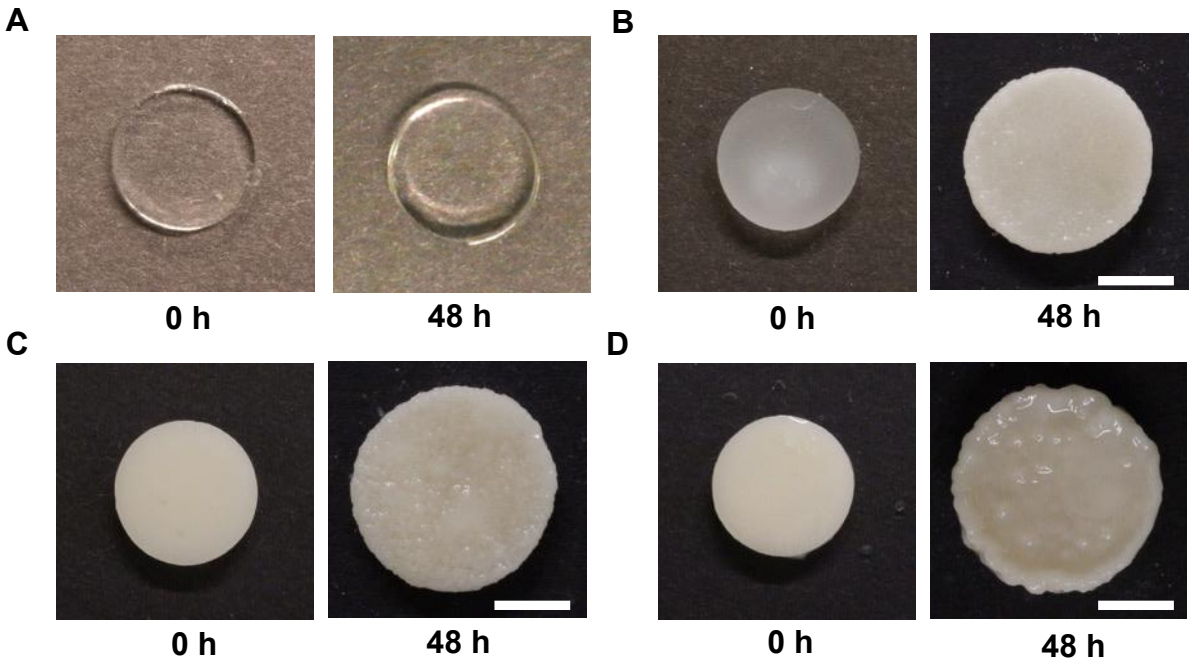

Figure A-2: Representative images of the living composites before and after incubation in media. Images of hydrogels without yeast (A) and composites with 1 wt% yeast (B), with 12 wt% yeast (C), and 18 wt% yeast (D) (Scale bars: 5 mm). Each experiment had 3 replicates. All samples were incubated at 30ºC in YPD media under static conditions with media changed every 6 h. Reprinted with permission from [197]. Copyright (2020) exclusive licensee American Association for the Advancement of Science. Distributed under a Creative Commons Attribution License 4.0 (CC BY).

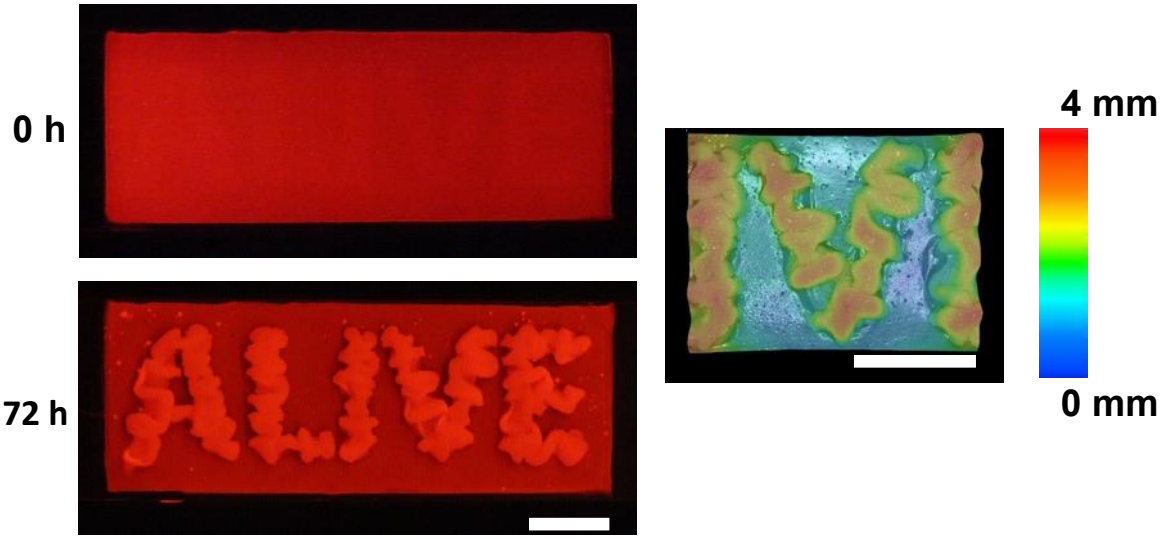

Figure A-3: Buckling pattern in living composite coated on a glass substrate. Fluorescence images of a living composite after UV patterning (top) and after incubation in YPD (bottom) (Scale bar: 10 mm). Topography of an initially flat living composite after exposure to YPD (right) (Scale bar: 10 mm). Samples were incubated at 30ºC in YPD media under static conditions with media changed every 12 h. Reprinted with permission from [197]. Copyright (2020) exclusive licensee American Association for the Advancement of Science. Distributed under a Creative Commons Attribution License 4.0 (CC BY).

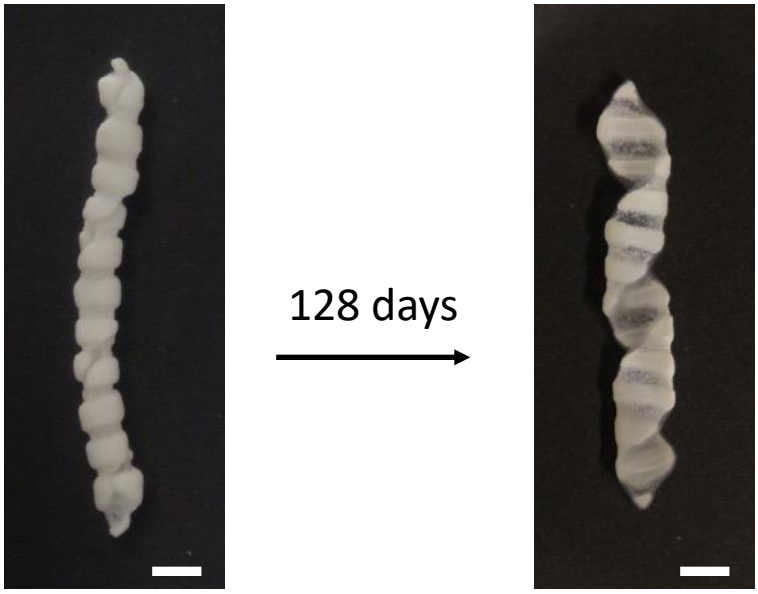

Figure A-4 Shape change stability. Helical structure after growth (left) and after storage for 128 days. Samples were stored in dH_2O at room temperature (Scale bars: 5 mm). Shape change due to proliferation is largely stable. Reprinted with permission from [197]. Copyright (2020) exclusive licensee American Association for the Advancement of Science. Distributed under a Creative Commons Attribution License 4.0 (CC BY).

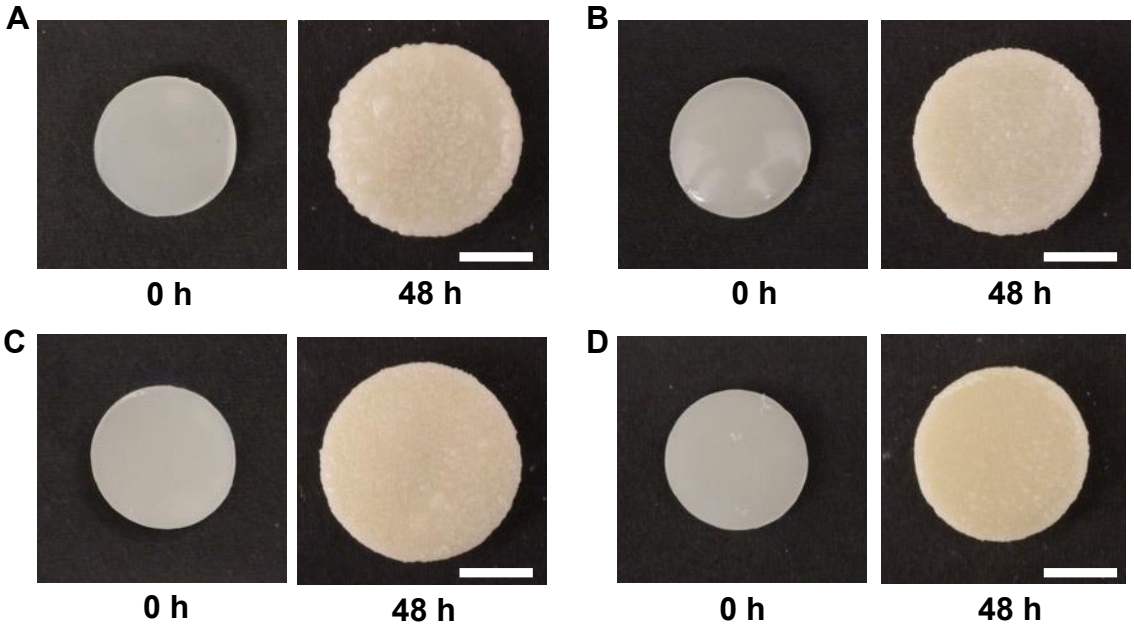

Figure A-5: Representative images of the macroscopic expansion of living composites with varying crosslinker density. Images of living composites synthesized with 0.05 wt% crosslinker (A), 0.1 wt% crosslinker (B), 0.3 wt% crosslinker (C), and 0.6 wt% crosslinker (D) (Scale bars: 5 mm). Each experiment had 3 replicates. All samples were incubated at 30ºC in YPD media under static conditions with media changed every 6 h. Reprinted with permission from [197]. Copyright (2020) exclusive licensee American Association for the Advancement of Science. Distributed under a Creative Commons Attribution License 4.0 (CC BY).

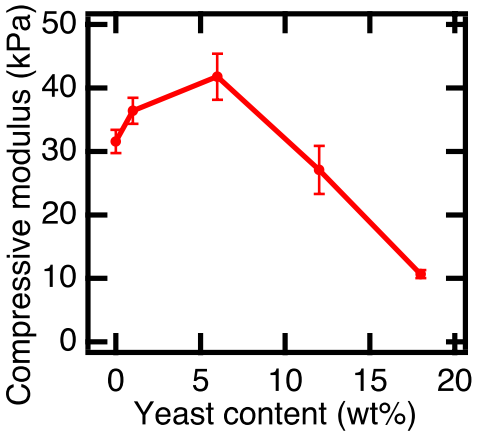

Figure A-6: Characterization of living composites with varying yeast content. Compressive modulus of living composites with varying yeast content. Each data point represents the mean (n=3), and error bars represent standard deviation. Trend lines are only intended to guide the eye. Reprinted with permission from [197]. Copyright (2020) exclusive licensee American Association for the Advancement of Science. Distributed under a Creative Commons Attribution License 4.0 (CC BY).

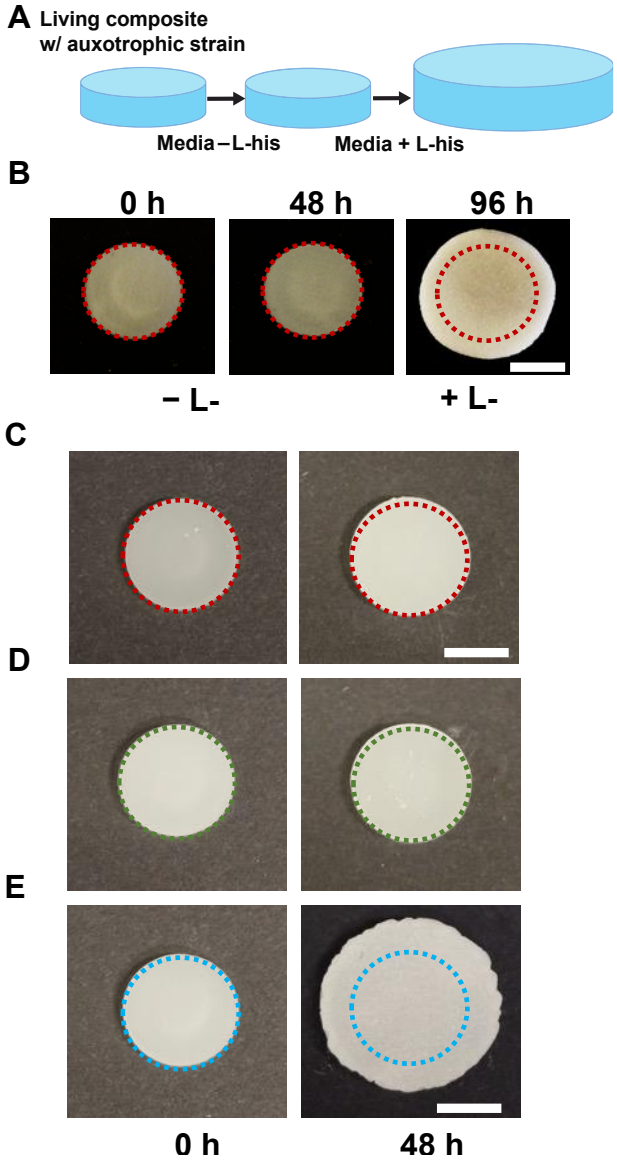

Figure A-7: Living composite shape change induced by adding a specific biochemical. (A) Schematic of a genetically modified living composite with growth triggered by the addition of L-histidine (B) Composites do not change in volume substantially in media lacking L-histidine but grow after L-histidine is supplemented into the media (Scale bar: 5 mm). Representative images of the macroscopic expansion of auxotrophic living composites incubated in media without histidine (A), with the stereoisomer D-histidine (B), and with L-histidine (C) (Scale bars: 5 mm). All samples were incubated at 30ºC under static conditions and media was changed every 12 h. Dotted circles represent initial area and are used to guide the eye after composites growth. Reprinted with permission from [197]. Copyright (2020) exclusive licensee American Association for the Advancement of Science. Distributed under a Creative Commons Attribution License 4.0 (CC BY).

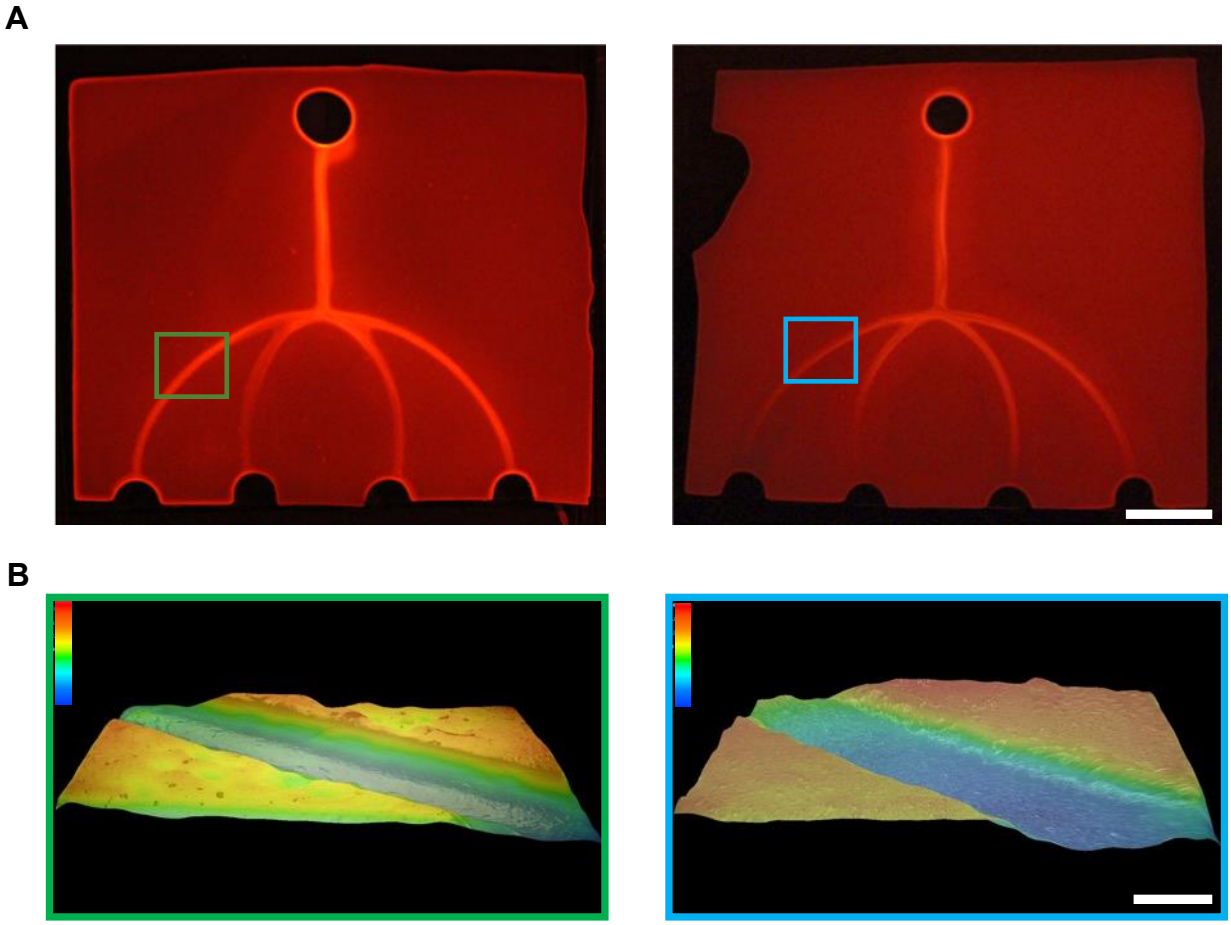

Figure A-8: Microfluidic device exposed to media without L-histidine. (A) Fluorescence image of fluid traversing the microfluidic device before exposure to media (left) (Scale bar 10 mm). Fluorescence image of fluid traversing the microfluidic device after media lacking L-histidine flows for 48 h through the channels. Growth of areas with living cells is not affected by media flow (right). (B) Topography of a living channel recorded before (left) and after (right) growth (Scale bar: 0.5 mm) (Color scale: 0-0.3 mm). Reprinted with permission from [197]. Copyright (2020) exclusive licensee American Association for the Advancement of Science. Distributed under a Creative Commons Attribution License 4.0 (CC BY).

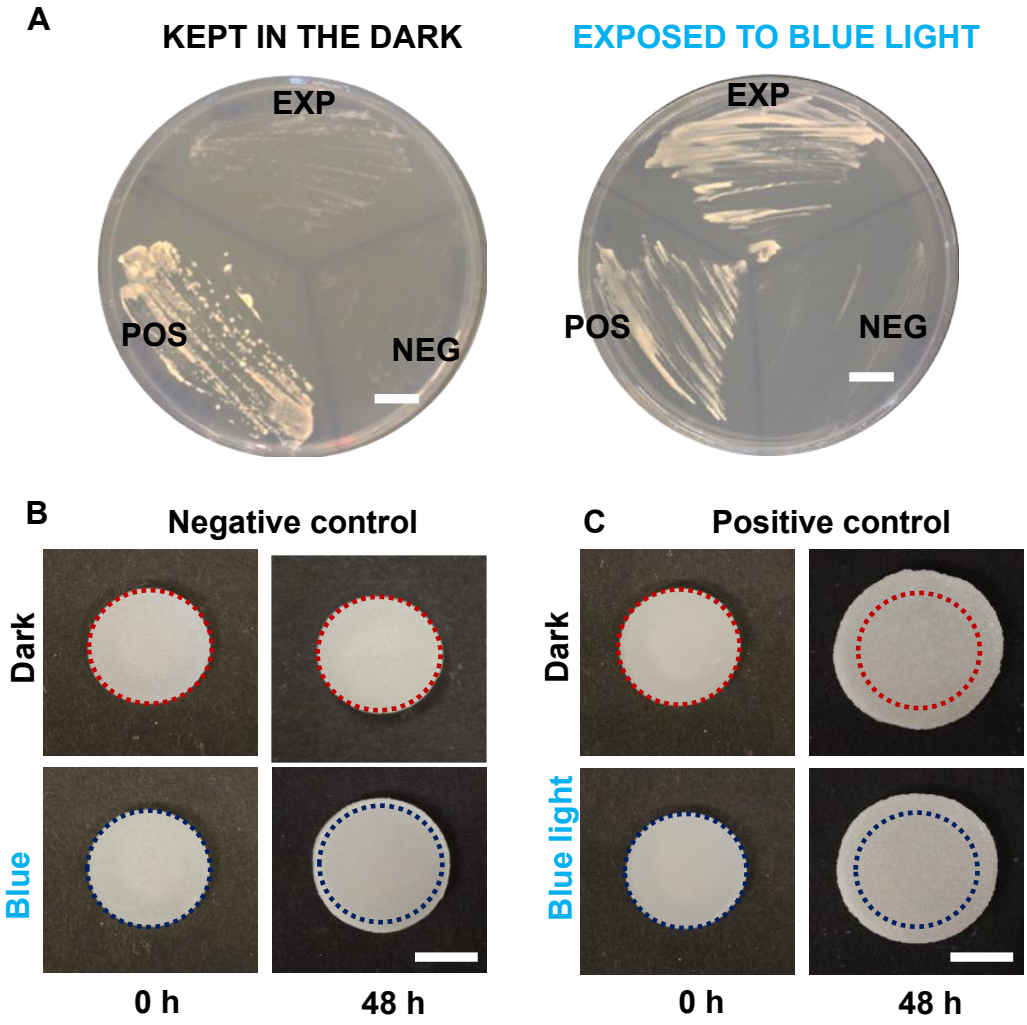

Figure A-9: Yeast proliferation on minimal agar media. (A)Yeast strains growing on minimal SD agar without L-Histidine and with competitive inhibitor 3AT. Plates were incubated at 30ºC for 36 h. The plate on the left was wrapped in aluminum foil to avoid light exposure, and the plate on the right was exposed to blue light at 455 nm of wavelength with 2.7 mW/cm^2 2 s pulses every 2 min (Scales bars: 10 mm). POS refers to the positive control strain. NEG refers to the negative control strain. EXP refers to the experimental strain. Representative images of living composites kept in the dark or exposed to blue light. Negative control composites are shown in (B) and positive control composites in (C) (Scale bars: 5 mm). Composites are incubated at 30ºC in media without L-Histidine for 48 h with media change every 12 h. Composites kept in the dark are wrapped in aluminum foil and light exposed composites are irradiated with 455 nm wavelength light with intensity of 2.7 mW/cm^2 for 2 s every 2 min. Dotted circles represent initial area and are used to guide the eye after composites growth. Reprinted with permission from [197]. Copyright (2020) exclusive licensee American Association for the Advancement of Science. Distributed under a Creative Commons Attribution License 4.0 (CC BY).

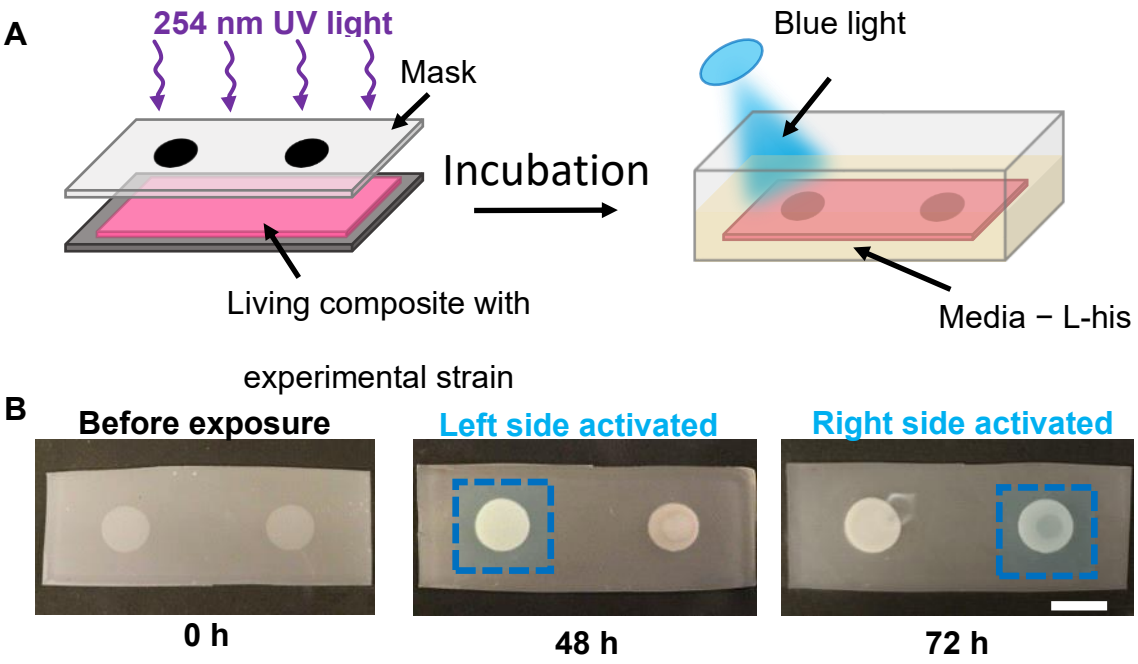

Figure A-10: Optogenetic control of shape change in genetically engineered living composites. (A) Schematic of the UV patterning of a free-standing film. Area indicated by the two circles contain living yeast while the area surrounding these circles contain cells that are UV-killed. After patterning, the living composite is equilibrated in dH_2O and incubated in media without L Histidine. During incubation, the living composite is irradiated with 455 nm wavelength blue light with an intensity of 2.7 mW/cm^2 for 2 s every 2 min over a portion of the sample. (B) Patterned composites before exposure to blue light (left), after incubation in media without L-histidine and only irradiating the left circle (middle), and irradiation of right circle only (right) (Scale bar: 10 mm). Reprinted with permission from [197]. Copyright (2020) exclusive licensee American Association for the Advancement of Science. Distributed under a Creative Commons Attribution License 4.0 (CC BY).

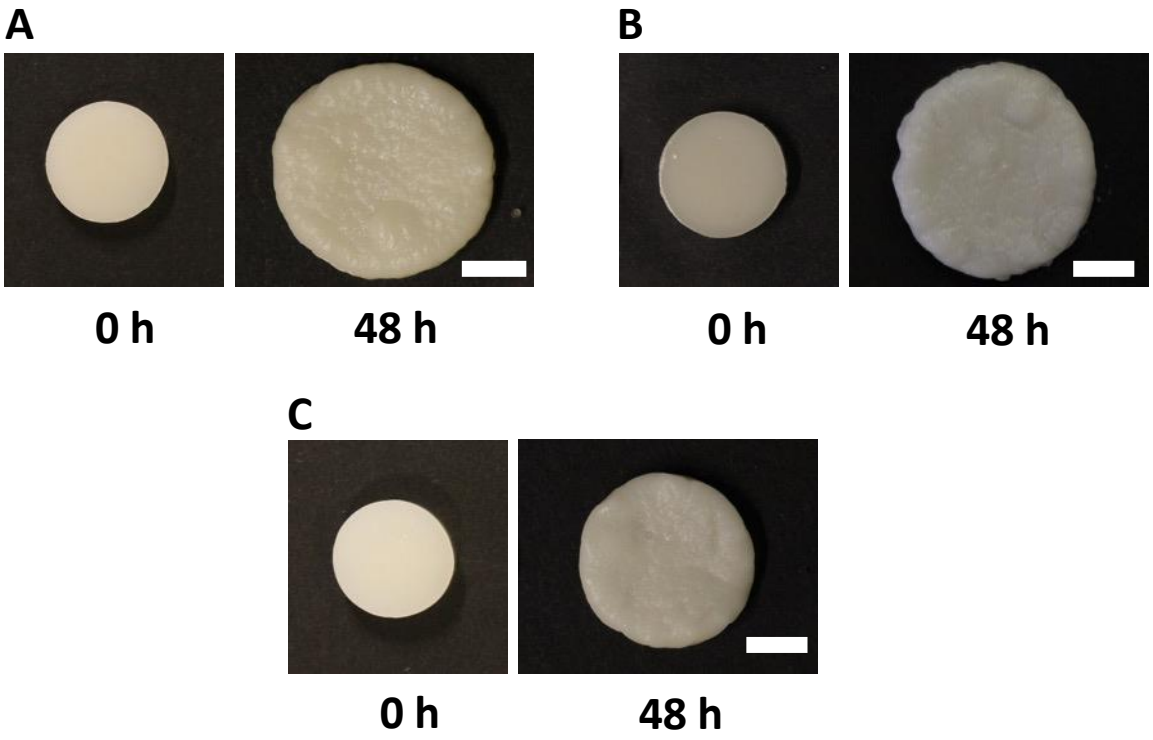

Figure A-11: Representative images of ELMs containing active dried yeast before and after growth in synthetic complete medium. Images of ELMS with (A) 5 wt % CNC, with (B) 8 wt % CNC, and with (C) 14 wt % CNC. (Scale bars: 5 mm). Each experiment had 3 replicates. All ELMs were grown in synthetic complete medium at 30 ^{o}C under shaking and aerobic conditions. Medium was changed every 12 h. Reprinted with permission from [296]. Copyright (2021) Wiley-VCH.

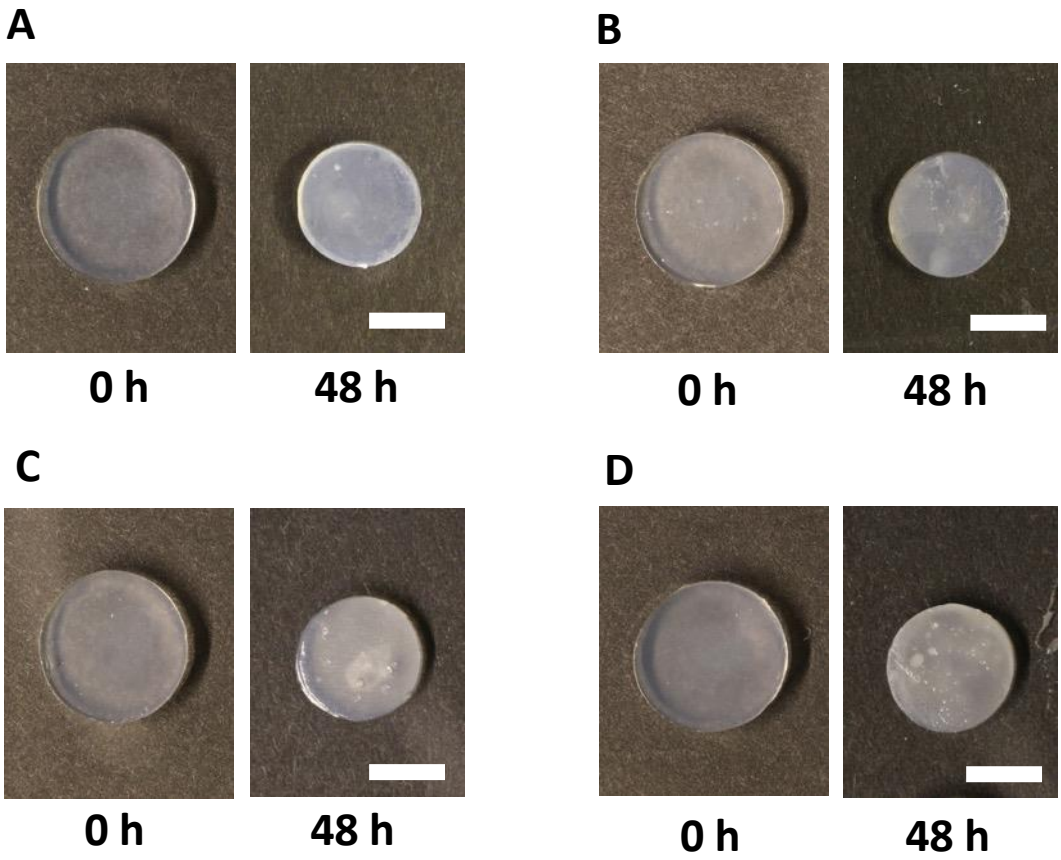

Figure A-12: Representative images of cell-free hydrogels before and after growth in synthetic complete medium. Images of cell-free hydrogels with (A) 11 wt % CNC, with (B) 16 wt % CNC, with (C) 19 wt % CNC, and with (D) 22 wt % CNC (Scale bars: 5 mm). Each experiment had 3 replicates. All cell-free hydrogels were placed in the same flasks containing ELMs growing in synthetic complete medium at 30 ºC under shaking and aerobic conditions. Medium was changed every 12 h. Reprinted with permission from [296]. Copyright (2021) Wiley-VCH.

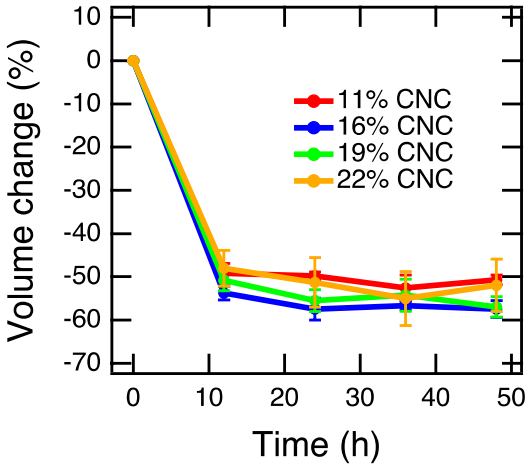

Figure A-13: Influence of CNC at varying concentrations on volume change of cell-free hydrogels. Volume change as a function of time for each cell-free hydrogel composed of different concentrations of CNCs. Reprinted with permission from [296]. Copyright (2021) Wiley-VCH.

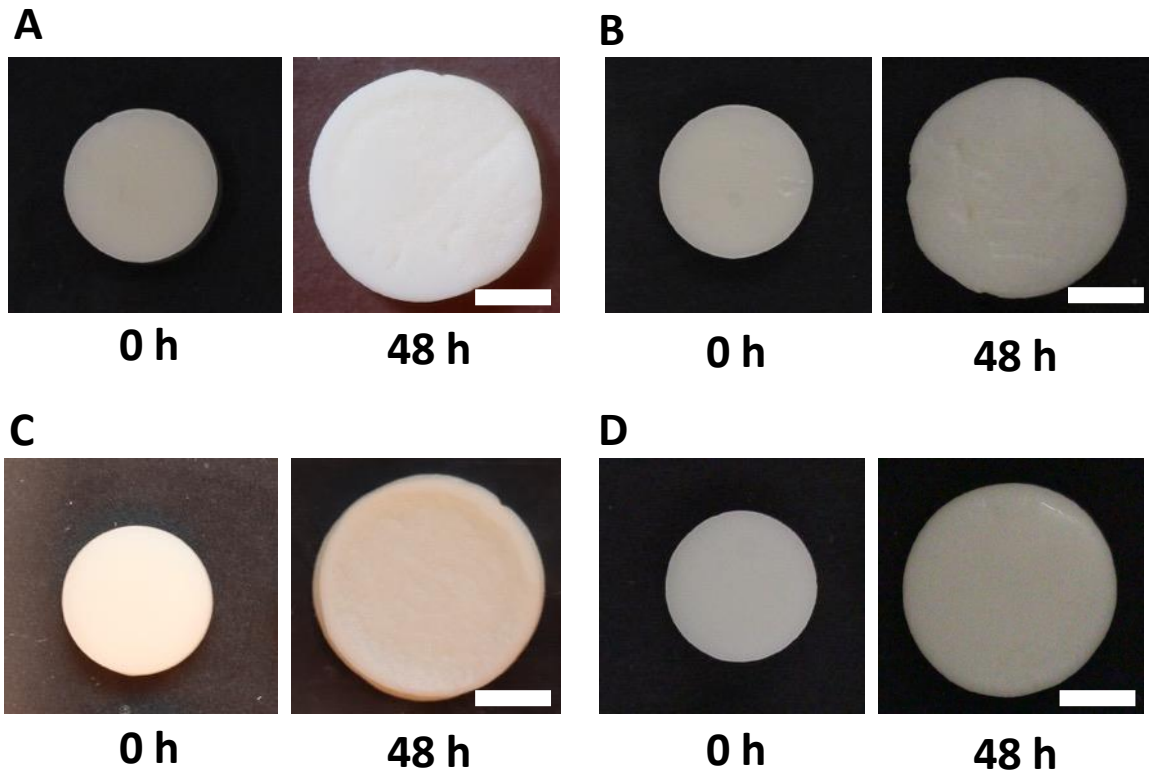

Figure A-14: Representative images of ELMs containing genetically engineered *S. boulardii* before and after growth in synthetic medium with the corresponding amino acid or nucleotide. Images of ELMs containing (A) *S. boulardii*-URA3, containing (B) *S. boulardii*-TRP1, containing (C) *S. boulardii*-HIS3, and containing (D) *S. boulardii*-LEU2 (Scale bars: 5 mm). Each experiment had 3 replicates and was repeated 3 times. All ELMs were grown in synthetic medium with the corresponding amino acid or nucleotide at 30 ºC under shaking and aerobic conditions. Medium was changed every 12 h. Reprinted with permission from [296]. Copyright (2021) Wiley-VCH.

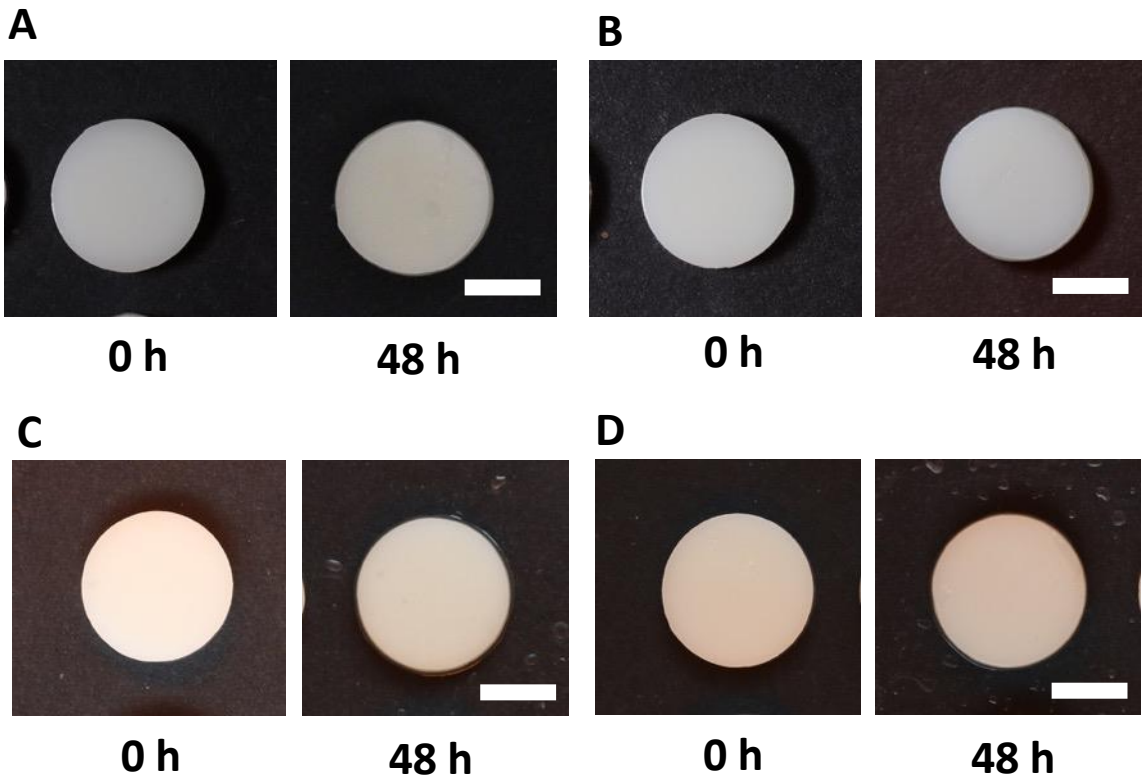

Figure A-15: Representative images of ELMs containing genetically engineered *S. boulardii* before and after growth in synthetic medium without the corresponding amino acid or nucleotide. Images of ELMs containing (A) *S. boulardii*-URA3, containing (B) *S. boulardii*-TRP1, containing (C) *S. boulardii*-HIS3, and containing D) *S. boulardii*-LEU2 (Scale bars: 5 mm). Each experiment had 3 replicates and was repeated 3 times. All ELMs were grown in synthetic medium without the corresponding amino acid or nucleotide at 30 ºC under shaking and aerobic conditions. Medium was changed every 12 h. Reprinted with permission from [296]. Copyright (2021) Wiley-VCH.

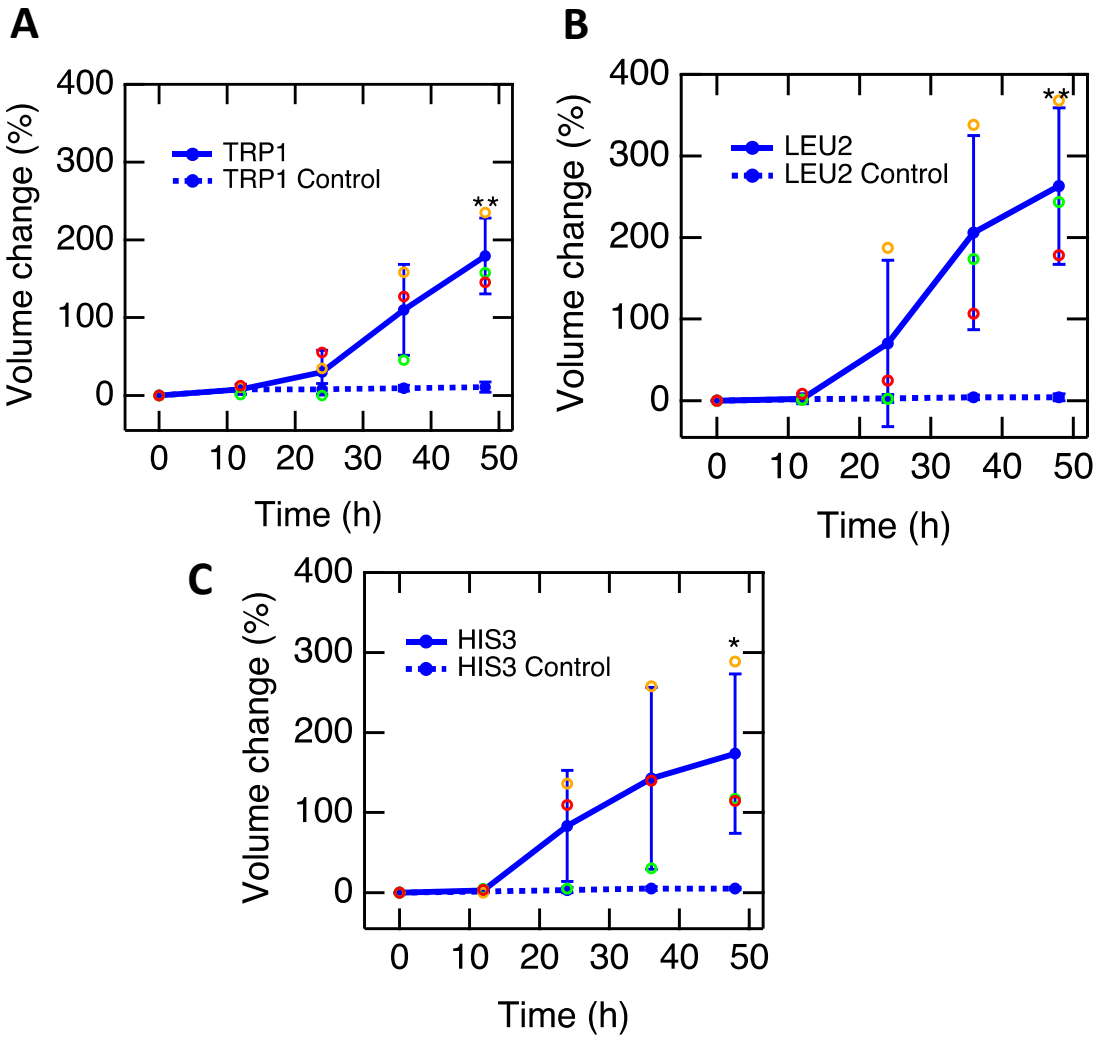

Figure A-16: Volume change of ELMs containing genetically engineered *S. boulardii*. Volume change over time of ELM disks containing (A) *S. boulardii*-TRP1, containing (B) *S. boulardii*-LEU2, and containing (C) *S. boulardii*-HIS3. Each experiment had 3 replicates and was repeated 3 times. All ELMs were grown in synthetic medium with and without the corresponding amino acid at 30 ºC under shaking and aerobic conditions. Medium was changed every 12 h. Each data point represents the mean (n = 3), and error bars represent standard deviation. Trend lines are only intended to guide the eye. To better visualized the data, open dots show the individual data points for ELMs grown in the presence of uracil. Statistical analysis: *t*-test, * P-value < 0.05, ** P-value < 0.01. Reprinted with permission from [296]. Copyright (2021) Wiley-VCH.

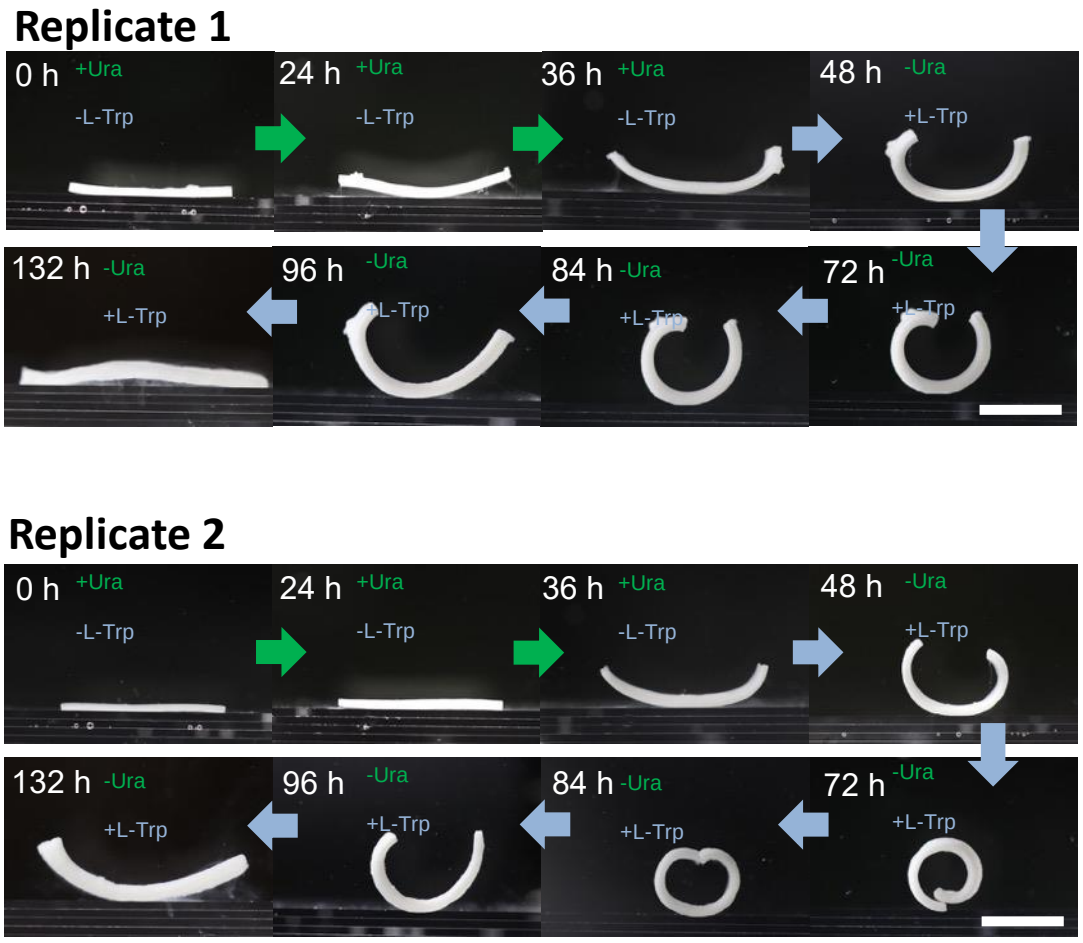

Figure A-17. Sequential shape change of ELM bilayers. Replicates of bilayers fabricated to contain a layer of *S. boulardii*-URA3 and a layer of *S. boulardii*-TRP1 (1 and 2) (Scale bars: 10 mm). Bilayers were grown in synthetic medium with uracil but lacking L-tryptophan for 48 h and then they were grown in synthetic medium with L-tryptophan but lacking uracil for 84 h. Bilayers were at 30 ºC under shaking and aerobic conditions. Medium was changed every 12 h. Reprinted with permission from [296]. Copyright (2021) Wiley-VCH.

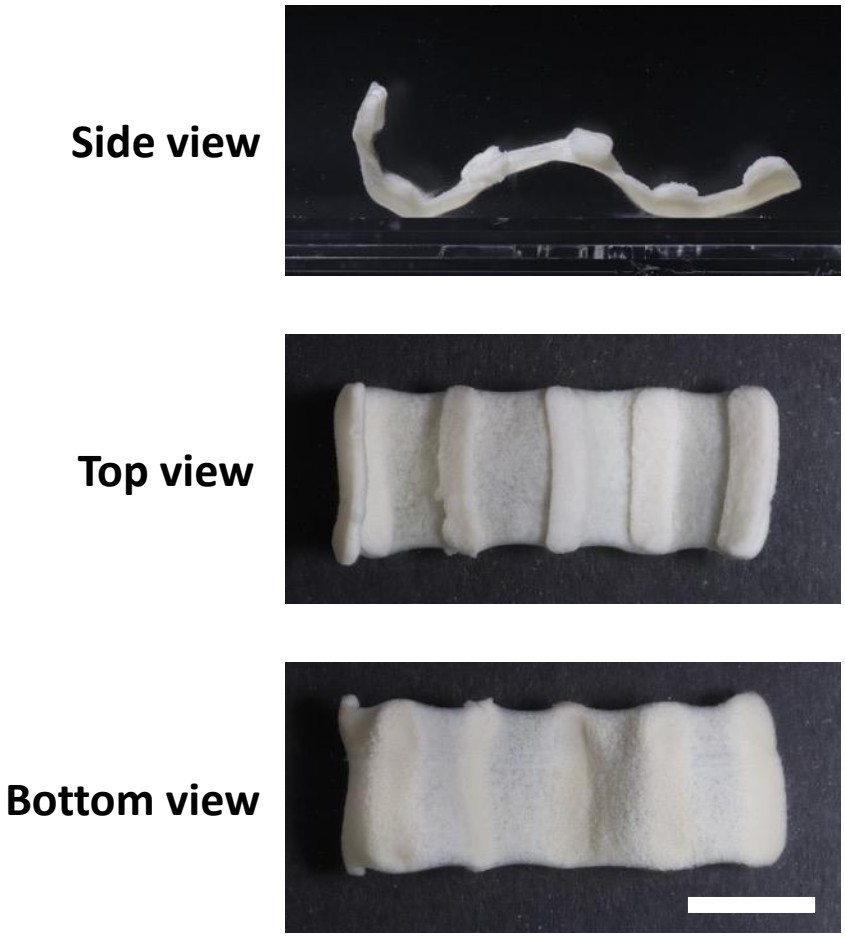

Figure A-18: Shape change of 4D printed structure in response to a second stimulus. Growth of patterned bilayer in medium containing the second biochemical stimulus for 144 h (Scale bar: 10 mm). Printed structures were first grown in synthetic medium with L-tryptophan but lacking L-leucine for 48 h (as shown in Figure 6) and then they were grown in synthetic medium with L-leucine but lacking L-tryptophan for 144 h. Bilayers were grown at 30 ºC under shaking and aerobic conditions. Medium was changed every 12 h. Reprinted with permission from [296]. Copyright (2021) Wiley-VCH.

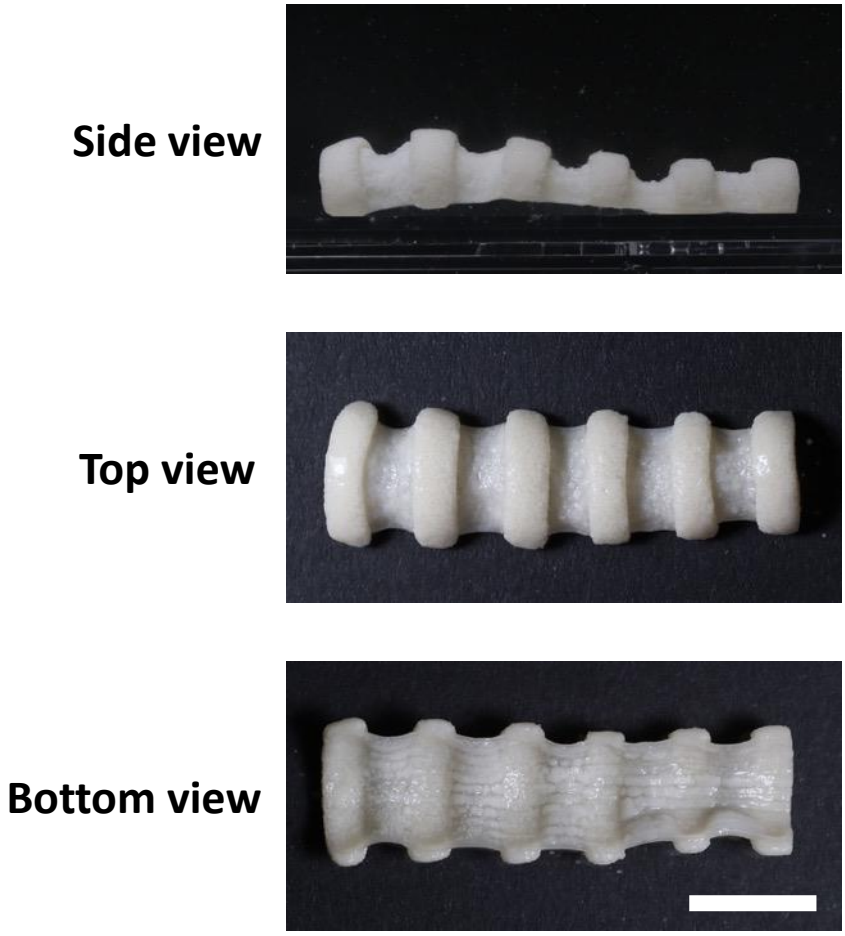

Figure A-19: Shape change of 4D printed structure in response to a second stimulus. Growth of patterned bilayer in medium containing the second biochemical stimulus for 144 h (Scale bar: 10 mm). Printed structures were first grown in synthetic medium with L-leucine but lacking L-tryptophan for 48 h (as shown in Figure 3-6) and then they were grown in synthetic medium with L-tryptophan but lacking L-leucine for 144 h. Bilayers were grown at 30 ºC under shaking and aerobic conditions. Medium was changed every 12 h. Reprinted with permission from [296]. Copyright (2021) Wiley-VCH.

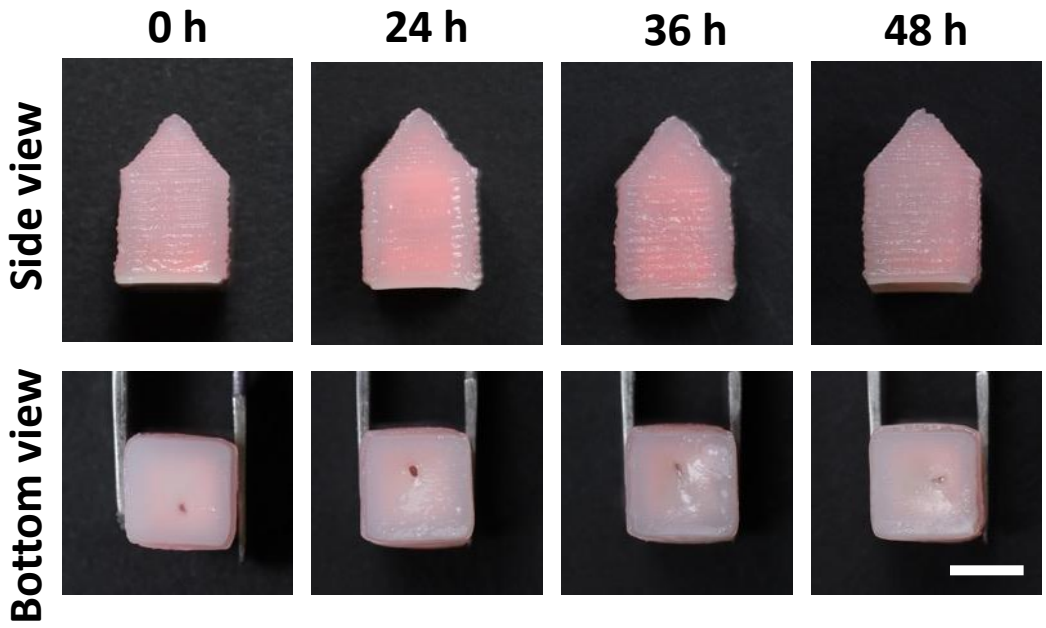

Figure A-20: Representative images of positive control printed drug delivery device. Positive control of printed capsule encapsulating model drug (fluorescent microparticles). Bottom of the capsule contains *S.boulardii*-TRP1 (Scale bar: 5 mm). The device is manually ruptured on the bottom and then incubated in synthetic medium lacking the amino acid L-tryptophan for 48 h. Devices were grown at 37 ºC under shaking and aerobic conditions. Medium was changed every 12 h. Reprinted with permission from [296]. Copyright (2021) Wiley-VCH.

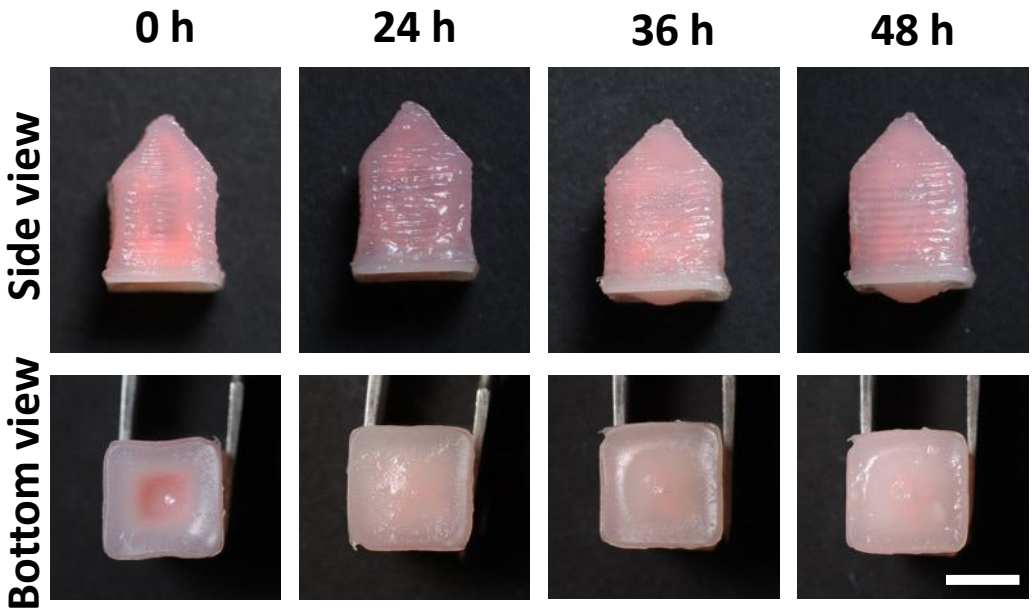

Figure A-21: Representative images of negative control printed drug delivery device. Negative control of printed capsule encapsulating model drug (fluorescent microparticles). Bottom of the capsule contains *S.boulardii*-TRP1 (Scale bar: 5 mm). The device is incubated in synthetic medium lacking the amino acid L-tryptophan for 48 h. Devices were grown at 37 ºC under shaking and aerobic conditions. Medium was changed every 12 h. Reprinted with permission from [296]. Copyright (2021) Wiley-VCH.

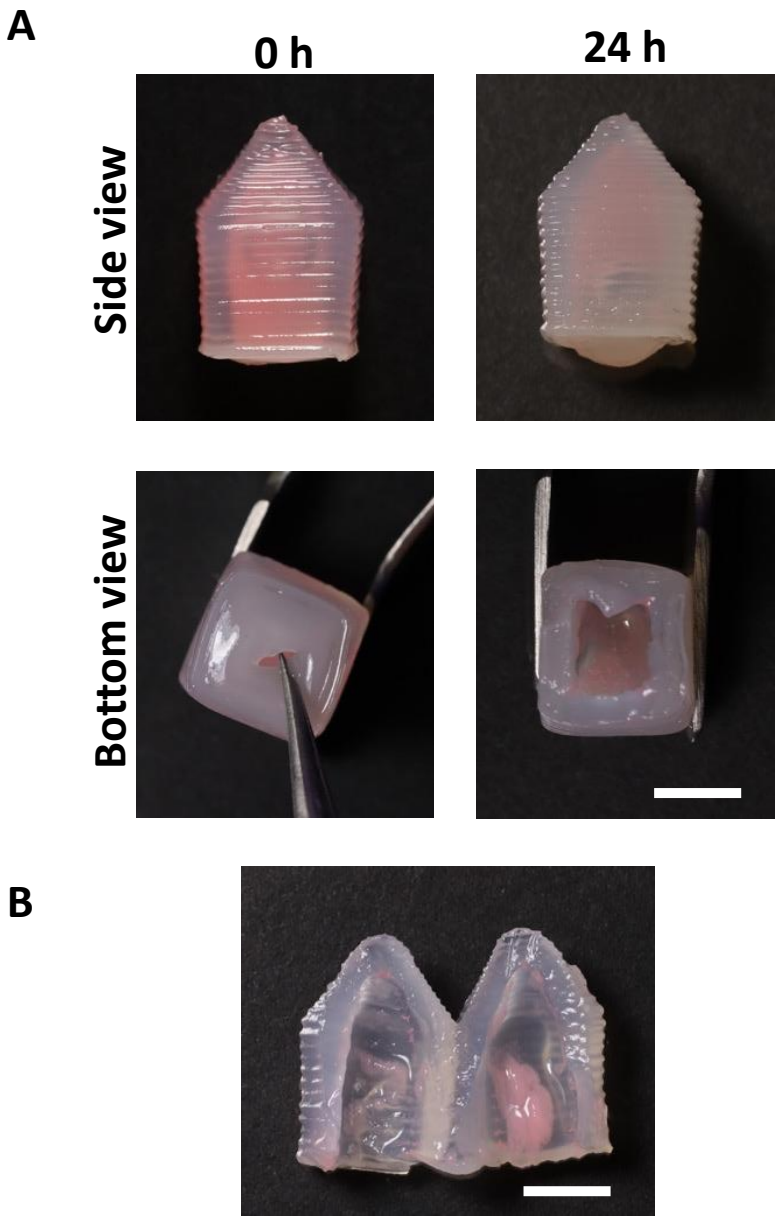

Figure A-22: Representative images of positive control printed drug delivery device. (A) Positive controls were manually ruptured on the bottom and then incubated for 24 h. After incubation, the base of the capsules were cut to observe the retained model drug within the reservoir. (B) The same capsules were cut through the side to observe the retained contents (Scale bars: 5 mm). Reprinted with permission from [296]. Copyright (2021) Wiley-VCH.

Table A-1. Power law flow index results. Table shows the flow indexes of bioinks and cell-free inks made with different concentrations of CNC. Reprinted with permission from [296]. Copyright (2021) Wiley-VCH.

Bioinks		**Cell-free inks**	
CNC (wt %)	**Flow index (*n*)**	**CNC (wt %)**	**Flow index (*n*)**
5	**0.01 ± 0.01**	**11**	**0.04 ± 0.01**
8	**0.03 ± 0.02**	**16**	**0.03 ± 0.01**
11	**0.01 ± 0.01**	**19**	**0.04 ± 0.03**
		22	**0.00 ± 0.00**